

Rowan University

Rowan Digital Works

Theses and Dissertations

3-10-2017

Analysis of aggregate mineralogy using LIBS

Bless Ann Varghese
Rowan University

Follow this and additional works at: <https://rdw.rowan.edu/etd>



Part of the [Civil and Environmental Engineering Commons](#)

Recommended Citation

Varghese, Bless Ann, "Analysis of aggregate mineralogy using LIBS" (2017). *Theses and Dissertations*. 2370.

<https://rdw.rowan.edu/etd/2370>

This Thesis is brought to you for free and open access by Rowan Digital Works. It has been accepted for inclusion in Theses and Dissertations by an authorized administrator of Rowan Digital Works. For more information, please contact graduateresearch@rowan.edu.

ANALYSIS OF AGGREGATE MINERALOGY USING LIBS

by

Bless Ann Varghese

A Thesis

Submitted to the
Department of Civil and Environmental Engineering
College of Engineering
In partial fulfillment of the requirement
For the degree of
Master of Science in Civil Engineering
at
Rowan University
June 22, 2016

Thesis Chair: Beena Sukumaran, Ph.D.

Dedications

I would like to dedicate this thesis to my grandparents; Melathekallelil
Geevarghese Abraham and Aleyamma Abraham, and Geevarghese and Sosamma
Varghese.

Acknowledgments

The success and outcome of this project required a lot of guidance and assistance from many people and I am extremely fortunate to have got this all along the completion of my project work. All I have done is only due to such guidance and assistance and I would not forget to thank them.

I would like to thank Dr. Beena Sukumaran; chair of the Rowan University Department of Civil Engineering and my advisor, for the opportunity to work on this project, her continued support and advice, and for her unwavering desire to see her students and advisees succeed in both their education and professional careers. A special note of thanks to Dr. Michael Lim from the Rowan University Physics Department and Dr. Ravi Ramachandran from the Rowan University Department of Electrical and Computer Engineering for their time, support, and assistance in making this research complete on time.

I would like to thank my family and friends for their continuous support throughout this research. I would like to thank all the undergraduate students who worked alongside me toward the completion of this research, and wish them all luck in all their future endeavors. I would also like to extend a special thanks to Andrew Branin for his continual support and assistance during the first half of this research. I owe my profound gratitude to Aaron Nolan and Danilo Zeppilli for all their support, encouragement and unlisted help from the beginning of this project.

Finally, I would like to thank the New Jersey Department of Transportation and University Transportation Research Center (UTRC) for their continued support, assistance, and for the research grant which made this research possible.

Abstract

Bless Ann Varghese
ANALYSIS OF AGGREGATE MINERALOGY USING LIBS
2016-2017

Beena Sukumaran, Ph.D.
Master of Science in Civil Engineering

The New Jersey Department of Transport (NJDOT) has a vested interest in the determination of the chemical composition and thereby the mineralogy of aggregates. Depending on the mineralogy of an aggregate sample, it may be inappropriate to use for construction and roadwork purposes. Current methods of determining the mineralogy of aggregates are costly in terms of time, money and convenience. As such, there is a desire for the development of an alternative and efficient method for aggregate mineralogical determination in the field.

The focus of this study is to develop a portable system for aggregate analysis in the field and compare the results with X-Ray Fluorescence (XRF) data provided by the NJDOT. Laser Induced Breakdown Spectroscopy (LIBS), which involves firing a laser pulse at a sample to determine its composition from light spectra emitted via a spectrometer and a custom program, was chosen to be the basis of the portable system. Along with system development, results were analyzed via Partial Least Squares Regression (PLSR). The current analysis technique utilizes split-training and y-scaling to analyze spectra data and performs well for most samples.

Table of Contents

Abstract	v
List of Figures	xi
List of Tables	xv
Chapter 1: Introduction	1
Hypothesis.....	1
Significance of Research.....	2
Study Objectives	2
Research Approach	3
Thesis Structure	4
Chapter 2: Literature Review	5
Geology of New Jersey.....	5
Coastal Plain	5
Piedmont Region.....	6
Highlands	7
Valley and Ridge Region	7
Key Rock Types Used by New Jersey Department of Transportation	8
Carbonate Rocks	8
Dolomite	8
Limestone.....	9
Gneiss.....	9
Basalt.....	9
Quartzite.....	10

Table of Contents (Continued)

Shale.....	10
Argillite.....	11
Various Analysis Methods for Aggregate Mineralogy.....	11
Atomic Absorption Spectroscopy (AAS)	11
Inductively Coupled Plasma-Mass Spectroscopy (ICP-MS).....	12
X-Ray Fluorescence (XRF)	12
Electron Probe Micro-Analysis (EPMA).....	13
Laser Induced Breakdown Spectroscopy (LIBS)	13
Configuration of LIBS	14
Laser Ablation.....	15
Laser Plasma	16
Plasma Cooling.....	16
Data Acquisition Time and Delay.....	17
Application of LIBS.....	18
Metal Industry Applications	18
Biological Applications	18
Geologic Applications	19
Advantages of LIBS.....	20
Experimental Errors	21
Analysis of Aggregate Mineralogy by NJDOT	23
Data Analysis Methods.....	23
Artificial Neural Network (ANN).....	24

Table of Contents (Continued)

Principal Component Analysis (PCA)	24
Partial Least Square Regression (PLSR) Analysis	25
Chapter 3: Methodology	27
Laboratory Setup	27
Field Setup	30
Data Acquisition and Testing Procedure	31
Data Collection	35
Calibration Set	35
Testing Set	38
Spectrum Analysis	38
Base Model	38
Y Scaling	38
Split Training Strategy	39
Combination Model	39
Classification Methods for Split Training	39
One-Dimensional Classification	39
Two-Dimensional Line Classification	40
Two-Dimensional Ratio Classification	41
Three-Way Split Classification	42
Chapter 4: Results and Discussions	44
Spectrum Analysis Methods	44
Base Model	44

Table of Contents (Continued)

Y Scaling.....	47
Split Training	50
Split Training and Y Scaling.....	53
Classification Methods for Split Training.....	56
One-Dimensional Classification	56
Two-Dimensional Line Classification	59
Two-Dimensional Ratio Classification.....	63
Three-Way Split Classification.....	66
Accuracy of Models	70
R Square Values.....	70
ANOVA (Analysis of Variance).....	72
High-Pass Filter of LIBS Spectrum	76
Moving Average Subtraction (MAS).....	77
Moving Slope Analysis (MSA)	78
Frequency Cut Off and Slope Detection.....	81
Determination of a Suitable Sample Size	83
Development of a User-Friendly Program.....	84
Testing of the Portable Equipment to Assess Ruggedness and Impact of Environmental Factors	86
Vibration/Impact Test	86
Temperature Test	88
Effect of Aggregate Moisture Content on Results.....	90

Table of Contents (Continued)

Building a More Affordable and Portable Equipment Setup.....	92
Chapter 5: Conclusions.....	94
Summary of Findings.....	94
Future Recommendations	98
References.....	99
Appendix A: X-Ray Fluorescence Data of Rocks	103
Appendix B: Algorithm for Three-Way Split Classification.....	106

List of Figures

Figure	Page
Figure 1. Layout of the 1:100,000 Scale of Geologic Map of New Jersey.....	5
Figure 2. Overview of LIBS System.....	15
Figure 3. Laser Ablation	16
Figure 4. Temporal History of LIBS Plasma	18
Figure 5. Artificial Neuron Network	24
Figure 6. Flowchart of Laser Equipment	28
Figure 7. Laboratory Setup	29
Figure 8. Portable LIBS setup.....	31
Figure 9. Laser Power Switch.....	32
Figure 10. Aurora Software Initialization.....	33
Figure 11. Spectrometer Lights.....	33
Figure 12. A Sample Spectrum.....	35
Figure 13. The Classification of Rocks Based on CaO%	40
Figure 14. The Classification of Rocks Based on the Threshold Line	41
Figure 15. The Classification of Rocks Based on the Threshold Ratio of 3.....	42
Figure 16. The Classification of Rocks Based on the Ratio Square Method.....	43
Figure 17. Results of SiO ₂ of Base Model.....	45
Figure 18. Results of Al ₂ O ₃ of Base Model.....	45
Figure 19. Results of Fe ₂ O ₃ of Base Model.....	46
Figure 20. Results of CaO of Base Model	46
Figure 21. Results of MgO of Base Model.....	47

Figure 22. Results of SiO ₂ of Y Scaling	48
Figure 23. Results of Al ₂ O ₃ of Y Scaling	48
Figure 24. Results of Fe ₂ O ₃ of Y Scaling	49
Figure 25. Results of CaO of Y Scaling	49
Figure 26. Results of MgO of Y Scaling	50
Figure 27. Results of SiO ₂ of Split Training.....	51
Figure 28. Results of Al ₂ O ₃ of Split Training.....	51
Figure 29. Results of Fe ₂ O ₃ of Split Training.....	52
Figure 30. Results of CaO of Split Training.....	52
Figure 31. Results of MgO of Split Training.....	53
Figure 32. Results of SiO ₂ of Split- Y Scaling	54
Figure 33. Results of Al ₂ O ₃ of Split- Y Scaling	54
Figure 34. Results of Fe ₂ O ₃ of Split- Y Scaling	55
Figure 35. Results of CaO of Split- Y Scaling.....	55
Figure 36. Results of MgO of Split- Y Scaling	56
Figure 37. Results of SiO ₂ Using Calcium Oxide Classification.....	57
Figure 38. Results of Al ₂ O ₃ Using Calcium Oxide Classification.....	58
Figure 39. Results of Fe ₂ O ₃ Using Calcium Oxide Classification.....	58
Figure 40. Results of CaO Using Calcium Oxide Classification.....	59
Figure 41. Results of MgO Using Calcium Oxide Classification.....	59
Figure 42. Results of SiO ₂ Using Line Classification.....	61
Figure 43. Results of Al ₂ O ₃ Using Line Classification.....	61
Figure 44. Results of Fe ₂ O ₃ Using Line Classification.....	62

Figure 45. Results of CaO Using Line Classification.....	62
Figure 46. Results of MgO Using Line Classification.....	63
Figure 47. Results of SiO ₂ Using Ratio Classification	64
Figure 48. Results of Al ₂ O ₃ Using Ratio Classification	64
Figure 49. Results of Fe ₂ O ₃ Using Ratio Classification	65
Figure 50. Results of CaO Using Ratio Classification	65
Figure 51. Results of MgO Using Ratio Classification	66
Figure 52. Results of SiO ₂ Using Ratio Square Classification	68
Figure 53. Results of Al ₂ O ₃ Using Ratio Square Classification	68
Figure 54. Results of Fe ₂ O ₃ Using Ratio Square Classification	69
Figure 55. Results of CaO Using Ratio Square Classification	69
Figure 56. Results of MgO Using Ratio Square Classification	70
Figure 57. ANOVA Results of Various Models for Carbonates	73
Figure 58. ANOVA Results of Various Models for Trap Rocks.....	74
Figure 59. ANOVA Results of Various Models for Non-Carbonates	74
Figure 60. ANOVA Results of Various Split Training Methods for Carbonates.....	75
Figure 61. ANOVA Results of Various Split Training Methods for Trap Rocks	76
Figure 62. ANOVA Results of Various Split Training Methods for Non-Carbonates....	76
Figure 63. Left to Right: Unfiltered Atkinson Quartzite data, Moving Average of Data, Subtraction of Data, Subtraction of Moving Average from Original Data, Filtered Data Adjusted to Eliminate Negative Values.....	77
Figure 64. Subtraction from MAS Filtration Method Showing the Moving Average N=180 to Best Conserve Relevant Information	78
Figure 65. Left to Right: Unfiltered Atkinson Quartzite Data, Moving Slope Analysis Data, Showing Preservation of Intensity Information, Filtered Data Subtracted from Unfiltered Data Leaving Only the Baseline.....	79

Figure 66. Left to Right: Unfiltered Atkinson Quartzite Data, Moving Slope Analysis Preserving Data with Slope \geq 10, Moving Slope Analysis Preserving Data with slope \geq 100, Moving Slope Analysis Preserving Data with Slope \geq 1000.....	79
Figure 67. Comparing the Output of the PLSR Calculation of Atkinson Quartzite, Error Bars Showing Uncertainty of Data with 95% Certainty.....	80
Figure 68. Comparing the Output of the PLSR Calculation of Carbonate Dolomite, Error Bars Showing Uncertainty of Data with 95% Certainty.....	80
Figure 69. Comparing the Output of the PLSR Calculation of EI Hamburg Gneiss, Error Bars Showing Uncertainty of Data with 95% Certainty.....	81
Figure 70. High Pass Filtering of LIBS Spectrum.....	82
Figure 71. Results of High Pass Filtering of LIBS Spectrum.....	83
Figure 72. Testing Set Size.....	84
Figure 73. Laser Data Analysis Tool.....	85
Figure 74. Update Calibration Tool.....	85
Figure 75. Vibration/ Impact Test Results, Carbonate Dolomite.....	86
Figure 76. Vibration/ Impact Test Results, Plumstead Argillite Stockpile.....	87
Figure 77. Vibration/ Impact Test Results, Bechtelsville Gneiss 15179.....	87
Figure 78. Temperature Test Results, Carbonate Dolomite.....	89
Figure 79. Temperature Test Results, Plumstead Argillite Stockpile.....	89
Figure 80. LIBS Spectrum Obtained at 34 Deg. F.....	90
Figure 81. LIBS Spectrum Obtained at 68 Deg. F. (Laboratory Condition).....	90
Figure 82. Aggregate Moisture Content Test results, Carbonate Dolomite.....	91
Figure 83. Aggregate Moisture Content Test results, Plumstead Argillite Stockpile.....	91
Figure 84. Testing of the Equipment Using Low Resolution Spectrometer.....	92

List of Tables

Table	Page
Table 1. Aggregates Used for Calibration	36
Table 2. Outliers of One Dimensional Classification	57
Table 3. Outliers of Two-Dimensional Line Classification	60
Table 4. Outliers of Two-Dimensional Ratio Classification	63
Table 5. Outliers of Three- Way Split Classification	67
Table 6. R Square Values of Each Method Against Each Compound.....	71
Table 7. R Square Values of Carbonates, Trap Rocks and Non- Carbonates for Various Split Training Methods	72
Table 8. Accuracy of the Model Selected for Final Use.....	96

Chapter 1

Introduction

Strength and durability of a pavement is derived from the quality of materials used for its construction. The main structural component used for both HMA and concrete pavements are aggregates. In fact, the quality of aggregate determines the performance of the pavements. Aggregate quality is dependent on its strength, water absorption, resistance to abrasion and resistance to forces of weathering, which all depends on the mineral composition of the aggregate. Certain deleterious minerals like clay lumps, soft organic impurities and chert are undesirable for use in concrete and asphalt. New Jersey Department of Transportation uses X-Ray Fluorescence technique, chemical analysis and petrographic examinations to identify the mineral composition of aggregates. But, these methods do not provide real time data. These methods also involve complex sample preparations and are time consuming.

This research is to develop portable equipment for the *in situ* characterization of qualitative as well as quantitative analysis of aggregate mineralogy using Laser Induced Breakdown Spectroscopy technology. This equipment can give rapid test results in less than an hour using a fresh breaking aggregate sample surface with absolutely no sample preparation.

Hypothesis

1. Laser Induce Breakdown Spectroscopy (LIBS) can be used to quantify the chemical composition of aggregate stone samples
2. Partial Least Square Regression Analysis (PLSR) can be used to develop predictive models to predict the aggregate composition.

3. Spectrum processing methods such as split training strategy with Y-scaling produce accurate results
4. A Graphical User Interface program facilitates rapid model testing and future refinement of models.
5. The new equipment is feasible and affordable as a portable tool for field use.

Significance of Research

X-Ray Fluorescence (XRF) technique used by New Jersey Department of Transportation is reliable but expensive, non-portable and time consuming. XRF also requires sample preparation, which does not allow for many samples to be tested. Development of a portable, reliable system to quantify the chemical composition of aggregate helps for a rapid in-situ characterization with no sample preparation. This testing method helps to fast track the construction timeline; and ensures and enforces the New Jersey State standards for quality control. New Jersey State allows a maximum of five percent mix of aggregate varieties in the same batch of an aggregate type. Mixing of aggregates causes poor mix design for both HMA and concrete. With the new LIBS equipment, ensuring quality of aggregates in a timely manner is critical and pavement construction will be able to proceed smoothly. The portable equipment can be placed in the back of a truck and taken to the field as needed and should provide results in thirty minutes or less.

Study Objectives

This study will focus on the development of a portable tool for the in-situ characterization and quality control of aggregates using laser analysis. The primary objectives of this research are as follows:

1. To obtain the characteristic laser spectra models for various aggregate sources from New Jersey and surrounding areas;
2. To calibrate the model using laser spectrums of newly added rocks to identify real time aggregate properties such as mineralogy;
3. To determine if the field and laboratory setup produce consistent results;
4. To improve the accuracy of the results with the expanded calibration dataset;
5. To develop a user friendly program for rapid analysis of laser spectra with batch capability and for future refinement of the models as new stones are added;
6. To determine the feasibility of laser technology as a portable tool for identification of real time aggregate mineralogy;
7. To determine the feasibility and affordability of laboratory based laser technology applications for field use;
8. To field test the use of lasers for real time property identification;
9. To demonstrate the use of laser technology in the field for aggregate property determination and as a means of quality control;
10. To develop a user-friendly manual for operation and regular maintenance of the portable laser setup; and
11. To train the personnel in the use of the laser technology.

Research Approach

This section gives an overview of the research process to achieve the above research objectives. This research includes a thorough literature review of the geological formations and classifications of rocks in New Jersey; conventional techniques of mineral

characterization; selection of operating variables; model refinement for accurate predictions; design of portable tool; and field testing and analysis.

Thesis Structure

Chapter 1 of this thesis gives an overview of this research which includes introduction, problem statement, hypothesis of this research and its significance. Chapter 2 consists of a detailed literature review to understand the background of this research. This chapter begins with the geology of the state of New Jersey and surrounding areas to obtain a better understanding of the geologic origin of key rock types used by New Jersey Department of Transportation. Next, this chapter discusses various conventional methods used for the qualitative as well as quantitative analysis of rock mineralogy. Then it describes the concept and detailed overview of Laser Induced Breakdown Spectroscopy, its previous applications in various field and its experimental limitations or errors. Finally, this chapter describes in detail various statistical analysis methods, and provides details of the various techniques used in this study.

Chapter 3 describes in detail the experimental setup, field setup and various methods and standards employed to collect data. This chapter also describes various spectrum preprocessing methods, classification methods and other strategies.

Chapter 4 discusses the results from the validation of field setup, various classification methods and testing results and expanded calibration results. It also includes results from field testing, and feasibility and affordability of the field setup.

Chapter 5 discuss the conclusions of this research, a user-friendly manual developed for the field equipment, how this equipment can be used as a means of quality control and future areas of study.

Chapter 2

Literature Review

Geology of New Jersey

New Jersey is the fourth smallest state in the United States of America, and boasts an impressive geological variety. New Jersey contains four geographic regions known as physiographic provinces, with characteristic mineralogy. These regions are the Coastal Plain, the Piedmont, the Highlands, and the Valley and Ridge regions as shown in the figure 1 [1].

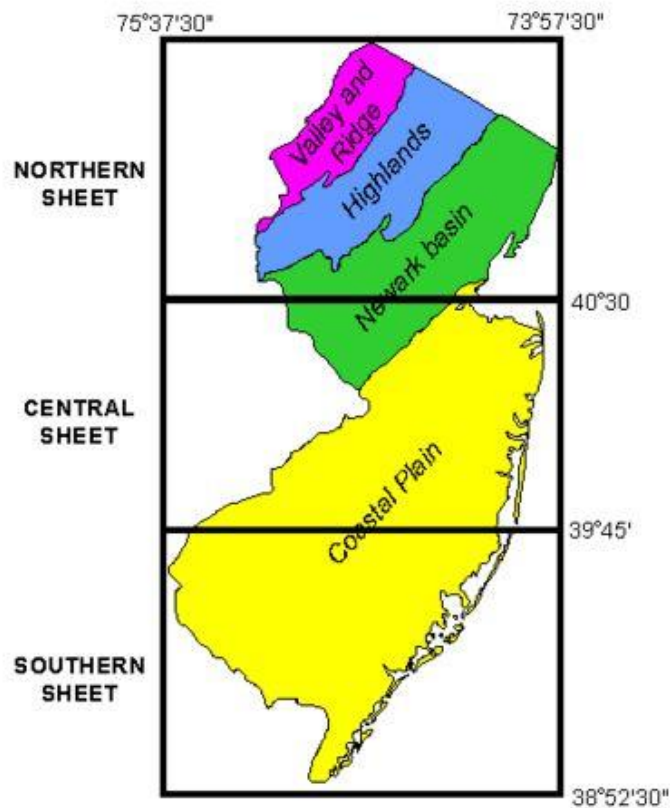


Figure 1. Layout of the 1:100,000 Scale of Geologic Map of New Jersey [2].

Coastal plain. Starting near Trenton and extending downwards to the southern end of the state, the Coastal Plain contains a flat or lightly rolling topography. There are

however, some higher elevation areas consisting of erosion resistant gravel and iron-cemented sediment. The majority of the Coastal Plain region consists of sand, silt, and clay sediments deposited in the environment due to the fluctuation of the sea level in the Cretaceous and Tertiary time periods around 145.5-2.58 million years ago [2]. There also exist wide bands of sand from the late tertiary and early Quaternary periods (~2.58-1.8 million years ago, [2]) along with gravel from river deposits [1].

This region was once the location of bog iron, glass sand, foundry sand, ceramic and brick clay mining. Recently mining has shifted over to glass sand and sand and gravel for construction material. The large sand deposits also serve as aquifers and ground water reservoirs [1].

Piedmont region. From the area around Trenton to a series of major faults, such as the Ramapo fault, lies the Piedmont region. Boasting rocks from the late Triassic and early Jurassic periods (~201.3 million years ago [2]) rather than the Cretaceous through Quaternary periods, the Piedmont region contains valleys known as rift basins formed by large crustal blocks dropping downwards during the elongation of the Atlantic Ocean. Sediment from higher elevation areas compacted in these basins over time, forming sandstone, siltstone, and shale deposits. These mineral deposits often have a reddish-brown color [3]. Along with the sandstone and shale is basalt and diabase from ancient volcanic activity. These volcanic deposits help to form a ridged topography in the region due to the greater erosion resistance of basalt and diabase when compared to the other sediments. Further north near the fault lines that make up the border of the piedmont region, some granite and gneiss can be found [1].

In the past “brownstone,” a once popular building material regarded as the state rock of New Jersey, was quarried from the sandstone deposits [4]. Presently, basalt and diabase are quarried for crushed stone. Some copper is also obtained from the sandstone and shale associated with the basalt and diabase deposits [1].

Highlands. Extending from the Ramapo fault to a border formed from a line from Franklin to Andover through to the Delaware River is the Highland region. The highlands primarily contain granite, gneiss, and Precambrian era (541 million or more years ago [2]) marble. The geology of the region came about from the melting and recrystallization of sedimentary rocks under high pressure and temperature from 1.3 billion to 750 million years ago, making the rocks in this region the oldest in New Jersey [1]. The erosion resistant properties of the granite and gneiss lend themselves to a hilly upland with valleys containing streams.

The highlands were once a source of magnetite ore deposits but are now quarried for crushed stone [1]. The Franklin Marble located in Ogdensburg, New Jersey is a mine containing a mineralogically unique zinc ore. This area of the highland region contains several unique fluorescent minerals that cannot be found elsewhere [5].

Valley and ridge region. The remaining northeastern portion of New Jersey is known as the Valley and Ridge region which encompasses an area around 530 square miles. This region was formerly covered in seas and floodplains, depositing sand, mud, and lime sediment in the area. Over a period of time ranging from the Cambrian to the Devonian eras (541-485.4 and 419.2-358.9 million years ago, [2]), these sediments formed into sandstone, shale and limestone. During the Ordovician era (485.4-443.8 million years ago, [2]) and the Pennsylvanian to Permian time (323.2-252.17 million

years ago, [2]) these minerals were compressed into folds along fault lines, resulting in linear belts of different minerals in the region. Alternating belts of erosion resistant sandstone and erosion susceptible shale and limestone led to the creation of ridges and valleys for which the region is named [1].

Limestone deposits in the valley and ridge region are quarried for construction purposes as well as to serve as an important ingredient for cement. Limestone can also yield large amounts of ground water, making the deposits good aquifers [1].

Key Rock Types Used by New Jersey Department of Transportation

While not representative of the absolute range of rocks found in aggregate, focus was placed on gneiss, limestone, dolomite, basalt, quartzite, argillite, and shale. These are the rocks collected and used by NJDOT for various highway construction purposes.

Carbonate rocks. The term carbonate is used in the aggregates industry to define aggregates that consist mainly of dolomite ($\text{Ca Mg}(\text{CO}_3)_2$) or Calcite (CaCO_3). Some examples of carbonates are limestone, dolomite, marl and chalk. An alkali-carbonate reaction can be potentially detrimental to the strength of a concrete mix. An alkali-carbonate reaction occurs when the alkali hydroxides in the binder react with the carbonates in aggregates, which leads to a decrease in the performance of a concrete. This reaction is relatively rare because most aggregates with high enough reactive carbonates are generally not suitable for concrete for some other reason like a low potential strength [6].

Dolomite. Dolomite is a sedimentary rock chiefly composed of calcium magnesium carbonate ($\text{Ca Mg}(\text{CO}_3)_2$). While containing a carbonate group, dolomite behaves differently from calcium carbonate ($\text{Ca}(\text{CO}_3)$) based limestone. While carbonate

minerals such as limestone are known to effervesce in a hydrochloric acid solution, dolomite only does so slowly as a powder and not at all as a crystal [7]. Dolomite is much weaker as an acid soluble material; however, dolomite is still not a recommended aggregate.

Limestone. Calcium carbonate ($\text{Ca}(\text{CO}_3)$) containing limestone is a key material for evaluation in aggregate applications. A common sedimentary rock, limestone has properties that make it unsuitable for aggregate applications. Limestone is weak to abrasion and will polish and become smooth when exposed to weathering and wheel loads [8]. A smoother roadway surface as a result of limestone-containing asphalt will show poor tire adhesion and be at a risk for hydroplaning. Limestone is also an Acid Soluble Material (ASM). In a solution of hydrochloric acid, limestone aggregate will dissolve. Thus, the acidity of rainwater causes limestone to breakdown, making the rock a poor fit for outdoor applications [9].

Gneiss. Gneiss is a high-grade metamorphic rock where the grains recrystallize under high heat and pressure and form into distinctive bands of varying mineral composition. The recrystallization of grains causes the grain size to increase and segregates them into distinctive bands. Gneiss is not defined by its mineral composition but most gneiss contains interlocking grains of quartz and feldspar. Gneiss and most metamorphic rocks generally do not split across its planar imperfections. This property allows gneiss to be used as a crushed stone in the cement and construction industry [10].

Basalt. Basalt is a fine grained igneous rock that is lightweight, with a glassy dark color. Basalt is an extrusive igneous rock, which means it is formed when molten rock cools either near or at the surface of the earth. [3] It is the most common igneous rock due

to its low viscosity which allows it to flow long distances. Basalts are generally comprised of pyroxene (Ca, Na) (Mg, Fe, Al) (Al, Si)₂O₆, plagioclase CaAl₂Si₂O₈ or NaAlSi₃O₈ and olivine (Mg, Fe)₂SiO₄. The SiO₄ content in basalts is 45%-52%. Basalts are used as an aggregate for the construction and pavement industry and for these applications it is preferred a low olivine content [11]

Quartzite. Quartzite is a metamorphic rock formed when quartz sandstone is exposed or weathered under considerable heat and pressure. Due to quartzite's quartz basis, the aggregate is primarily identified via its SiO₂ content. Due to its chemical makeup, quartzite is susceptible to alkali-silica reaction. Like quartz, quartzite is hard and durable. Quartzite also demonstrates an angular surface when broken. The pressure and heat responsible for quartzite formation causes the aggregate to be made up of quartz crystals instead of quartz grains. This leads to a flatter surface than pure quartz, since quartzite will break across quartz grains rather than around them [7]. Quartzite's inherent hardness makes it wear resistant and the angular pieces can interlock to impart greater stability to the overall structure of the application [9]. While not always used in road work applications, use of quartzite can be advantageous.

Shale. Shale is a sedimentary rock composed of hardened mud and contains appreciable amounts of mica and quartz along with the more predominant clay minerals. Shale breaks into small angular block, referred to as mudstone or siltstone dependent upon grain size [7]. Shale commonly reacts with dehydrated limestone and breaks down into CaO and CO₂ to produce cement powder [10]. As an aggregate, however, shale shows deleterious effects. Crushed shale can break down into a clay powder. Clay

expands when exposed to water and will cause surface stripping, making shale as a pure aggregate a poor fit for asphalt applications [12].

Argillite. Argillite is a very hard mudstone. Mudstones are fine-grained sedimentary rocks with grain sizes less than 0.06 mm and are comprised of a mixture of clay and silt sized particles that form when mud hardens. Argillite is not fissile, meaning it does not break along closely spaced bedding spaces like shale [11]. Argillites are weak compared to other similar sized aggregate and are very angular, which would increase the amount of binder needed. Despite these negative properties argillite still has applications as an aggregate in low strength concrete applications [13].

Various Analysis Methods for Aggregate Mineralogy

Various methods for the analysis of aggregate mineralogy were studied and Laser Induced Breakdown Spectroscopy is selected for this research.

Atomic Absorption Spectroscopy (AAS). Atomic Absorption Spectroscopy can accurately measure the concentration of metal elements present in a sample [14]. A sample is first atomized before a certain wavelength of light is passed through the sample. This can be done in several ways, but the most common method is flame atomization. Depending on the atomic composition of the sample, a certain wavelength of radiation (i.e. a certain energy input) is required to excite the electrons of a given element from one specific shell to another. A detector analyzes the radiation flux between tests with and without the sample, and these values as a ratio can be used to find elemental concentrations using the Beer-Lambert Law [14]. This method is dependent on the property of metals that they absorb specific, discrete wavelengths and return

characteristic spectrographic spectra, therefore this method cannot be used to determine non-metallic elemental compositions accurately [15].

Inductively Coupled Plasma-Mass Spectrometry (ICP-MS). Inductively Coupled Plasma-Mass Spectrometry (ICP-MS) ionizes an aerosol mass of the sample to be analyzed by introducing it into an argon plasma. Sample ions are collected and then separated using a spectrometer according to the ratio between the mass and charge of each ion [16]. By this method, the concentration and distribution of each element within the sample can be found [17]. This method has been proven to determine sample composition with only 1% error, as shown by J. Ludden et al. [18]. However, this process takes a significant amount of time due to the necessity of powdering the sample and adding it to an acid solution before testing [19]. This negates the possibility of *in situ* testing due to the amount of sample preparation required. Additionally, the ICP-MS instrument is large and is not feasible as a portable device.

X-Ray Fluorescence (XRF). X-ray fluorescence (XRF) spectrometry uses an x-ray instrument to analyze the chemical composition of aggregate samples. X radiation is directed at an aggregate sample. The sample then ionizes and loses inner-shell electrons. As outer-shell electrons move into the lower energy orbit, the sample emits x-rays of wavelengths unique to the individual elements present [20], [21]. For this method, the sample must be powdered and vitrified [19]. This method produces accurate results when conducted using relatively large sample sizes (>1 gram), [19]. However, it takes two weeks to conduct this test from preparation to results, and the equipment is expensive and cumbersome. As such, XRF spectrometry is not a viable option for field testing.

Electron Probe Micro-Analysis (EPMA). Electron Probe Micro-Analysis is a method for determining sample chemical composition using the same principles as x-ray diffraction. The significant differences are that EPMA analysis uses a focused electron beam rather than x-rays to ionize the sample, and EPMA analysis uses multiple sensors to record both emitted x-rays as well as electrons released by the sample [20], [22]. This test is conducted on a small point on a sample (1-2 microns across) and is subsequently relatively non-destructive [22]. However, the small size of the targeted area leads to potential inaccuracies in chemical composition determination of larger samples. Pownceby et al. included cathodoluminescence (CL) mapping to aid in determining the composition of minerals [23]. Due to the number of sensory instruments required to collect complete data from EPMA testing, the overall setup is too large to serve as a portable option.

Laser Induced Breakdown Spectroscopy (LIBS). Laser Induced Breakdown Spectroscopy can be used to quantify the concentrations of individual chemical compounds within a test sample. LIBS were developed in the 1960's as an alternative method of creating plasmas instantly out of any material from which a characteristic spectrum can be obtained. A high-energy laser pulse is used to ablate the sample surface to form plasma. The plasma is formed from the vaporized sample surface material which is caused by three body collisions between photons, electrons and atoms, or molecules [24]. The ionized sample releases light in wavelengths characteristic to its component elements. This light is directed to a spectrometer where it is analyzed, and a plot of wavelength versus intensities can be obtained. Greater intensities of light can reflect

larger portions of the corresponding element in the sample, thus by this method elemental composition can be determined [24].

Configuration of LIBS

The various components of a Laser Induced Breakdown spectroscopy apparatus are described. A laser connected to a power supply provides pulses of high-powered laser light at regular intervals, which are directed at a point on the sample of unknown material placed in a designated holding chamber or device. This laser light is focused with a lens onto a small spot on the surface of the sample. The sample responds by emitting wavelengths of light as the ionized particles return to lower energy levels. This process, known as laser ablation, is covered in the following section. A series of lenses and mirrors direct this released light and directs it to the spectrometer, which filters this light and measures the intensity of individual wavelengths ⁽²⁵⁾. The spectrometer is controlled by a computer program that can set specific variables, such as the delay of data collection, which is discussed further under plasma cooling. Within the spectrometer, collected light is first passed through an entrance slit to obtain a single beam of light, which is then directed at a diffraction grating ⁽²⁵⁾. This grating diffracts each wavelength of light from the original beam at a different angle out of an exit slit to a sensor array, which measures the intensity of each wavelength and outputs digitized data [24]. A diagram of this process is illustrated in Figure 2. LIBS technology is proven to can identify elemental composition of a variety of sample types, and can be compact and suitable as a portable testing system [25], [26].

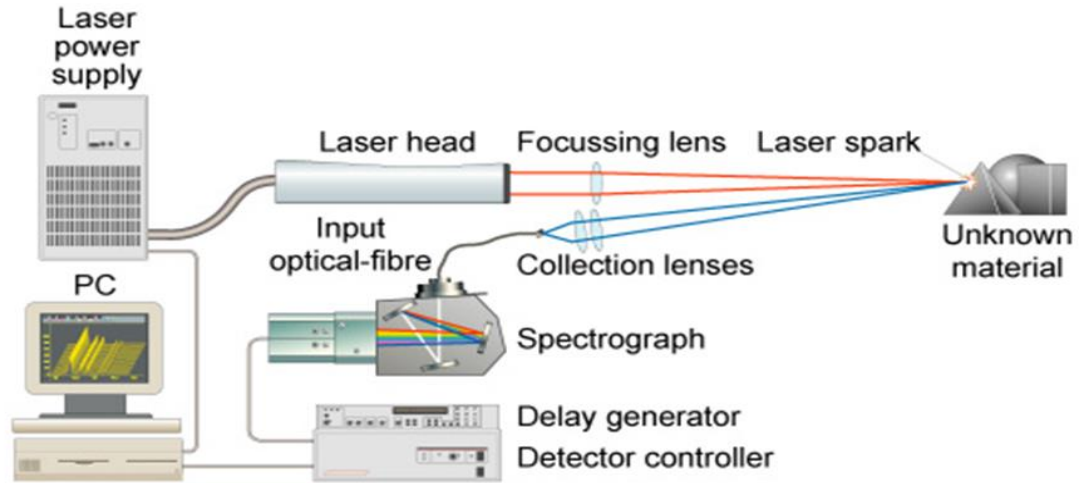


Figure 2. Overview of LIBS System [26].

Laser ablation. The LIBS method for analyzing the composition of a sample material is dependent on the characteristic light wavelengths that individual elements emit. In order to observe this characteristic, the sample must be charged with energy that it can then release in the form of visible light. This is done through laser ablation, in which a focused laser pulse ionizes the surface of the sample, creating a plume of material in the plasma state [27]. This process is represented in figure 3.

This process dissociates the inner-shell electrons from the atoms. As the outer-shell electrons lower their orbits, the ions in the plasma release light energy that is collected and analyzed. Heat energy is also released during this process, and the plasma rapidly cools and returns to a lower-energy state.

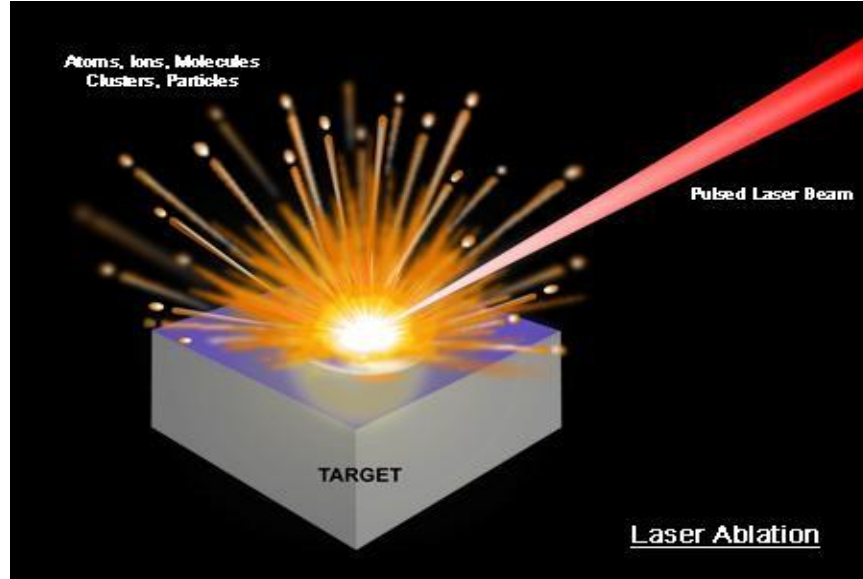


Figure 3. Laser Ablation [29].

Laser plasma. The main goal of LIBS technology is to create a thin plasma that completely and represent the sample elements and its concentrations. But this goal is usually approximate, depending on various conditions.

Plasma cooling. In the plasma, the sample particles are in an excited energy state. This plasma rapidly cools, and the ions return to a state of lower energy, releasing this energy partially in the form of light in the visible spectrum [24]. The power of the laser impacts the time it takes for this process to occur, as a higher power laser imparts more energy to the plasma and causes it to heat to a higher temperature. It will then require a longer period of time to cool. The ions release characteristic light wavelengths during this process that correspond to the elements present. In order to collect the highest intensity of this light possible for analysis, the spectrometer must be set to collect data on a specific delay with respect to the laser pulse. If the delay is too small, data collection will begin and end before most the light energy is released. If the delay is too long, the plasma will

have already cooled too much and the collected light intensity will be very low, reducing the definition of the resulting data. Optimal spectrometer delay also avoids blackbody radiation. Trial-and-error testing must be conducted to determine the optimal spectrometer delay, which is dependent on the power of the laser being used.

The laser emission depends on temperature and density of plasma. The plasma size, propagation speed and energy of the emitted light depends on the ambient gas into which the plasma expands. Gas pressure will influence plasma and the plasma energy distribution [60]. The three main features of plasma emitted light consisting of discrete lines, bands and an overlying continuum are wavelength, intensity, and shape. The feature depends on the atomic structure of the sample particles and their environment. Each atom of various element has different energy levels which determines its emission wavelengths. The wavelength line intensities depend on the amount of elements present in it.

Data Acquisition Time and Delay

The data acquisition time and delay depends on the elemental atoms excitation energy, laser energy and ambient pressures. The figure 4 shows the plasma initiated in air at 1 atm by a 5 to 10ns using a 1064-nm Nd: YAG laser. The time scale will change depending on longer (CO₂ laser) or much shorter (pico- or femtosecond lasers) laser pulses. Plasma lifetime varies proportionally with the ambient pressure since the trapping and recycling of absorbed energy in the plasma volume changes accordingly.

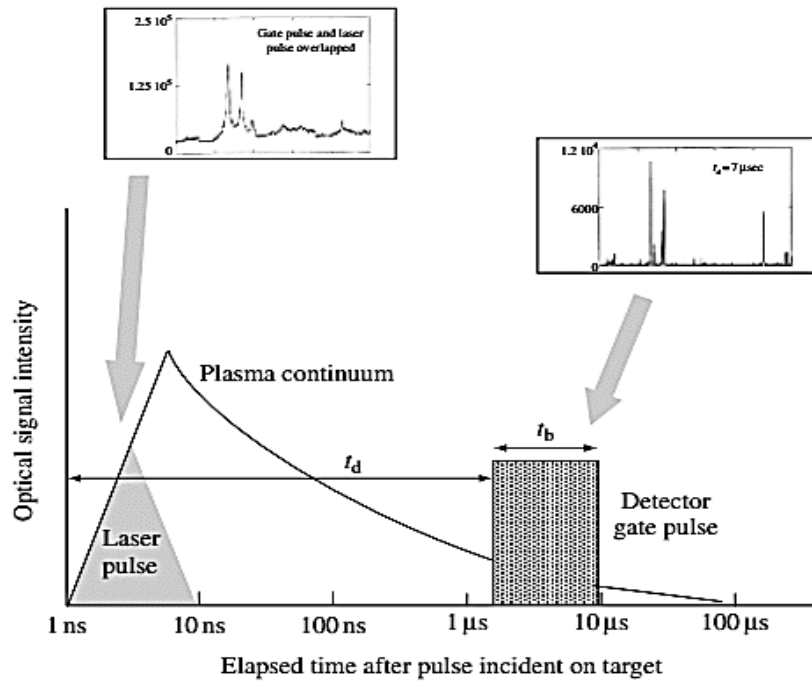


Figure 4. Temporal History of LIBS Plasma [25].

Application of LIBS

Metal industry applications. A LIBS sensor can be used to detect traces of explosives remotely [28], [29]. It is also used to detect the protective coating of metals in metallurgy [30], carbon content in molten steel [31], and quantify the minor constituents in molten aluminum alloys [32].

Biological applications. LIBS technology has been used for differentiating pathogens and viruses on substrates [33]. It is also used in determining the concentrations of hazardous materials in industrial waste water [34]. The industrial waste water has to undergo certain purification process to avoid contamination of soil and underground water. Hence, knowing the concentrations of toxic elements in waste water is useful and important.

Geologic applications. LIBS technology has been used as a portable tool for in situ characterizations of speleothems in Karstic caves [35]. It can also be used as a rapid analysis tool for petrochemical analysis of geological materials [36].

D-Cracking of aggregates by KSDOT. The Kansas Department of Transportation (KSDOT) used LIBS to analyze the likelihood of D-Cracking and to identify the source quarry of an aggregate sample. D-Cracking is a breakdown of aggregates, typically caused by freeze-thaw conditions, and the KSDOT uses two test methods; the KTMR-21 and KTMR-22 tests, as a criterion for determining an aggregate blend. To identify a source bed, a model was developed to classify an aggregate sample based on a branching algorithm which distinguishes an aggregate based on its spectrum meeting a unique criterion, or continuing to additional checks. A second model was generated to predict whether the aggregate would pass or fail the previously mentioned tests. The model predicted the result with perfect accuracy, indicating that a spectrum feature or features can be correlated to a susceptibility to D-Cracking [37].

To Acid Soluble Residue in Carbonate Aggregates by NY State DOT. The New York State Department of Transportation (NYSDOT) Materials Method 28 imposes limits on the use of carbonate aggregates in asphalt and concrete; namely that a carbonate aggregate must contain at least 20 Acid Insoluble Residue (AIR), i.e. silicates, or that the aggregate must be blended into a mix containing at least 20 percent silicates. One model was created and calibrated which predicts the AIR content of an aggregate sample, and another was created which determines the percent non-carbonated in an aggregate blend. Both models performed reasonably well, with the percent AIR model achieving very high

accuracy. It is worth noting however, that the NYSDOT models utilized large calibration and test samples [37].

Identifying Chert in aggregate by TXDOT. The Texas Department of Transportation (TXDOT) developed a three-model system to quantify the percent of reactive chert in an aggregate blend, classify the sample as highly reactive or not, and to identify a sample from a collection of several. Chert is a type of silica which is a major cause of Alkali Silica Reactive aggregates, which can experience damaging expansion within the concrete. The first model resulted in very high accuracy in quantifying chert content in the testing set. Similar to the KSDOT's model, the second model was developed by regressing samples against a yes/no or pass/fail system. While the model incorrectly classified some individual spectra, the model correctly classified aggregates when spectra were averaged. Individual sources of cherts were identified using a branching test model similar to the KSDOT, in which sources were differentiated based on a unique criterion [37].

Advantages of LIBS

LIBS technology needs little or no sample preparation. A fresh surface of the sample can be directly analyzed using a laser pulse. [42]

1. LIBS can be used for testing solids, liquids and gases. [42]
2. LIBS testing requires a very small amount of sample in milligrams, which can be a small part of a larger object. Hence, this method is a minimally destructive technique. [42]
3. Hardness of the material does not impact LIBS testing. [42]

Experimental Errors

In laser testing with LIBS, the following errors must be considered.

1. **Plasma Opacity:** When the emitted radiation escapes from the plasma without significant absorption or scattering, the plasma becomes optically thin. Optically thin plasma gives better LIBS results due to a greater amount of radiation escaping the plasma along the length of the plasma. Following ablation, plasma formed are not completely transparent, that will partially shield the light emitted by the particles, particularly towards the center of the plasma where the plasma is dense. This will skew data of some elements. However, the use of short laser pulses decreases the effect of non-transparent plasma [24].
2. **Atmospheric Plasma:** When LIBS is tested in atmospheric air, the laser pulse will cause plasma to form in the atmosphere immediately adjacent to where the laser hits the sample. The resulting atmospheric plasma, caused by the atmospheric elements, will show a high spike of nitrogen and oxygen in the LIBS spectrum. Testing in vacuum would eliminate the formation of atmospheric plasma. As it is more convenient to conduct on-site test on atmospheric conditions, this study is developed based on the results conducted in air. Calibrating the model in the same conditions where the sample is tested would somehow eliminate the effect of atmospheric plasma, and is more effective than the idea of testing in vacuum [24].
3. **Incomplete Vaporization:** Tendency of some elements to ablate more readily than other elements and the plasma opacity can cause in incomplete vaporization. Incomplete vaporization of material will produce as lower light intensities compared to completely vaporized samples. This can be mitigated either by the

use of a powdered sample, which will make the sample preparation more complex, or through the use of larger testing set size to limit the effect of non-vaporized particles [24].

4. **Baseline Light:** This is caused by background light on the sample chamber. This can be eliminated by testing in a dark chamber. Some baseline may continue to exist in the LIBS spectra due to the signal noise, however spectral filtration can remove the additional light [24].
5. **Accelerated ionization:** This is the increased tendency of the ionization of free electrons formed by the interaction of some particles, which can skew the distribution of various elements present in the sample. By using optimum delay and recording data at the end of the plasma glow, better results will be obtained [24].
6. **Stark broadening:** A reduction in effective resolution due to the local electric fields produced by the ionization of atoms in the plasma, which causes the electrons to fall into lower energy levels and vary the wavelength of light emitted by the particles. This causes the light emitted from certain species to have wider Gaussian distribution with respect to the wavelength. This distribution would likely overlap and result in the broadening of the spectrum baseline. This error can also be limited by collecting the light at the end of the plasma glow thereby eliminating the effect of the presence of electric fields in dense plasma [24].
7. **Chemical Matrix Effects:** Some elements ionize more quickly than others to produce more free electrons to recombine each other. This results in the higher concentration of neutral particles causing a non-uniform distribution of ions and

neutral particles. Studies show that interference of these ions can cause variation in the wavelength of the light produced by the original molecular composition [24].

8. **Surface Conditions:** The surface conditions of the material being tested can affect the data being collected. Surface dust or other contaminants present in the sample will represent the plasma formed and thus the light spectrum collected. It is determined that by firing an appropriate number of initial laser shots on a single point on the sample, the surface dust can be removed and the later laser shots can ablate the original molecular composition, which is collected as light spectrum. A proper testing procedure is developed in this study by neglecting the initial 200 laser shots and then collecting 100 subsequent laser shots [24].

Analysis of Aggregate Mineralogy by NJDOT

New Jersey Department of Transportation currently uses X-ray Fluorescence analysis and petrographic examination to fully characterize the aggregate source and quantify the mineral composition of aggregates. The petrographic examinations based on ASTM C-295 standards helps to quantify the amount of specific minerals like chert (microcrystalline quartz), pyrite and shale. It also helps to identify the expansive quartz that cause alkali-silica reactions in Portland Cement Concrete mixtures [38], [39]. X-Ray Fluorescence analysis method gives elemental composition of aggregate as described in the previous section.

Data Analysis Methods

Various data analysis methods used by previous application of LIBS technology in geological applications are described herein.

Artificial Neural Network (ANN). Artificial Neural Network is a mathematical modeling methodology capable of building nonlinear relationships between complicated inputs and outputs. It was developed by a physiologist, Frank Rosenblatt, inspired by the complicated neural networking of human brains [40].

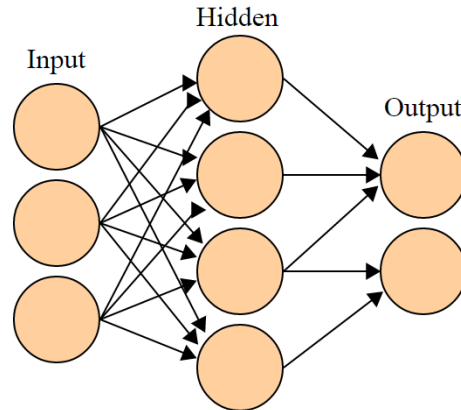


Figure 5. Artificial Neuron Network [43].

ANN uses a set of interconnected neurons to establish the inter-related layers or hidden layers between the inputs and outputs as shown in the figure. ANN is used in several applications in particular with LIBS technology such as material identification by NASA [41], rapid classification of archaeological ceramic [42] and polymer material identification [43]. This pattern recognition modelling was not considered for research as simpler methods were found to be effective.

Principal Component Analysis (PCA). Principal Component Analysis (PCA) is a statistical method similar to pattern recognition for identifying the variations among the input data and building a pattern or trend. PCA uses orthogonal transformation to convert original set of observations into a derived variable set, which are the linear combinations of original variables. These derived variables, which will be less than or equal to the

original number of data sets, are called principal components [44], [45]. PCA is used in chemometrics industry for the qualitative identification of ethanol and other products [46]. It is also used in waste recycling industry to broadly identify and classify various plastics by employing a Nd: YAG Laser and a spectrometer to obtain the characteristic spectrum of materials and using PCA and Mahalanobis distance (M) analysis to identify the type of plastic [47]

Partial Least Square Regression (PLSR) analysis. Partial Least Square Regression analysis is another statistical model, which is a combination of PCA and multiple regressions. It was developed by a Swedish Professor, Herman Wold [48]. When the input factors are large in number and are highly collinear, none of the standard regression functionalities will be suitable for analysis. PLSR is best used where the number of predictors is much higher than the number of observations [49]. PLS decomposes the X variables and Y labels into a product of orthogonal factors or score matrix and a loading matrix.

$$X = TP^T + E$$

$$Y = UQ^T + F$$

Where T is the X score matrix or the projections of X in new space of size $n \times l$ and U is the Y score matrix or the projections of Y in new space of size $n \times l$. T ($m \times l$) and U ($p \times l$) are the loading matrices of X ($n \times m$) and Y ($n \times p$) [49]. A function is then established in the original space capable of predicting Y's for any input X's.

PLSR increases the covariance between the orthogonal factors/ scores of X and Y such as T and U. A SIMPLS algorithm is used in this research where coefficients are determined by maximizing the covariance rather than minimizing the least squares as in

multi-linear regression function. PLSR has proven to be more a predictive oriented model than other regression functions [48]. PLSR is widely used in chemometrics as a basic tool to predict the chemical properties and biological activities based on its chemical structures [50]. Its ability to analyze large number of factors with noisy and highly collinear data gives its wide applications in industries.

PLSR is also used in spectral analysis of LIBS technology. Whang et.al used a multivariate dominant PLS model to determine the concentrations of Cu in brass alloys [51]. The characteristic light intensities obtained using LIBS depends on the elemental concentrations and the chemical interaction between the elements in the plasma. Since LIBS spectrum is highly sophisticated with uncontrollable experimental errors within the collected light intensities, its application is limited. Also, the light intensity peaks vary with experimental conditions; standard regression functions are incapable of handling LIBS spectrum. PLS-R due to its versatility to accommodate all these fluctuations has found to be the best predictive model for LIBS spectrum analysis.

The samples used in this research are largely heterogeneous rocks and hence to accommodate variations among the samples, PLS-R method is used to develop predictive models.

Chapter 3

Methodology

As discussed in Chapter 2, Laser Induced Breakdown Spectroscopy provides a unique spectrum for each aggregate sample provided, which is representative of its chemical composition. In this chapter, more details of the testing equipment and the operational procedure is provided. In addition, some of the data preprocessing techniques that can yield accurate mineralogical composition is also discussed.

Laboratory Setup

This setup uses a Quantel Ultra Laser, with a Nd³⁺ doped Yttrium Aluminum Garnet crystal gain medium (Nd: YAG), capable of emitting light with a wavelength of 1064 nm at a Pulse Repetition Frequency (PRF) of 10Hz. The pulsed laser operates in a Q-switch mode, in which an optical switch opens when the majority number of Neodymium ions are in higher excited energy states. Neodymium ions in various types of ionic crystals act as a laser gain medium. It emits 1064nm light from the atomic transition of Neodymium ions from higher excited state to the ground level after being pumped into excitation by an external trigger. This laser is built to withstand harsh environments. The energy of the laser is set to 100 mJ. A schematic diagram of the setup is shown in Figure 6.

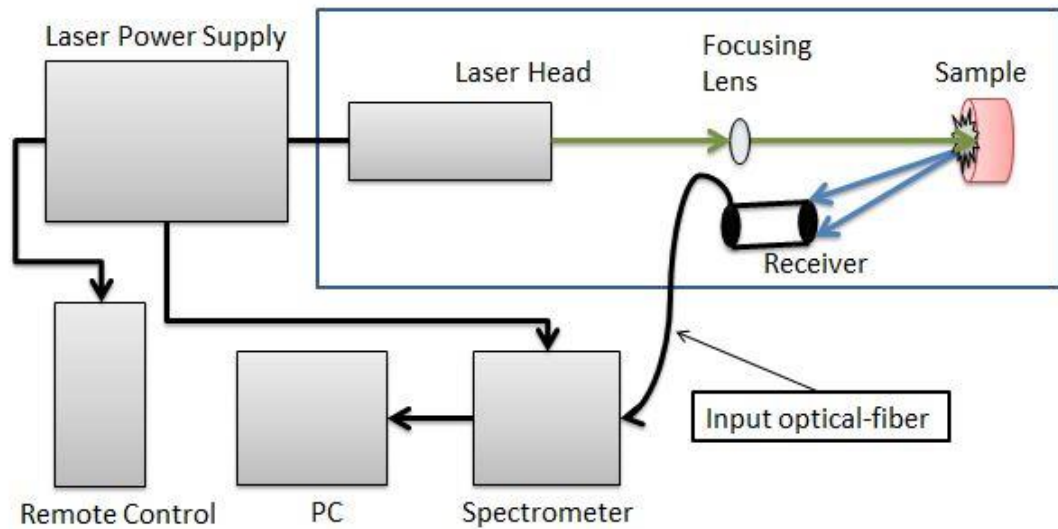
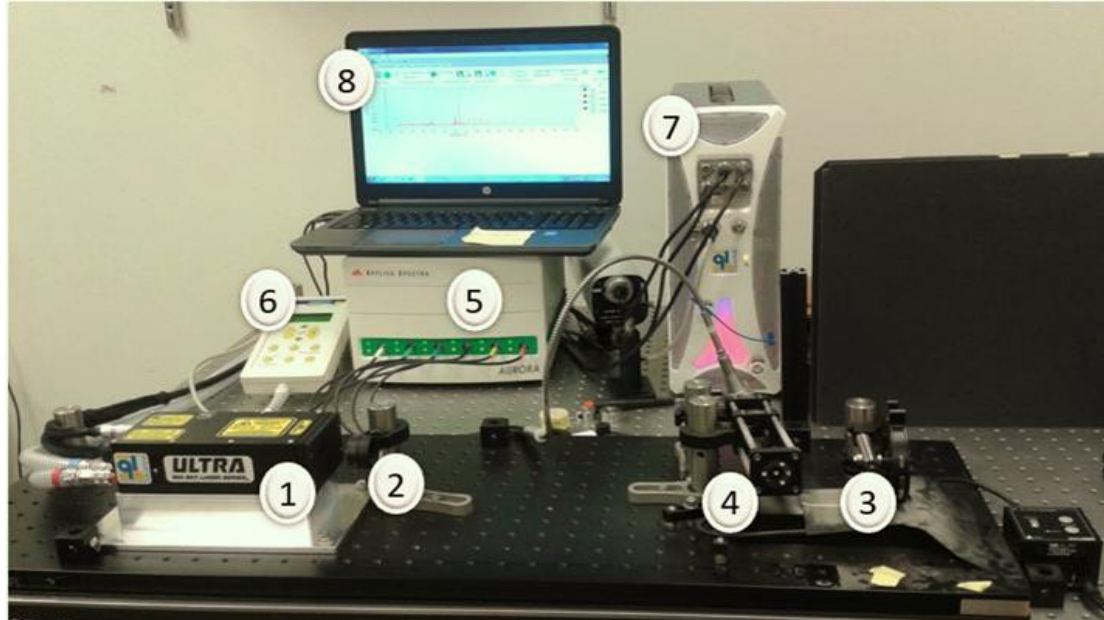


Figure 6. Flowchart of Laser Equipment.

The setup is arranged in a lightweight honeycomb breadboard of size 36 in. length and 12 in. width as shown in Figure 6 and the weight of the whole setup is reduced to 120 lbs. The laser head is aligned in line with the focusing lens and the sample so that maximum energy from the laser pulse is utilized to ablate the sample. A sample holder with a removable magnetic focus pointer is used to hold the sample in a vertical position in line with the laser beam. The position of the sample can be adjusted to correspond to the focal point of the beam by use of an automated translation stage. The sample is placed on an elevated holder, which prevents dust contamination during continuous testing. The light emitted from the sample is collected using an off-axis hyperbolic reflector and send to a spectrometer through fiber optic channels as shown as Label 4 in Figure 7.



- | | | |
|---------|----|-----------------------------|
| Labels: | 6. | Remote Control |
| 1. | 7. | Power Unit |
| 2. | 8. | Laptop with Aurora software |
| 3. | | |
| 4. | | |
| 5. | | |

Figure 7. Laboratory Setup.

The integrated spectrometer consists of 6 channels, with each channel corresponding to a specific spectral range. The resolution of the spectrum obtained is less than 0.1 nm for visible UV light and less than 0.11 nm for visible to near infrared. The timing generator is a fully integrated electronic pulse generator with independent external triggers such as a flashlamp and Q-switch. The optimal flashlamp Q-switch delay of 180 μ s is used. Too short or long delay between pump and Q-switch causes a decrease in the population of higher excited Neodymium ions caused by spontaneous emission resulting a loss in the output pulse energy. The spectrometer delay (aka acquisition delay) of 5 μ s is used to control the delay between the laser pulse and the onset of spectrometer data collection.

A dust control system has been implemented in this setup. The optics and sample holder are housed separately to prevent contamination by dust ablated from the sample. Two small holes are made in the chamber boxes to allow for the passage of the laser beam and to collect the light emitted by the sample. Two fans were fitted at the opposite end of the optics chamber to maintain airflow out of the box through the tiny holes. This prevents the dust particles from entering the chamber boxes through the holes. Heavy ablated particles will settle in the sample chamber. The sample chamber is cleaned regularly to prevent dust accumulation.

Field Setup

The field setup is assembled in a composite wooden crate to make it portable. The size of the portable equipment was 48 in X 24 in X 20 in and it weighs around 200 lbs. A power strip of 120 V is mounted on to the crate. This equipment is mounted on the back of a truck and can be transported to field sites for on-site testing.

Internal layout of components is designed and constructed using steel clamps to fix the components in position. The breadboard is placed on a vibration isolation pads and friction pads. This helps to minimize vibrations from being transmitted to any of the optics in the laser setup.

A layer of impact resistant foam is placed between the clamp and each component. This provides individual cushions for each component and it absorbs sudden impacts or shocks and protects the equipment from damage. This takes into consideration sudden movements caused by braking of the vehicle, potholes and vehicular accident damage. In addition, a set of bungee cords is used to secure the components to provide a layer of additional security. Figure 8 shows the final setup of portable equipment.



Figure 8. Portable LIBS Setup.

Data Acquisition and Testing Procedure

The following provides a step-by-step guide on how to operate the equipment and obtain testing data for analysis.

1. All operators should complete the safety training, the link for which is provided in the Appendix, before operating the equipment.
2. On the laser's control unit, switch the key to the ON position to turn on the laser unit. The laser's coolant must reach the operating temperature before the laser can be used. Figure 9 shows the laser power key switch and the coolant light when it is booted up.



Figure 9. Laser Power Switch.

3. Connect the spectrometer's power supply and ensure all connections and cables are in place.
4. Power up the laptop and connect the spectrometer to the laptop using the USB code. Ensure that all the green lights on the spectrometer are on. The green light indicates that the system is receiving power.
5. Start up the Data Analysis software and wait for the software to establish communication with the spectrometer. When the indicator light on the software turns green, the software and spectrometer are ready to be used. Figure 10 shows the green light when the spectrometer software, Aurora, is initialized.

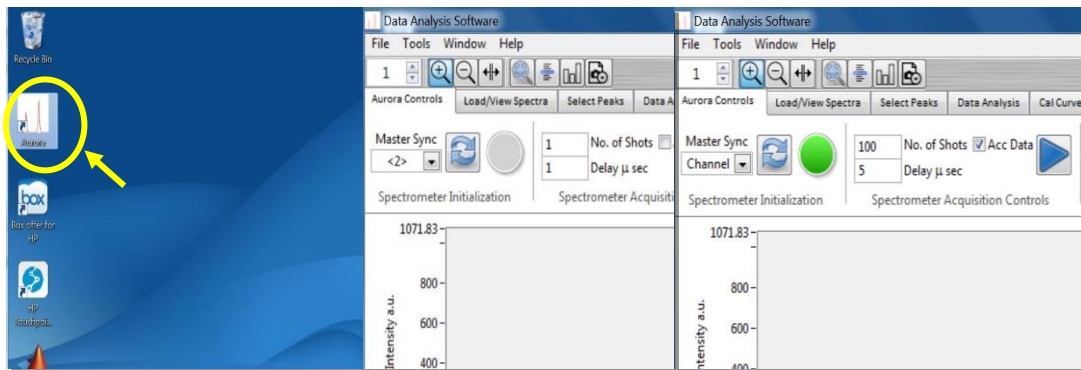


Figure 10. Aurora Software Initialization.

6. Check the front face of the spectrometer to ensure that the yellow lights are on for each channel. The yellow light indicates that it is ready to communicate with the software. Figure 11 shows the green and yellow lights on each 6 channels of spectrometer.



Figure 11. Spectrometer Lights.

7. Set all timing values in the software to their appropriate values. The flashlamp width, Q-switch width, and Q/S delay values should be set to 0 when the spectrometer is triggered externally. The integration time may be left at its default value. The spectrometer delay setting may be set as desired, but note that the

actual delay will be 1.3 μs greater than the setting. The spectrometer delay setting in this procedure is 5 μs giving a total delay of 6.3 μs . The number of shots to be collected can be set to some desired value. For the experiments performed thus far, 300 shots are fired, of which the first 200 are neglected and the data from the last 100 shots are collected.

8. Place the sample in the sample holder. Using the controller, the sample position is adjusted to the predetermined reference point that coincides with the laser focus.
9. Place the sample chamber box to prevent spectra disturbance due to ambient light.
10. To adjust the energy output of the laser, set the flashlamp-Q-switch delay time to 180 μs using the control pad. Increasing the delay time will decrease the energy output. A pulse energy of about 100 mJ is generally determined to be optimal for testing.
11. To activate the laser's flashlamp, press *Ready* and then *Start* on the top row of the control pad selection.
12. Before firing the laser, ensure that everyone present is wearing appropriate safety goggles and that any windows are covered. Observe any other safety measures as appropriate.
13. When ready to begin testing, press the Data Acquisition button on the spectrometer software (this button looks like a 'Play' symbol).
14. When ready to fire, press *Single Shot* to fire the laser pulse once. Continue firing laser pulses until the appropriate number of output spectra have been obtained.
15. The initial 200 shots are fired to remove any surface contaminants. These laser shots penetrate the sample and collect the light spectra for the next 100 shots.

16. After the appropriate number of shots has been fired, the software will automatically prompt the user to save the data. An appropriate naming convention should be selected for the data files. Previous test files have names which include the date, type of stone sample, and the number of the test.

To mitigate the effect of shot-to-shot variation on the data, the ‘Accumulate Data’ option in the software is checked, and 100 shots are collected per sample, per location. This results in a single output spectrum per location, which is the sum of the spectra for all 100 shots. In the event of a low-emission shot, this additive data collection ensures that the overall trends and peaks in the output data remain largely unaffected. To conduct these tests in a timely manner, the *continuous fire* option on the laser is utilized rather than the single shot option. It has been found that the software does not encounter issues when this option is utilized. A sample spectrum obtained after firing laser shots on rock is shown in Figure 12.

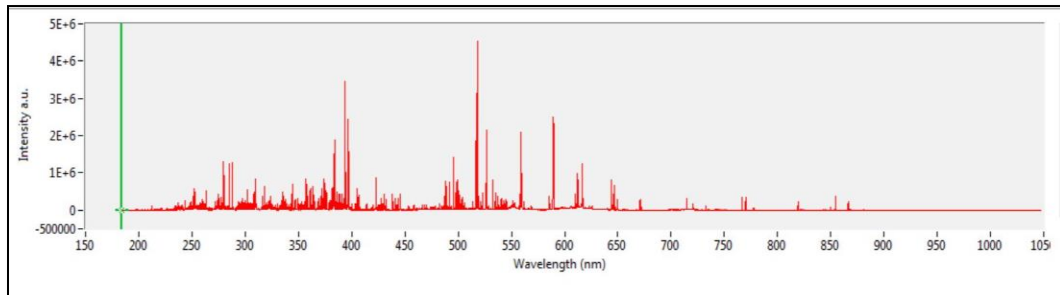


Figure 12. A Sample Spectrum.

Data Collection

Calibration set. A standard set of data is collected to calibrate the model using PLSR. 35 rock types are used for calibration. For each rock type, 10 rock samples are randomly selected. Each rock was tested at 5 different locations. 200 shots are fired and to ablate the sample of surface contaminants and stabilize the light intensity collected for

the next 100 shots. This calibration set consists of 35 rock types as mentioned earlier with 10 carbonates, 17 non-carbonates and 8 trap rocks as shown in Table 1.

Table 1

Aggregates Used for Calibration

	Name of the aggregate	Type of rock
1	Allen Myers Carbonate	Carbonate
2	Andreas Lehigh Carbonate	Carbonate
3	Bechtelsville Gneiss	Non-Carbonate
4	Braen Franklin Carbonate	Carbonate
5	Carbonate Dolomite	Carbonate
6	Dyer Quarry Diabase	Trap Rock
7	EI Hamburg Gneiss	Non-Carbonate
8	Eureka Milford Quartzite	Non-Carbonate
9	Fanwood Trap rock	Trap Rock
10	Hanson Glen Gneiss	Non-Carbonate
11	Kingston Argillite	Non-Carbonate
12	Kingston Trap Rock	Trap Rock
13	Lehigh Asphalt Carbonate	Carbonate
14	New Hope Crushed Stone Carbonate	Carbonate
15	OW Trap rock Orange Basalt	Trap Rock
16	Westfield Trap rock	Trap Rock
17	Pioneer Laflin Quartzite	Non-Carbonate

Table 1 (continued)

	Name of the aggregate	Type of rock
18	Temple Quartzite	Non-Carbonate
19	Atkinson Quartzite	Non-Carbonate
20	Woodboro Carbonate	Carbonate
21	Plumstead Argillite Belt	Non-Carbonate
22	Plumstead Argillite Stockpile	Non-Carbonate
23	Tilcon Diabase	Trap Rock
24	New hope Carbonate	Carbonate
25	Eastern Wantage Carbonate	Carbonate
26	Tilcon Oxford Carbonate	Carbonate
27	Plumstead Argillite Lockatong	Non-Carbonate
28	Tilcon Oxford Gneiss	Non-Carbonate
29	Eastern Hamburg Gneiss Losee	Non-Carbonate
30	Moores Argillite Trap rock Ind	Trap Rock
31	Bechtelsville Gneiss 15179	Non-Carbonate
32	Plumstead Argillite 15165	Non-Carbonate
33	Tarheel Quartzite	Non-Carbonate
34	Kingston Trap rock 15219	Trap Rock
35	Pyramid Gneiss	Non-Carbonate

Each spectrum collected is the accumulated light data of 100 shots which is averaged to minimize the shot to shot variations. For each rock type, 50 spectrums are collected to capture the heterogeneity in the rocks.

Testing set. A separate set of data is collected to validate the model and test the accuracy of each model. Initially, 5 samples were selected randomly and tested at 3 locations on each sample. Later, it was found that 30 data points were required to obtain a more representative dataset. Hence, the testing set size was increased to 10 samples and 3 locations each.

Spectrum Analysis

PLSR and various spectrum pre-processing techniques are used to analyze the data. The finalized methods are discussed below and all the models are compared with the Base Model.

Base Model. In the Base Model, the spectral amplitude is obtained by averaging 100 shots. Negative values which are considered signal noise are zeroed. Each spectrum is normalized by the total light intensity value, which is obtained by finding the area under the spectrum.

Y Scaling. While various techniques for optimizing the PLS model were studied, *Y-Scaling* between 0 and 1, described in Tuckers et al. (2010) was found to be the most effective. This method involves subtracting the minimum values for each compound and dividing by the range of values of that compound and thereby scaling the Y variables of each rock between 0 and 1. This is done to force the PLSR algorithm to consider the concentrations of all compounds equally. The Y-variables in this study are the XRF values of the 35 rocks that are provided by NJDOT.

Split Training strategy. Split Training is a strategy employed to reduce the range of values in the calibration set to two or more narrow sets of values. Tuckers et al. (2010) suggested that to make an ‘initial guess’, researchers should use the broad-based model and use a narrow more specialized model for classification of the rock. For the broad-based model (Base Model), 35 rocks types were used to make an initial guess of the composition. Then the rocks were classified based on the initial guess and put into corresponding more precise models such as carbonate, non-carbonate and trap rocks. Initially, the rocks were classified into two categories namely carbonates and non-carbonates, Non-carbonates included trap rocks. Later it was found to be more beneficial to classify the rocks into three categories.

Combination model. Various techniques are implemented with the combination of the Split Training strategy, however, Y-Scaling and the Split Training strategy is found to be the most effective combination with the pre-processing techniques employed with the Base Model.

Classification Methods for Split Training

Based on the initial guess of the composition of each rock type using the Base Model, the rocks were classified using various classification methods. These methods are described in the following sections.

One-Dimensional classification. The preliminary method used was the One-Dimensional Classification method. This method looks at the percentage composition of CaO of each rock as predicted by the Base Model. A threshold of 25% or below is used to classify the rock as a non-carbonate and anything above 25 is classified as a carbonate. This threshold is chosen based on the percentage of Calcium Oxide in XRF values for

each rock. Figure 13 shows the percent of CaO present in various rocks that are calibrated and the rock classification. The classification of the unknown sample is determined based on the initial guess. Since the initial guess is made using the Broad-Base Model of all the rocks, the predictions are not accurate to classify the rocks based on CaO percentage. Researchers studied various other classification methods and found useful.

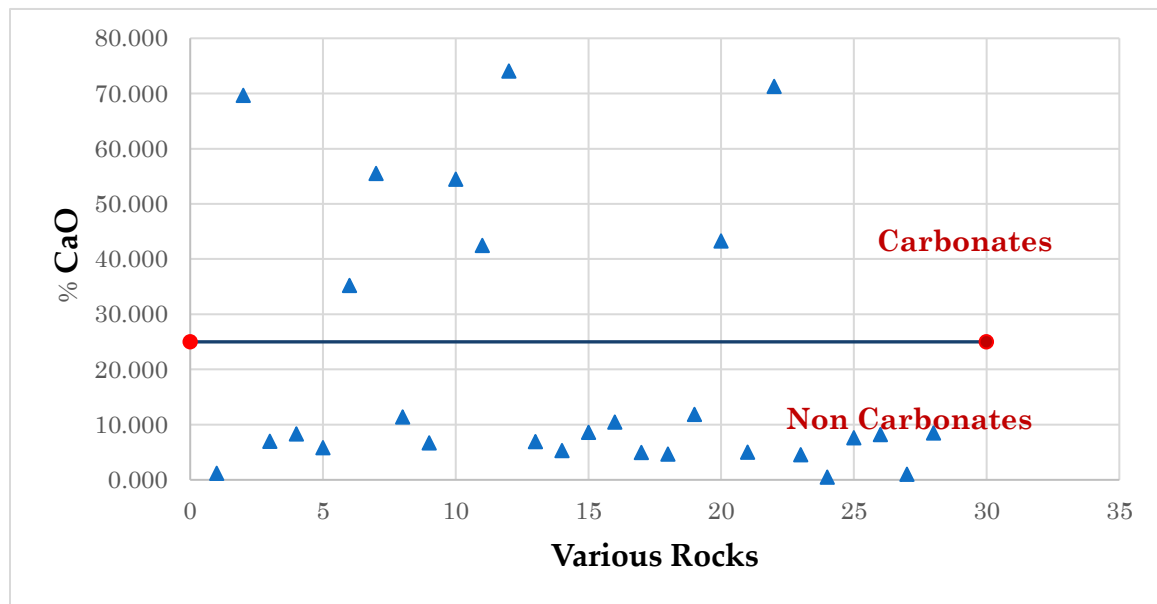


Figure 13. The Classification of Rocks Based on CaO%.

Two-Dimensional Line classification. This method is based on a graphical pattern observed when plotting the percent iron oxide (Fe_2O_3) and ratio of silica to calcium oxide (SiO_2/CaO). Figure 3.9 shows of the data for carbonates and non-carbonates. Carbonates with lower Fe_2O_3 and SiO_2/CaO values tended to move closer to zero and non-carbonates with higher Fe_2O_3 and SiO_2/CaO values tended to move away from both axes. A demarcation line separating carbonates and non-carbonates is found using trial and error maximizing the space between the threshold line and each data point. The equation of the line is:

$$Y + 0.286X - 5 = 0 \quad (3)$$

Where, X is the percentage of Fe_2O_3 and Y is the ratio of percentages of SiO_2 and CaO .

When $Y + 0.286X - 5$ is less than zero, it is classified as carbonate and when it is greater than zero, it is classified as a non-carbonate. Figure 14 shows the classification of rocks using a threshold line based on the XRF values of the known rocks.

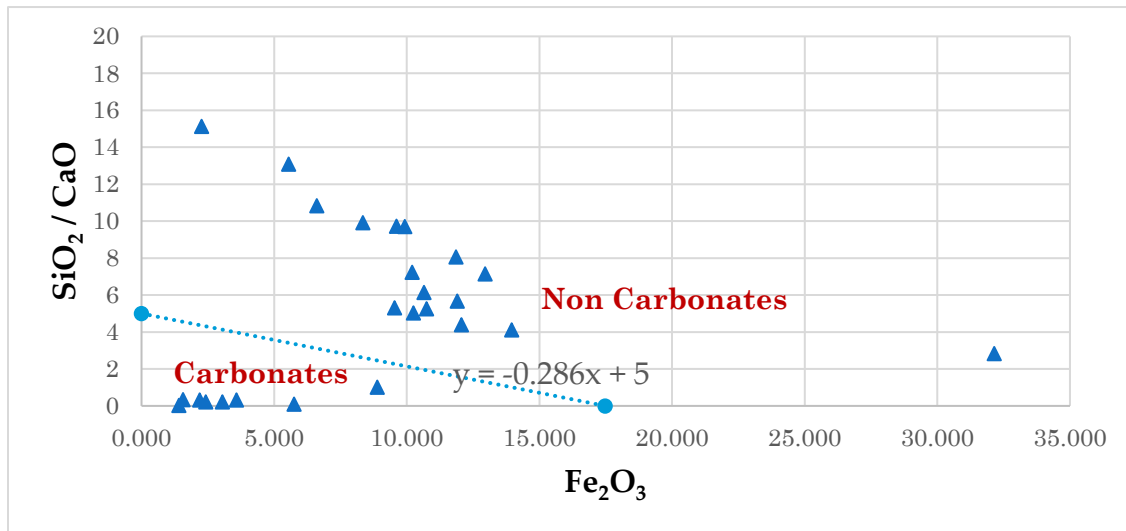


Figure 14. The Classification of Rocks Based on the Threshold Line.

Again, the classification system is based on the XRF values, however, the initial guesses are not accurate enough to classify certain rocks. This method fails to classify the Lehigh Asphalt carbonate and Trap Rocks; this method is not implemented.

Two-Dimensional Ratio classification. A Two-Dimensional Ratio classification method is implemented considering two compounds for classification. Carbonates tend to have higher percentages of Calcium Oxides (CaO) and non-carbonates tend to have higher percentages of SiO_2 . Hence a ratio of SiO_2 to CaO of is used to distinguish between carbonates and non-Carbonates. The threshold ratio is determined to be 3 as

shown in Figure 15. If the ratio is below 3, it is a Carbonate otherwise it is classified as a non-carbonate. This method proved versatile and is used for further analysis.

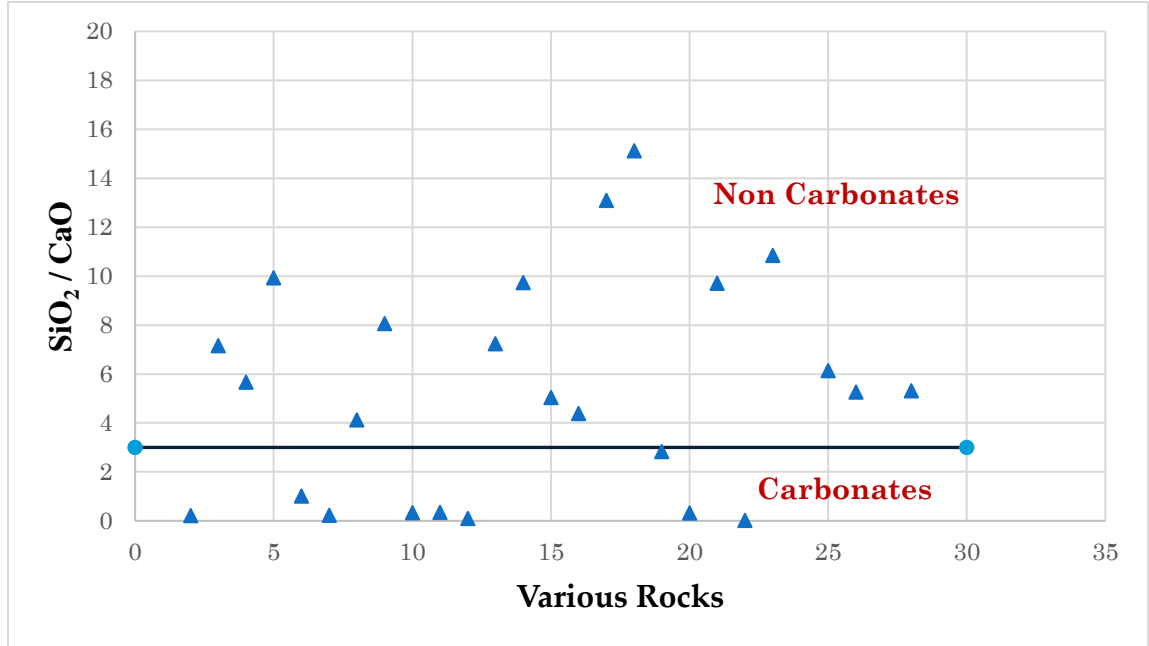


Figure 15. The Classification of Rocks Based on the Threshold Ratio of 3.

Three-Way Split classification. A Three-Way Split classification method is considered using three compounds silica (SiO₂), calcium oxide (CaO) and iron oxide (Fe₂O₃). The distinction between carbonates and non-carbonates is clearer when (SiO₂/CaO) ^2 * Fe₂O₃ is used and can be used to distinguish a special type of non-carbonate rocks called trap rocks. Hence the rocks are classified into 3 precise models Carbonates, Non-Carbonates and Trap Rocks. Figure 16 shows the classification of rocks into Carbonates, Trap Rocks and Non-Carbonates. Again, this classification threshold value is determined based on the XRF values of the known rocks as shown in figure. An initial guess is made using a Broad-Base Model to classify the unknown rock sample. Certain rocks failed to classify the rock correctly are either due to the contamination of

aggregates from the manufacturing source or may be due to the chemical composition changes due to the weathering of rocks.

$$\frac{SiO_2^2}{CaO} * Fe_2O_3 < 150 = \text{Carbonates} \quad (4)$$

$$150 < \frac{SiO_2^2}{CaO} * Fe_2O_3 < 500 = \text{Trap Rocks} \quad (5)$$

$$500 < \frac{SiO_2^2}{CaO} * Fe_2O_3 = \text{Non - Carbonates} \quad (6)$$

If the value of $(SiO_2/CaO)^2 * Fe_2O_3$ is less than 150, it is a Carbonate. If it is between 150 and 500, then it is a trap rock; otherwise it is a non-carbonate. The threshold values are chosen based on XRF values and further modified based on the initial guess values. Three-Way Split classification is found to be the best method for an accurate prediction of chemical composition.

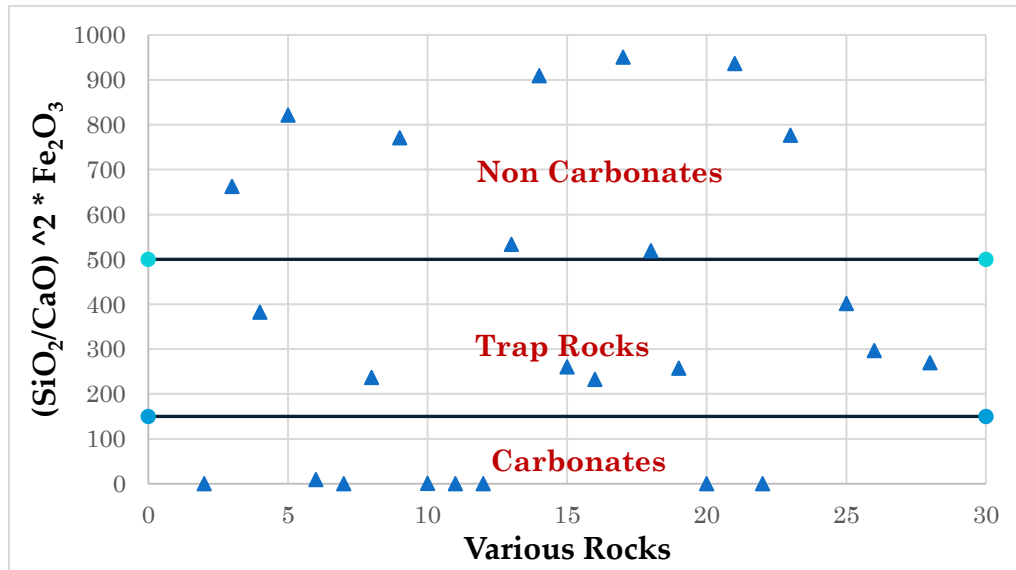


Figure 16. The Classification of Rocks Based on the Ratio Square Method.

Split Training in combination with Y-scaling using a Three-Way split is found to be the efficient model and is selected for final use. The results of various methods described herein this chapter is discussed in detail in chapter 4.

Chapter 4

Results and Discussions

This chapter discusses the results obtained from the mineralogical analyses using the laser induced breakdown spectroscopy approach and the various methods described in Chapter 3. Results are analyzed using statistical error analysis methods. The portable equipment developed is tested under various environmental conditions during field testing to ensure that accurate results can be obtained when outside temperature varies.

Spectrum Analysis Methods

Base Model. Before any alternative pre-processing options are explored, a Base Model is developed for comparison purposes. In the Base Model, the 100 shot total spectra are reduced in amplitude as previously described, negative values are removed through applying center clipping with a zero threshold, and spectra are normalized to the total light emission, as previously stated. Only the five most significant compounds are reported for visual clarity. Unless otherwise noted, each method below includes these steps.

Figures 17 through 21 shows the results for the Base Model. X-axis shows the predicted values or the LIBS spectrum analysis results. Y-axis shows the Known Values, in this case, the XRF values. A line is drawn which is the line of accuracy. If the data points come near to the line, then the results are more accurate. The data points of CaO and SiO₂ are closer to the line while the data points of the minor compounds Al₂O₃, Fe₂O₃ and MgO are scattered away from the line. The results of the Base Model provide an assurance that the Partial Least Square Regression analysis method for the quantitative

prediction of chemical composition will work. This encouraged the researchers to explore further spectrum analysis methods.

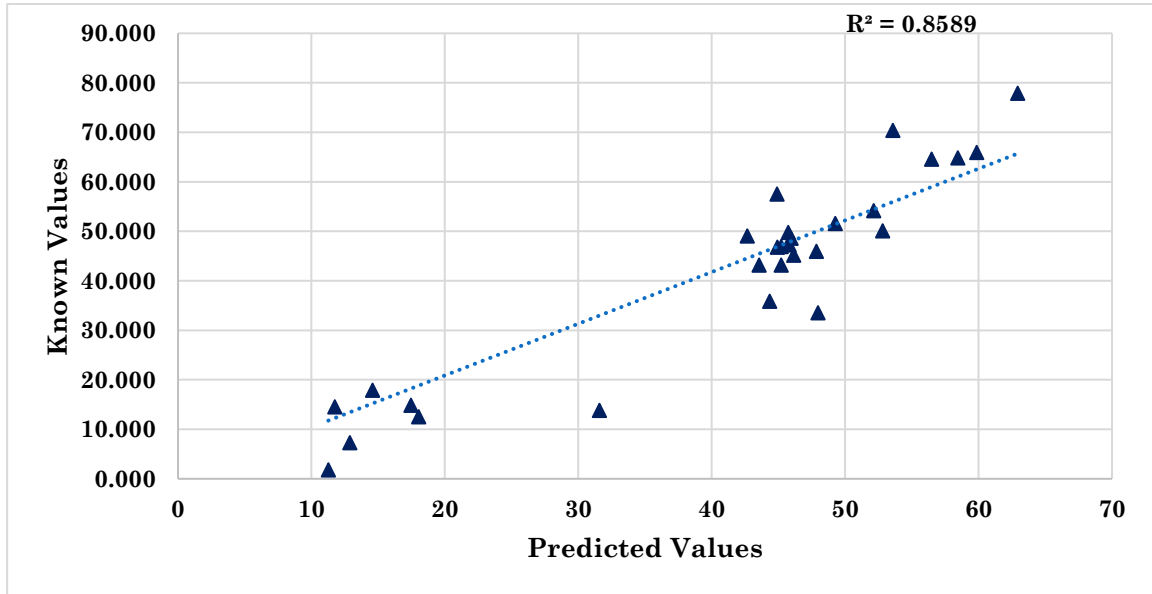


Figure 17. Results of SiO₂ of Base Model.

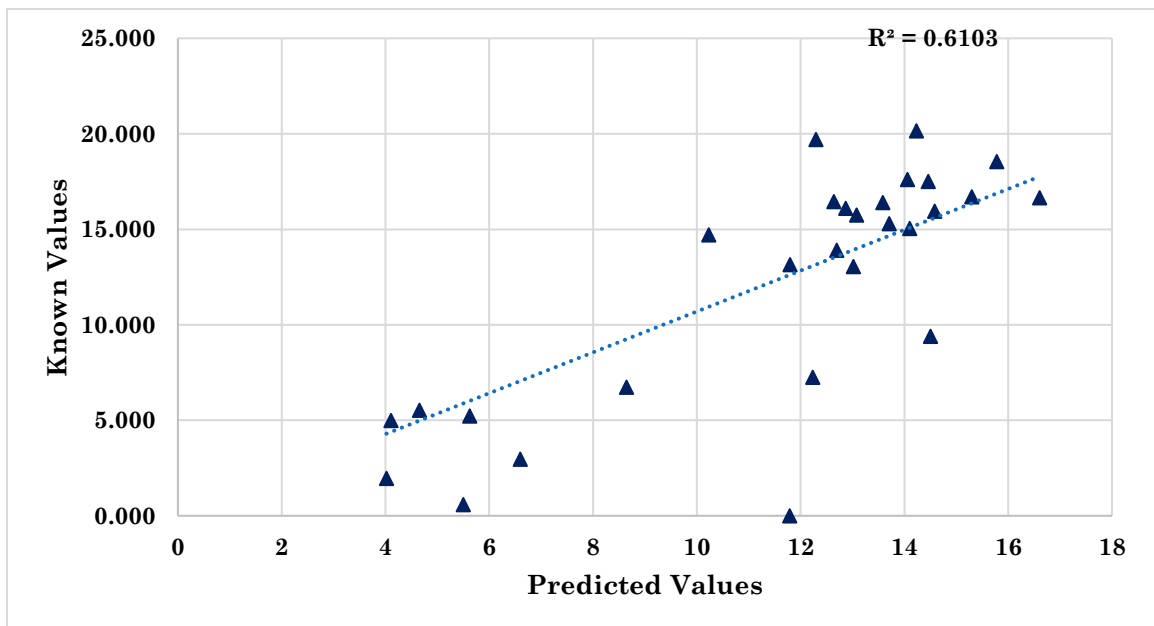


Figure 18. Results of Al₂O₃ of Base Model.

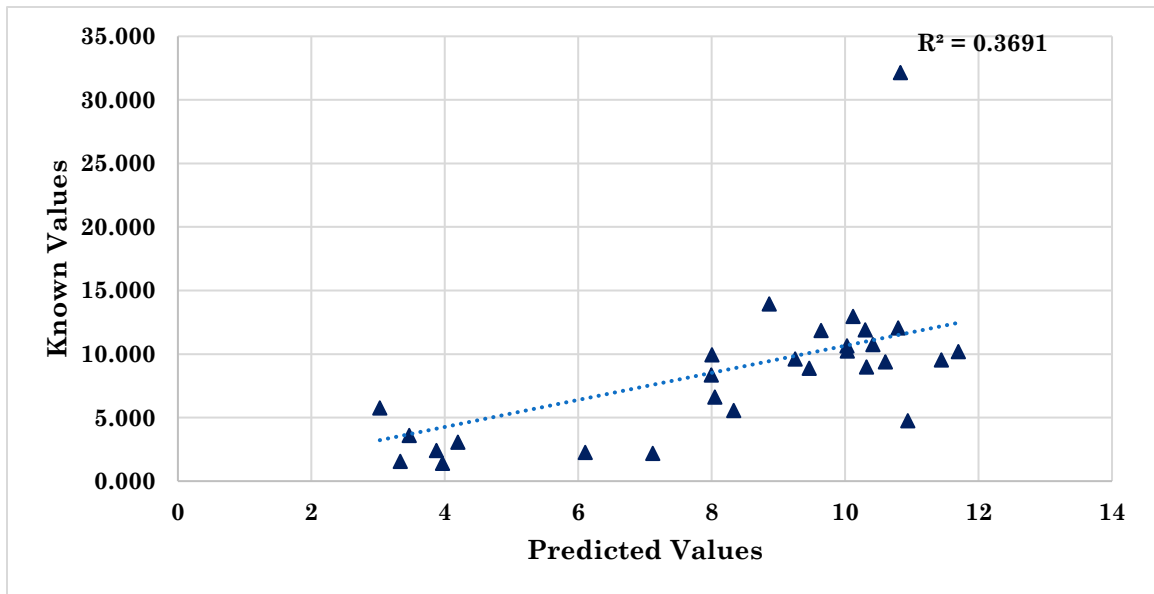


Figure 19. Results of Fe₂O₃ of Base Model.

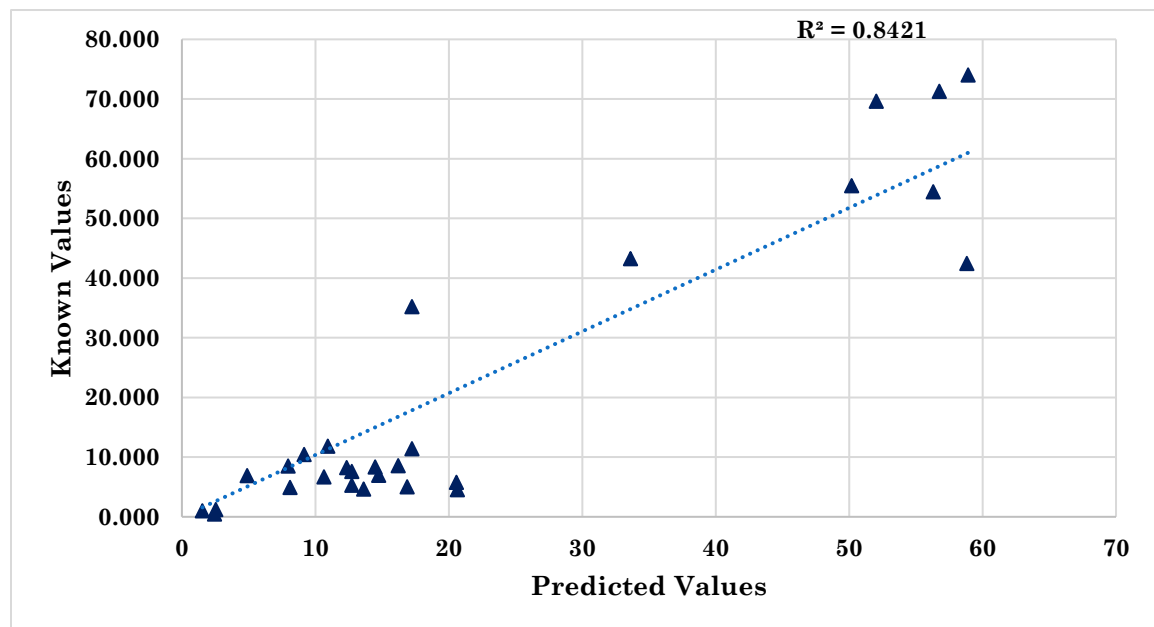


Figure 20. Results of CaO of Base Model.

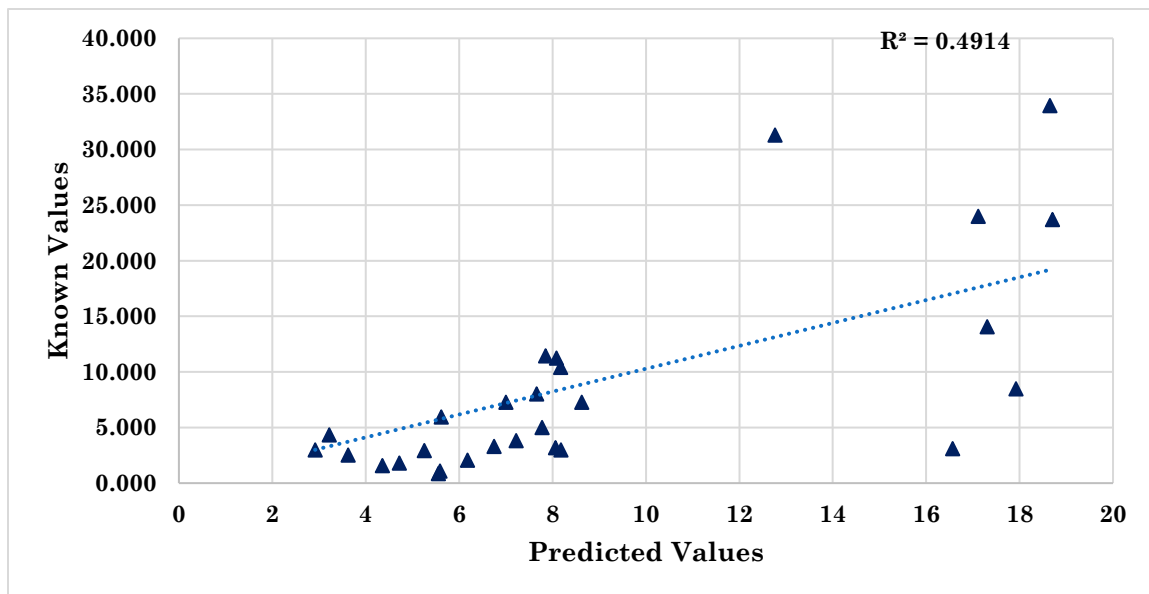


Figure 21. Results of MgO of Base Model.

Y Scaling. This method involves subtracting the minimum value of each compounds of all the aggregates' XRF values before dividing all remainders by the range for that compound, thereby, reducing each to a value between 0 and 1. The reverse adjustments must be applied to the predicted values to convert them to actual results. The results for each compound are shown in Figure 22 through 26. The accuracy of the results had improved compared to the base model shown in Figures 17 through 21. The R square values for the Y Scaling model remains more or less the same as the Base Model with a small improvement in the minor compounds Al_2O_3 , Fe_2O_3 and MgO. The data points of these minor compounds are slightly closer to the line compared to Base Model. Y Scaling prioritizes all compounds equally and therefore improves accuracy of the results.

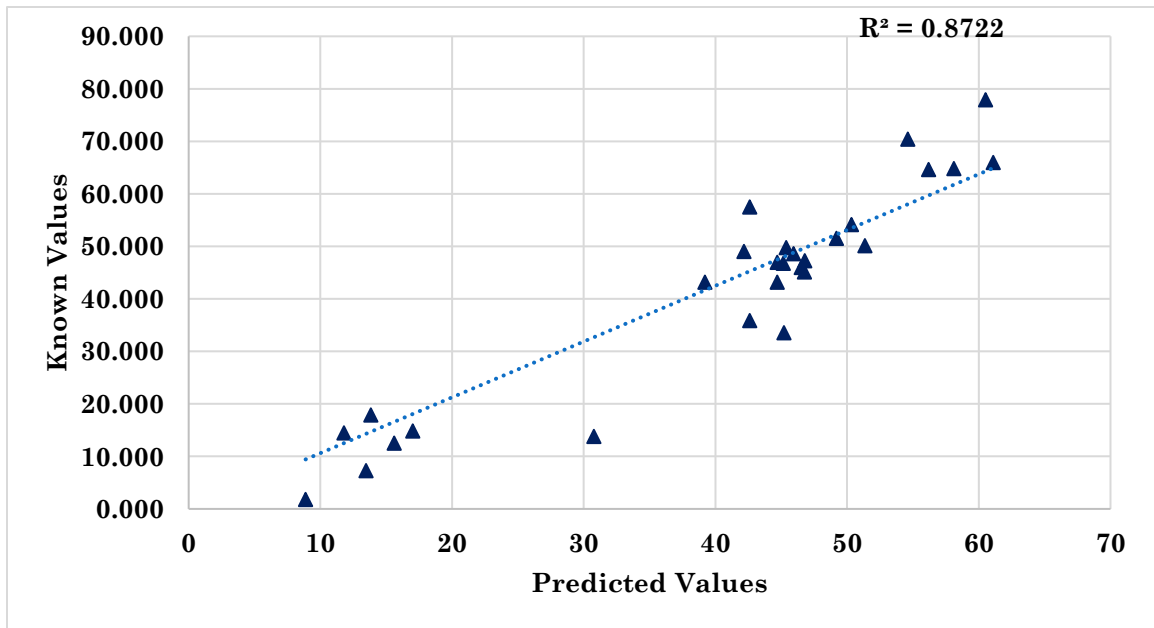


Figure 22. Results of SiO₂ of Y Scaling.

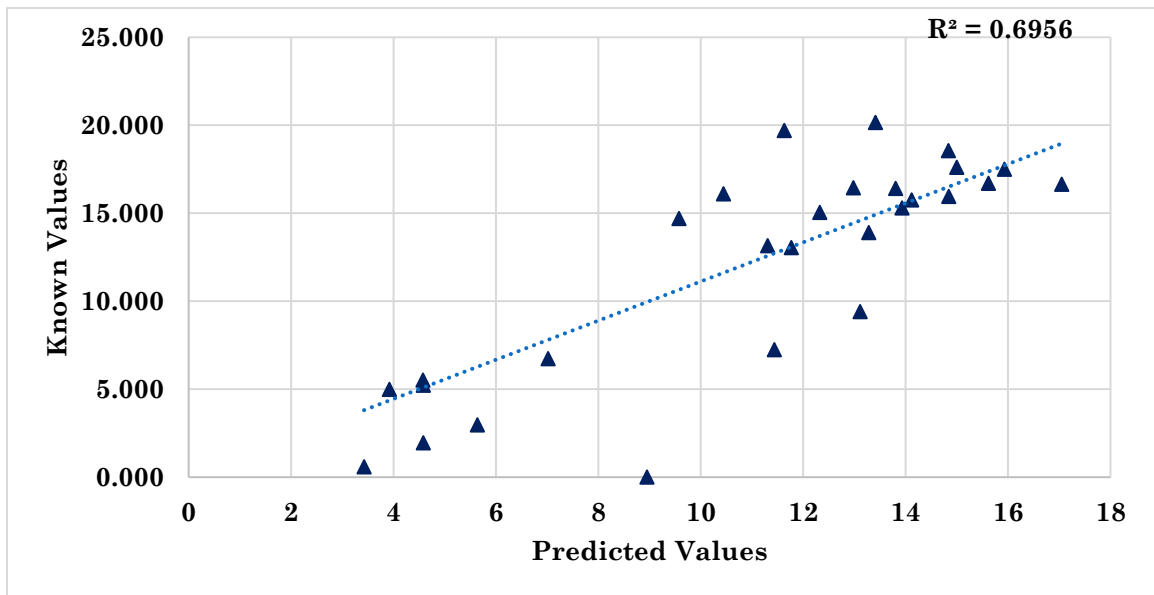


Figure 23. Results of Al₂O₃ of Y Scaling.

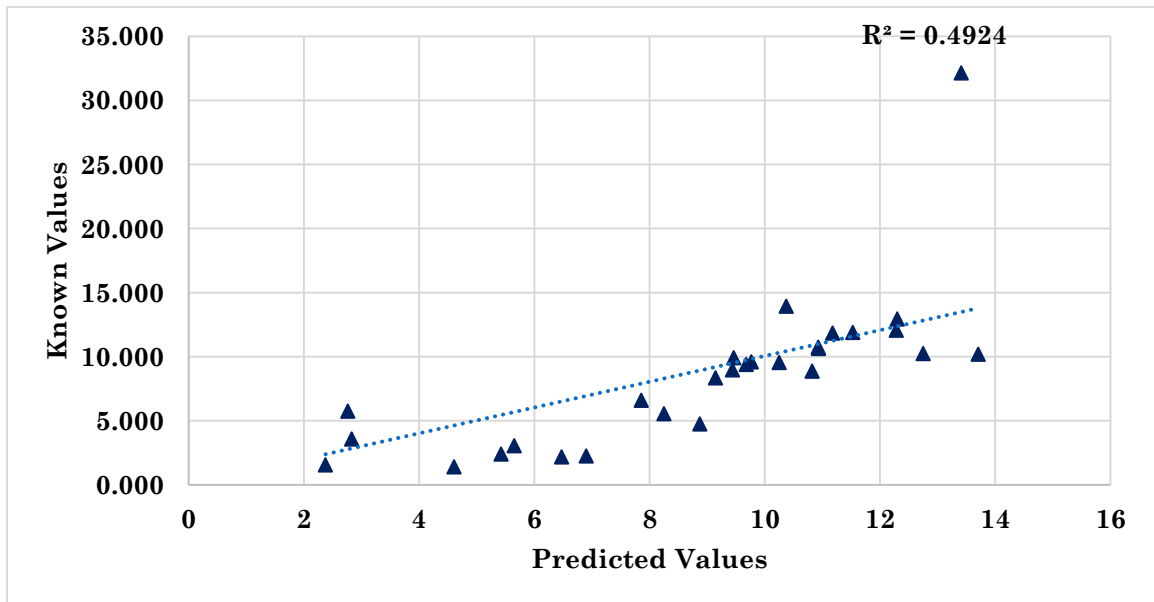


Figure 24. Results of Fe₂O₃ of Y Scaling.

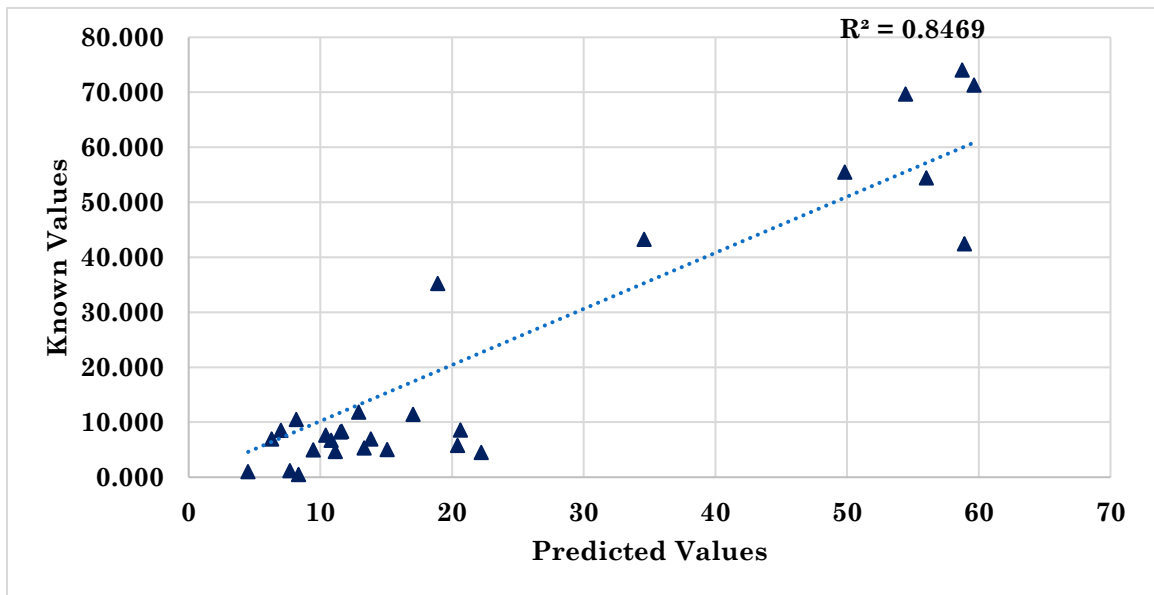


Figure 25. Results of CaO of Y Scaling.

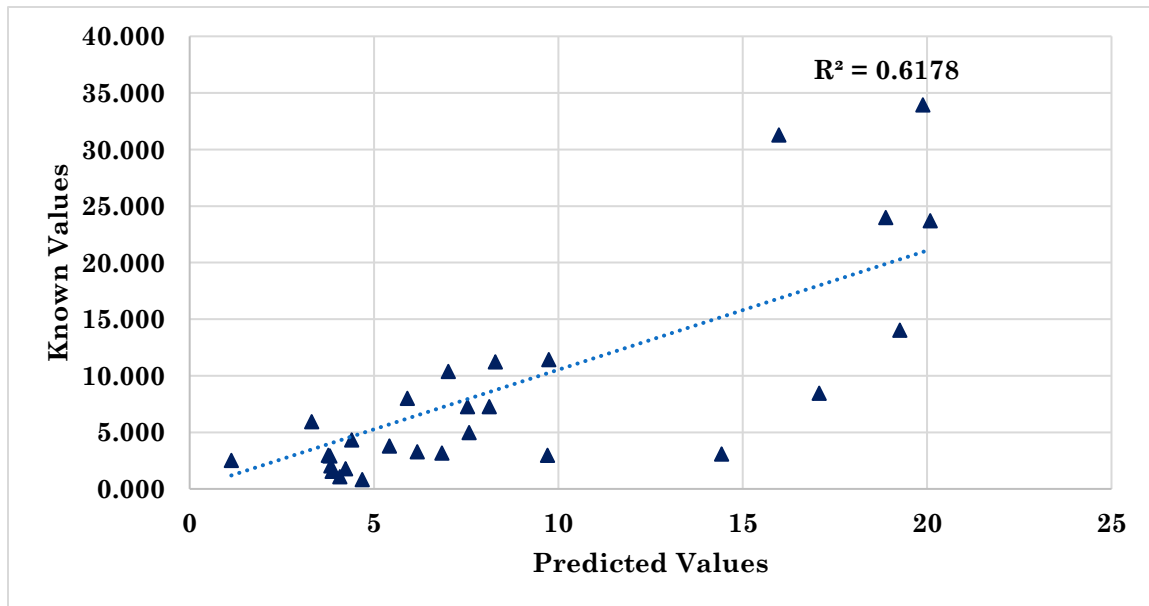


Figure 26. Results of MgO of Y Scaling.

Split Training. Split Training is a strategy used to make an ‘initial guess’ using a broad Base Model and then directing the aggregates into a more specialized model for more precise predictions. In this case, aggregates are classified into carbonates or non-carbonates based on the percentage of CaO in the initial guess of the rock. This strategy is applied along with the Base Model. Figure 27 through 31 shows the results for the model along with the stone’s broad classification; carbonate or non-carbonate. This strategy improved the accuracy of prediction over the Base Model and Y Scaling model as evidenced by the improvement in the R^2 value obtained for each of the five principal chemical constituents.

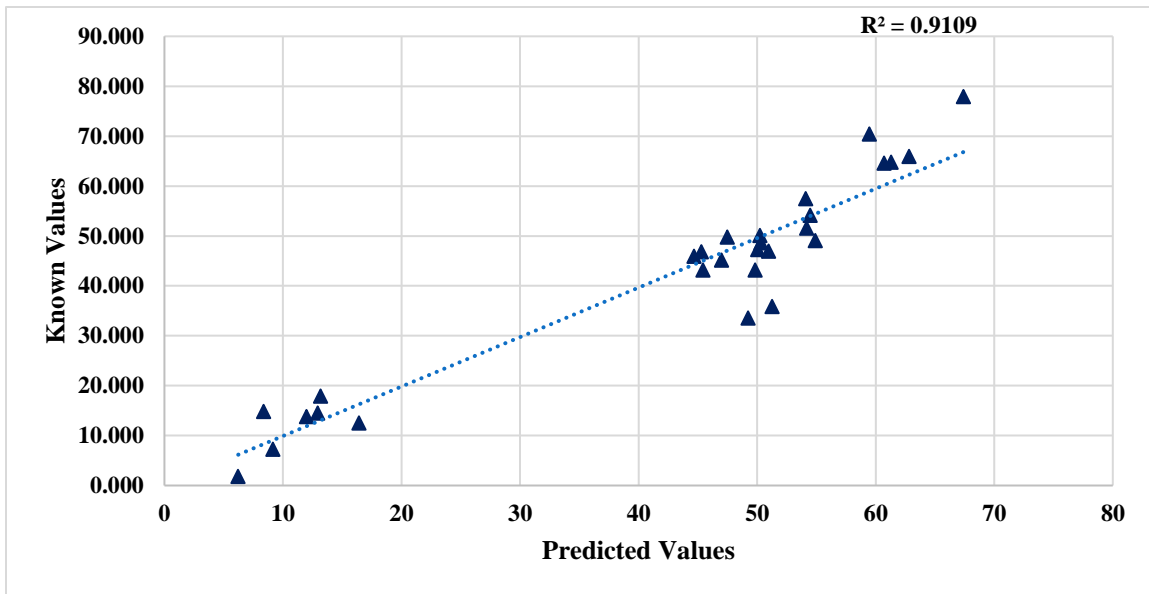


Figure 27. Results of SiO₂ of Split Training.

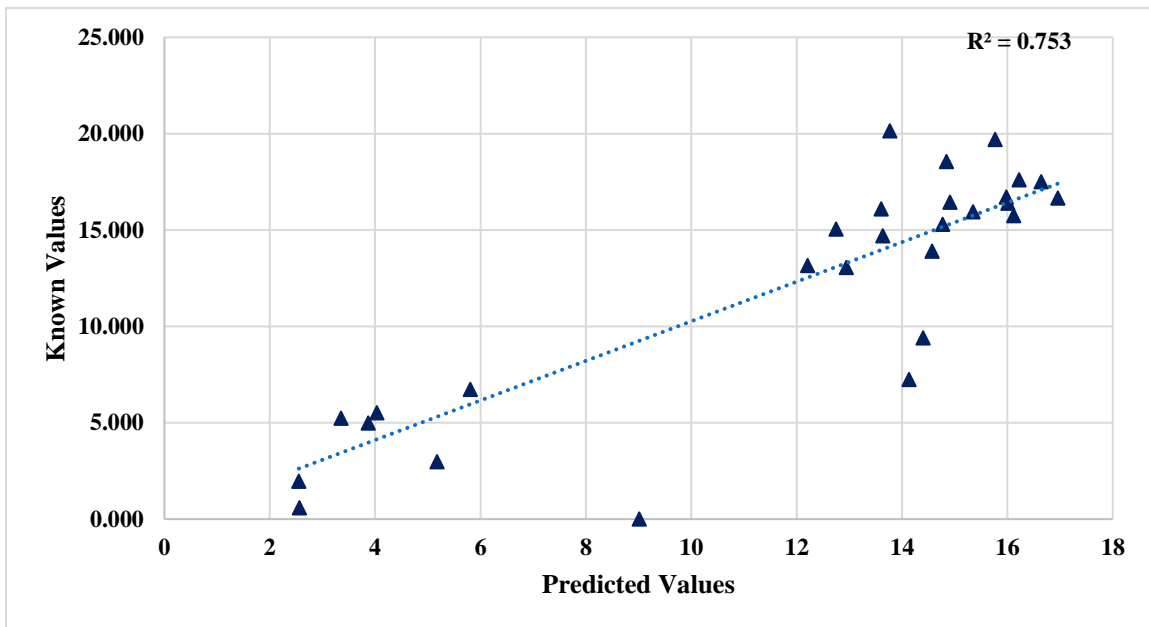


Figure 28. Results of Al₂O₃ of Split Training.

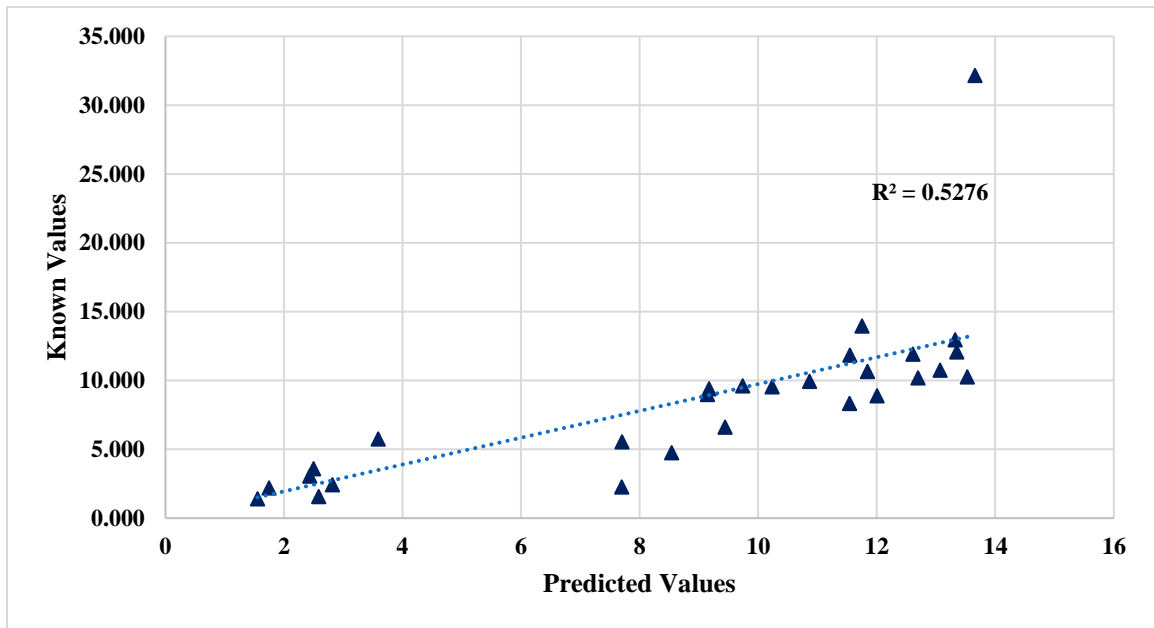


Figure 29. Results of Fe₂O₃ of Split Training.

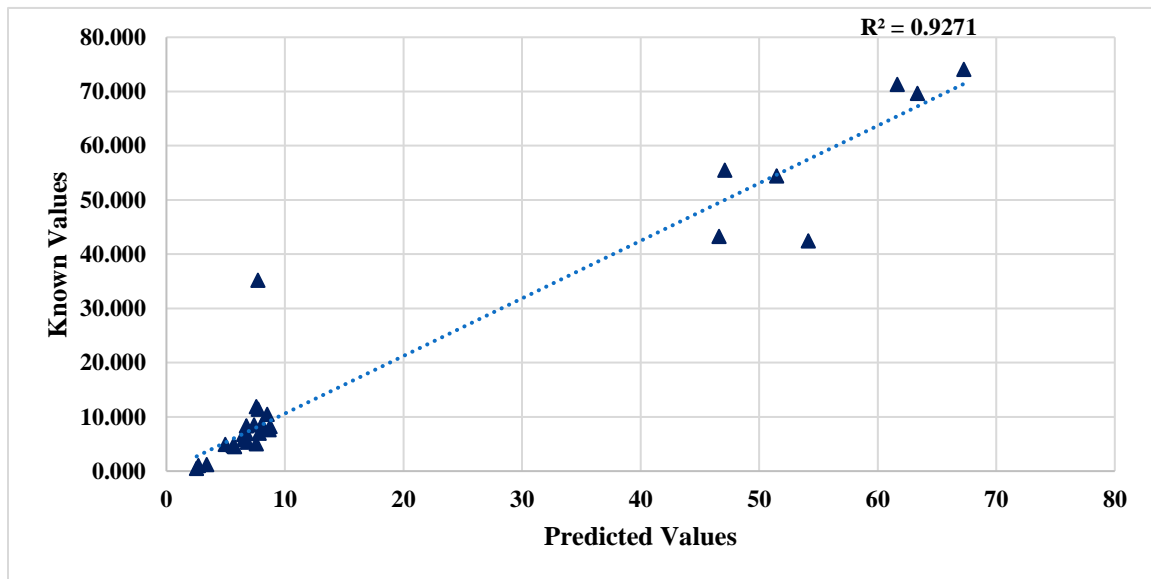


Figure 30. Results of CaO of Split Training.

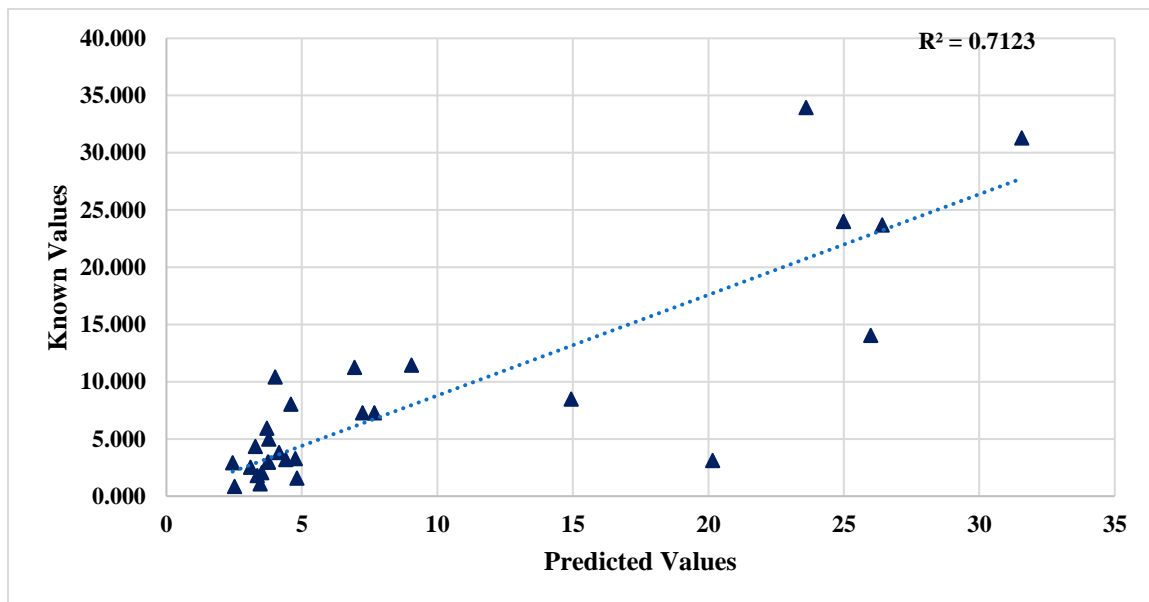


Figure 31. Results of MgO of Split Training.

Split Training and Y Scaling. The results of combining the Split Training model and Y Scaling are shown in Figures 32 through 36. Better results are produced through the use of Y Scaling and Split Training. Split Training combined with Y Scaling 0:1 produced accurate results and is selected as the analyses method for this research. This method uses a one-dimensional classification method based on the percentage of CaO. The predicted values are closer to the XRF values and hence it better fits the line of accuracy. SiO₂ and CaO points are closer to the line of accuracy, yet other compounds have to be improved. Although, this was successful for several aggregates, Lehigh Asphalt Carbonate, is found to be classified incorrectly. Thus, various classification methods were further explored to improve classification of the rocks.

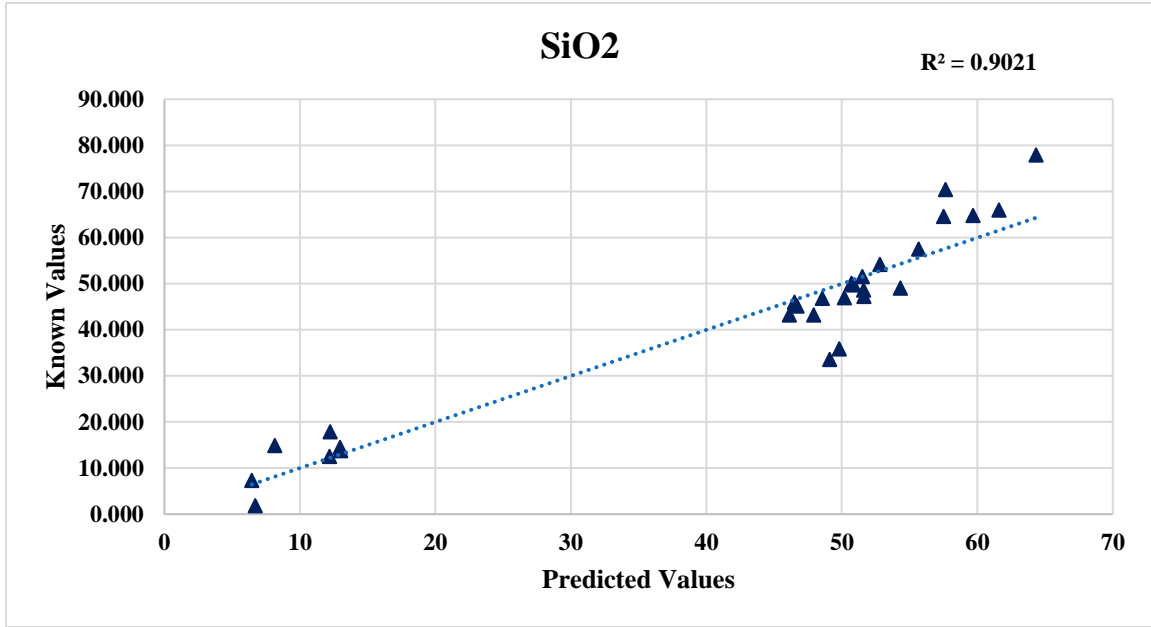


Figure 32. Results of SiO₂ of Split-Y Scaling.

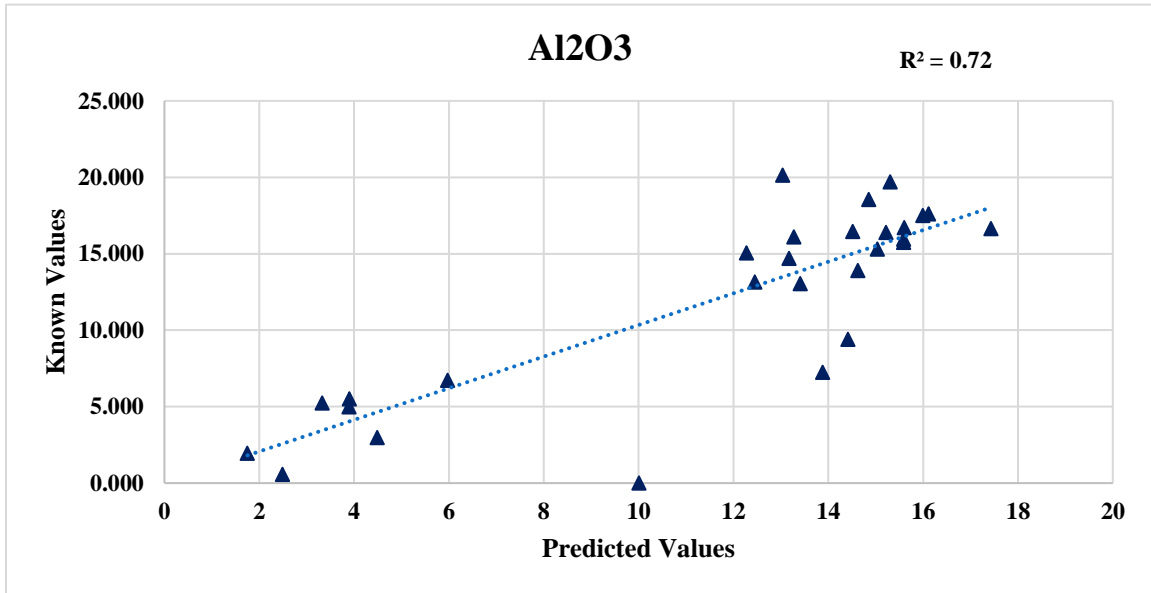


Figure 33. Results of Al₂O₃ of Split-Y Scaling.

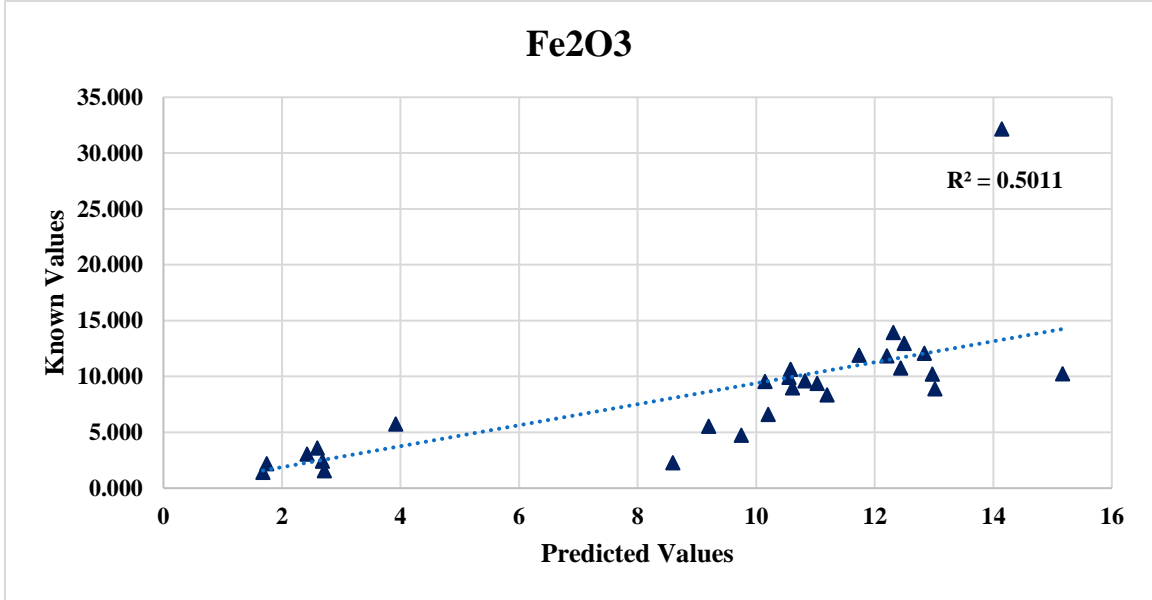


Figure 34. Results of Fe₂O₃ of Split-Y Scaling.

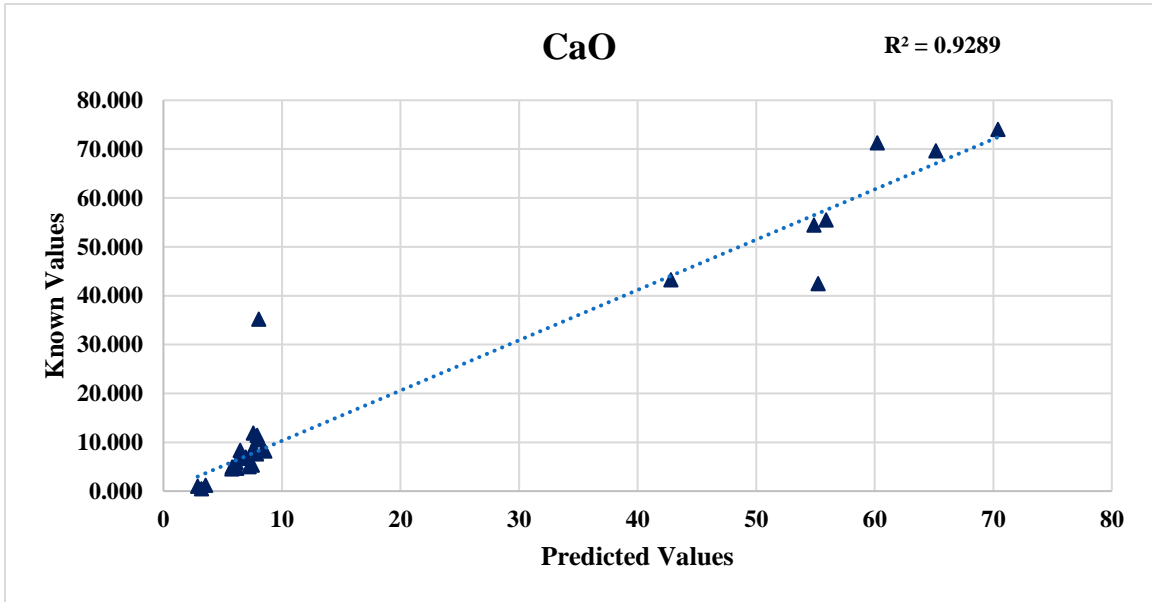


Figure 35. Results of CaO of Split-Y Scaling.

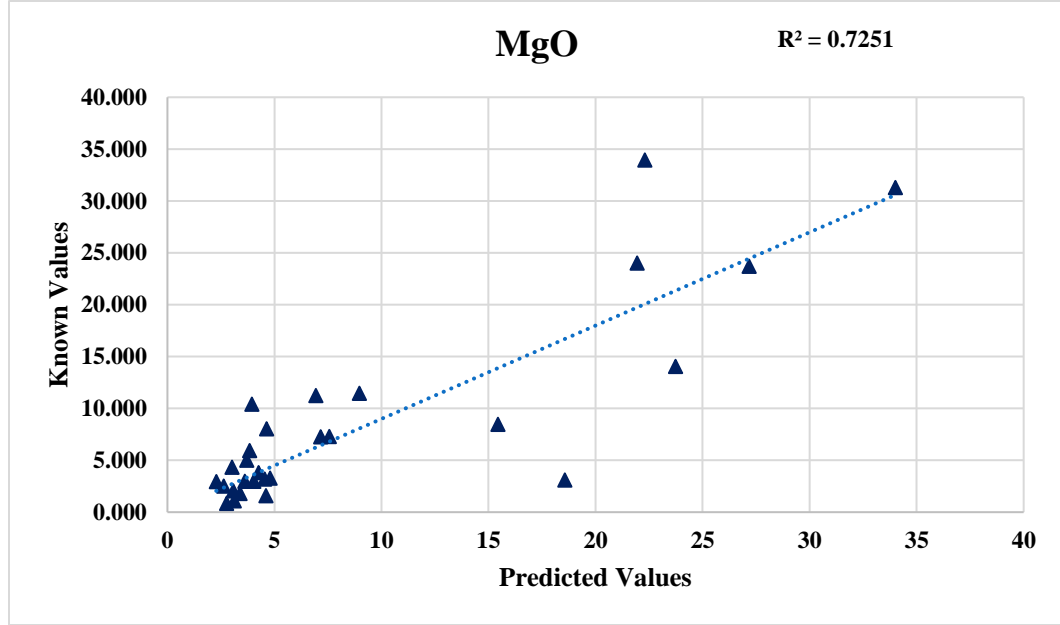


Figure 36. Results of MgO of Split-Y Scaling.

Classification Methods for Split Training

One-Dimensional classification. One-Dimensional classification is based on the percentage of CaO in the initial guess. Figure 37 through 41 shows the results utilizing the One-Dimensional classification method. The initial prediction values of CaO percentage of Andreas Lehigh Carbonate is 16.83% and of Lehigh Asphalt Carbonate is 11.12% which are less than the threshold ratio (25%) as shown in Table 2. Because of the low CaO content in Andreas Lehigh Carbonate and Lehigh Asphalt Carbonate, these rocks are not identified as Carbonates. Further study on classification system resolved this problem of classifying the low Calcium Oxide carbonates into right model.

Table 2

Outliers of One Dimensional Classification

Outlier	Threshold Value	Classified as:
Lehigh Asphalt Carbonate	11.12	Non-Carbonate
Andreas Lehigh Carbonate	16.83	Non-Carbonate

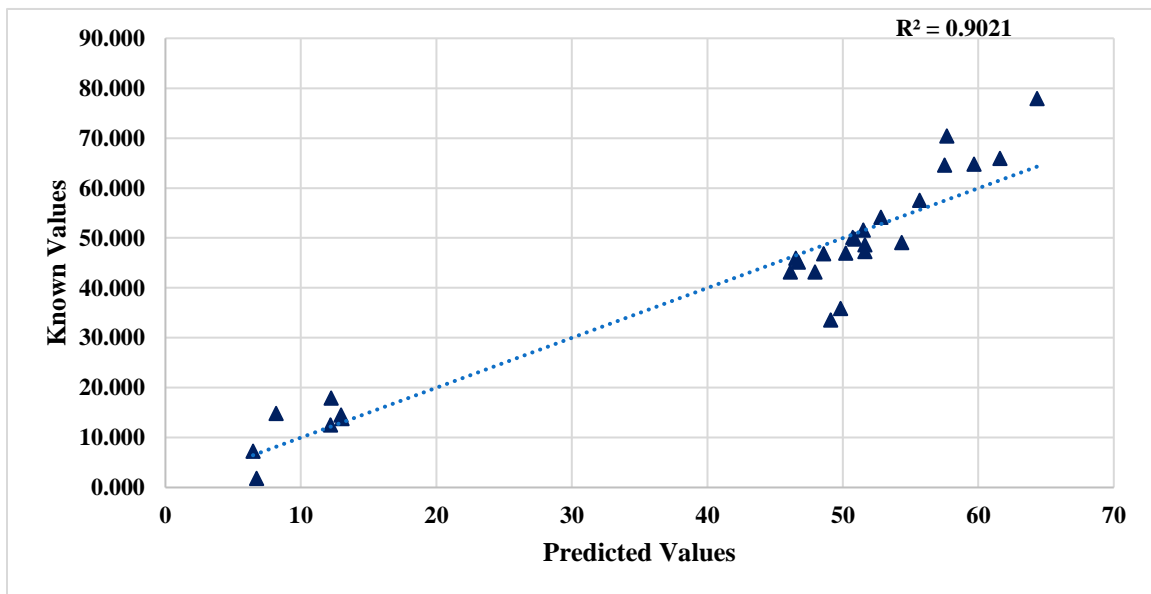


Figure 37. Results of SiO₂ Using Calcium Oxide Classification.

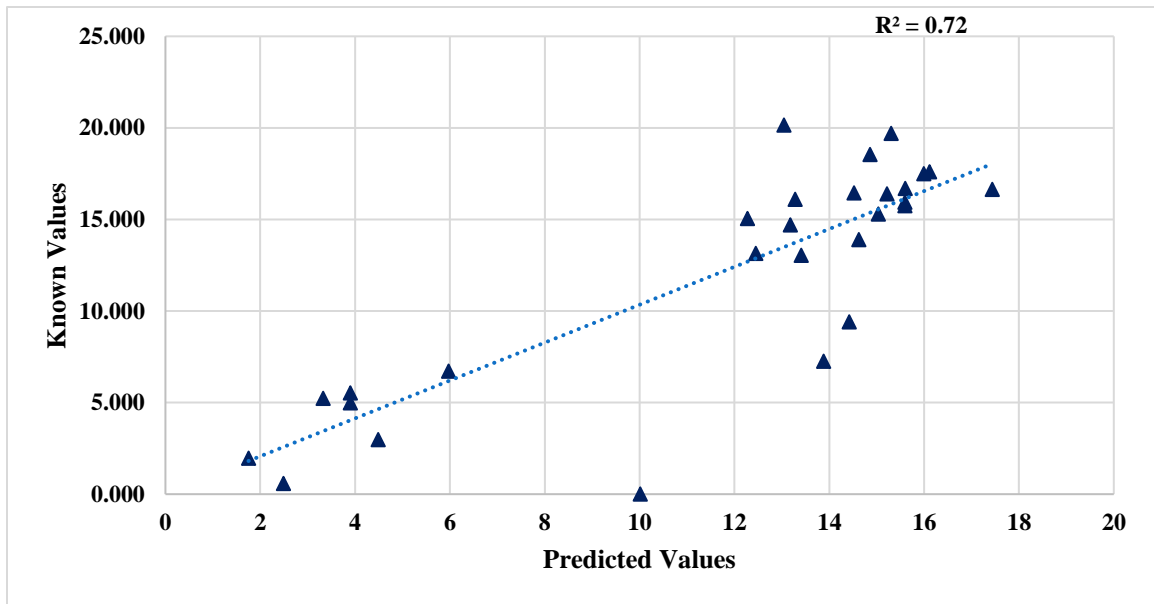


Figure 38. Results of Al₂O₃ Using Calcium Oxide Classification.

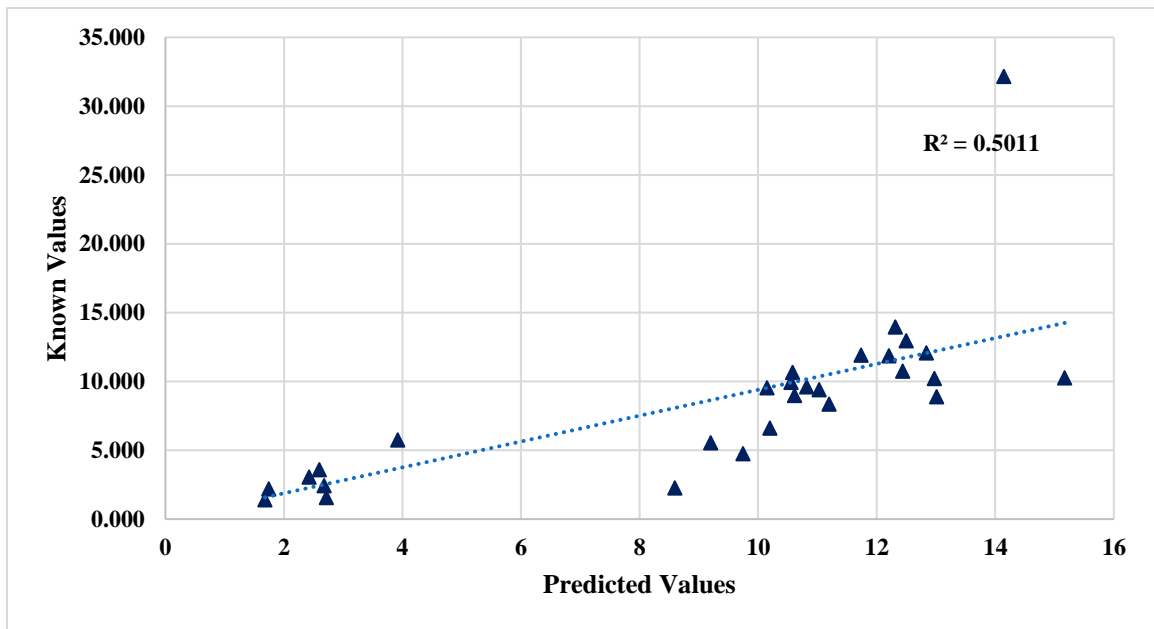


Figure 39. Results of Fe₂O₃ Using Calcium Oxide Classification.

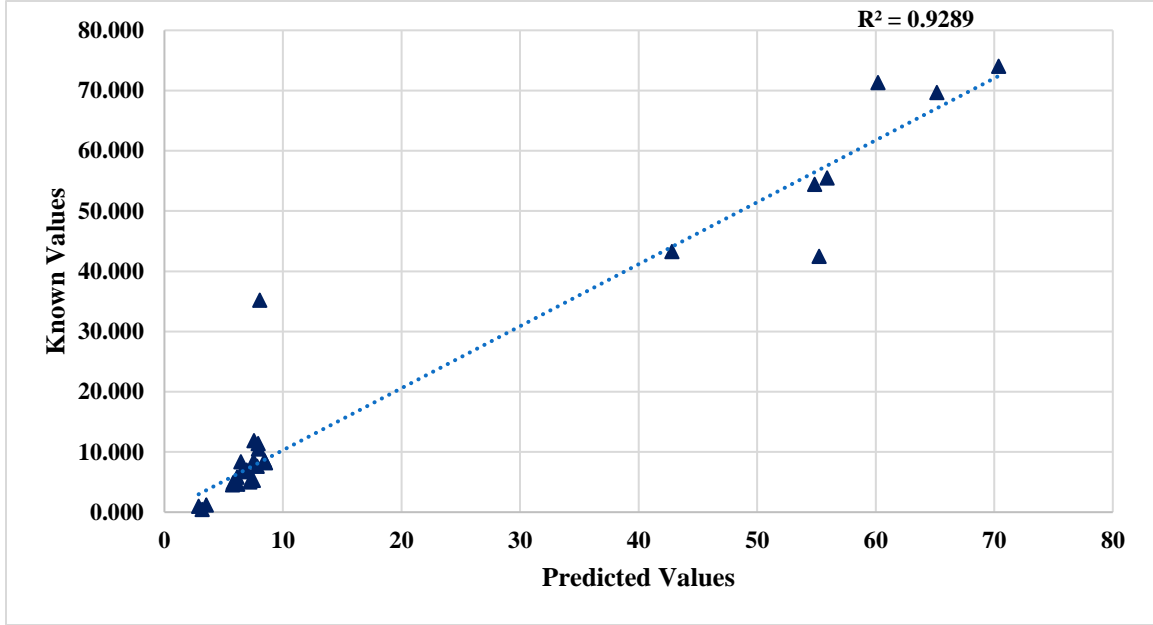


Figure 40. Results of CaO Using Calcium Oxide Classification.

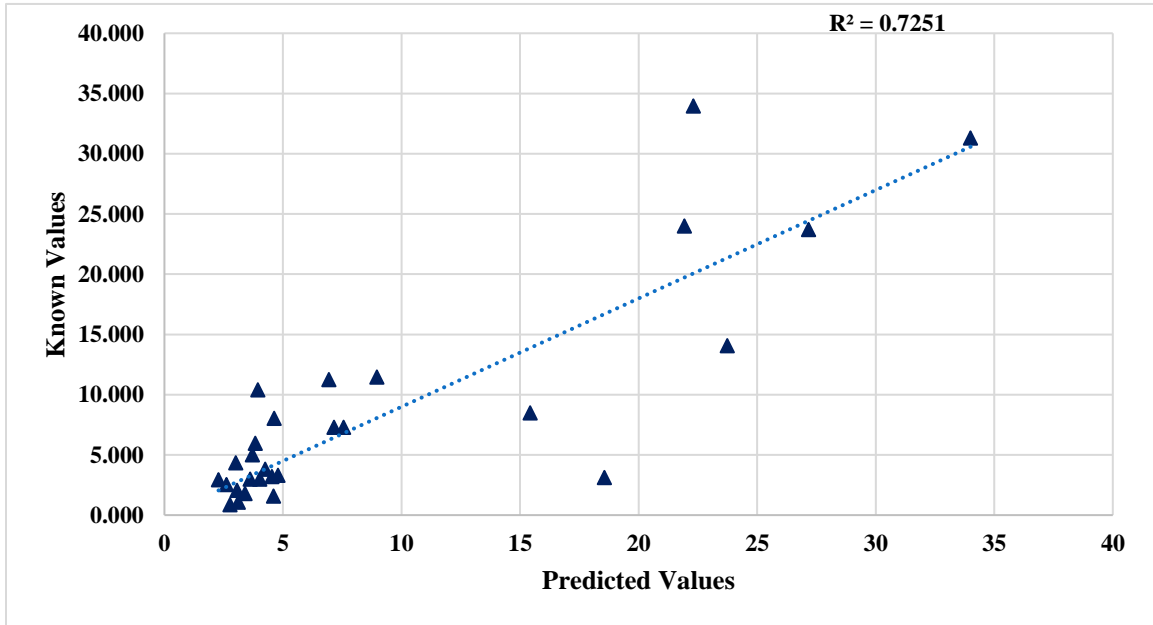


Figure 41. Results of MgO Using Calcium Oxide Classification.

Two-Dimensional Line classification. Figure 42 through 46 shows the results of Line Classification method. This showed the Two-Dimensional Line classification

method failed to classify carbonates and non-carbonates. This was because the trap rocks overlapped with both the Carbonates and Non-Carbonates models, and were therefore incorrectly classified. Lehigh Asphalt Carbonate was incorrectly classified as a Non-Carbonate and most of the trap rocks classified as Carbonates as shown in Table 3. This method gave the lowest R Square value; therefore, it was no longer used.

Table 3

Outliers of Two-Dimensional Line Classification

Outlier	Threshold Value	Classified as:
Bechtelsville Gneiss 15179	-0.53705	Carbonates
Dyer Quarry Diabase	-8.788	Carbonates
Outlier	Threshold Value	Classified as:
Hanson Glen Gneiss	-13.379	Carbonates
Kingston Argillite	-52.283	Carbonates
Kingston Trap Rock	-4.78	Carbonates
Plumstead Argillite	-12.371	Carbonates
Stockpile		
Temple Quartzite	-4.1864	Carbonates
Tilcon Diabase	-7.0635	Carbonates

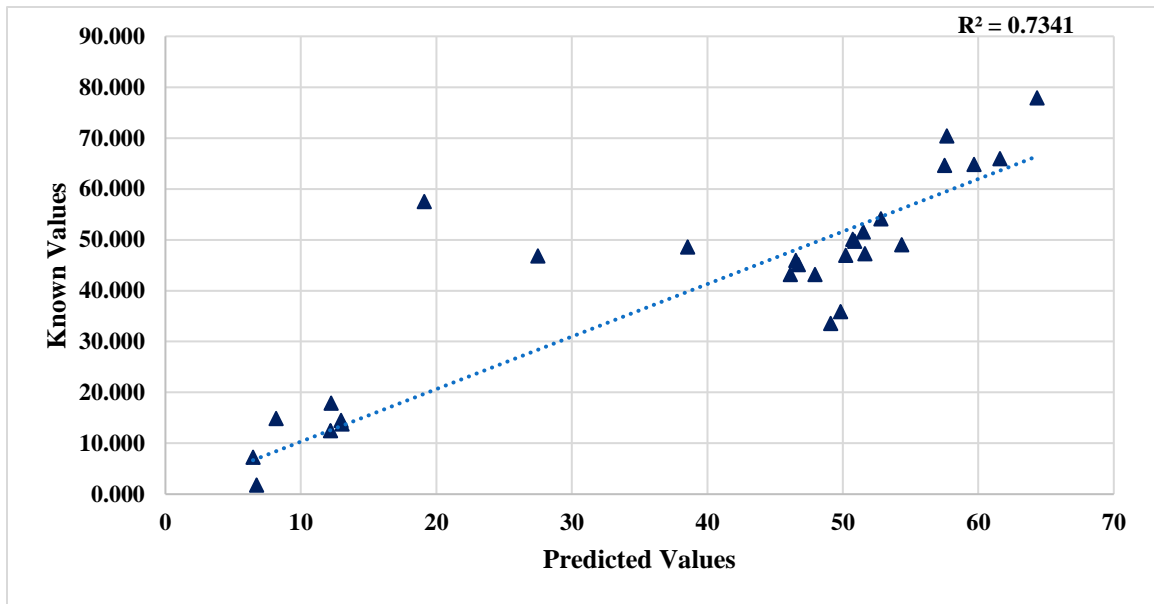


Figure 42. Results of SiO₂ Using Line Classification.

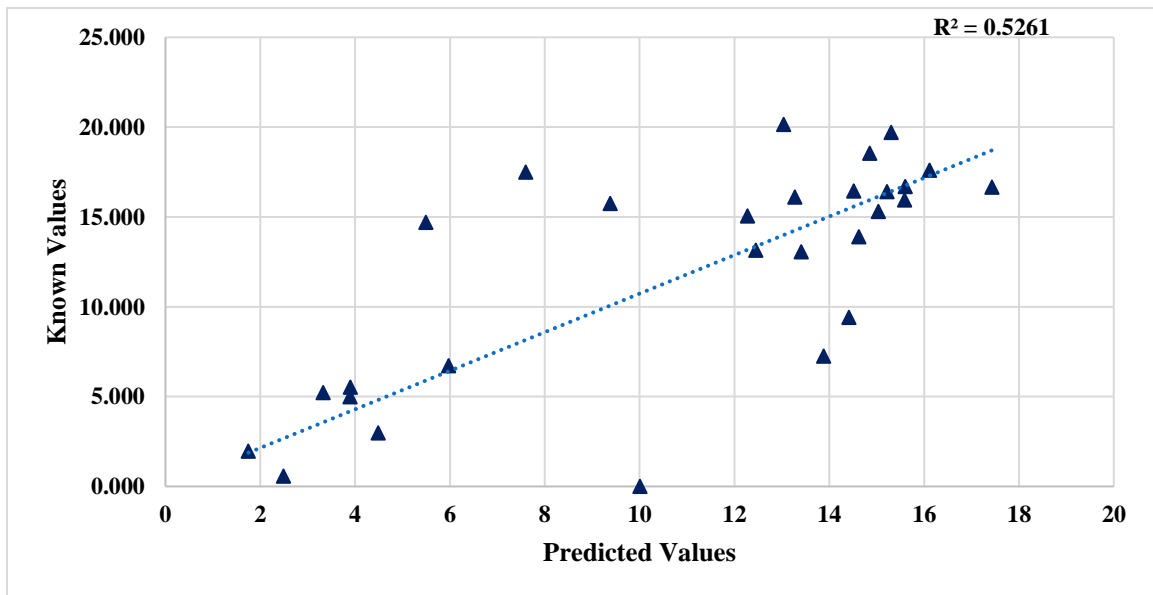


Figure 43. Results of Al₂O₃ Using Line Classification.

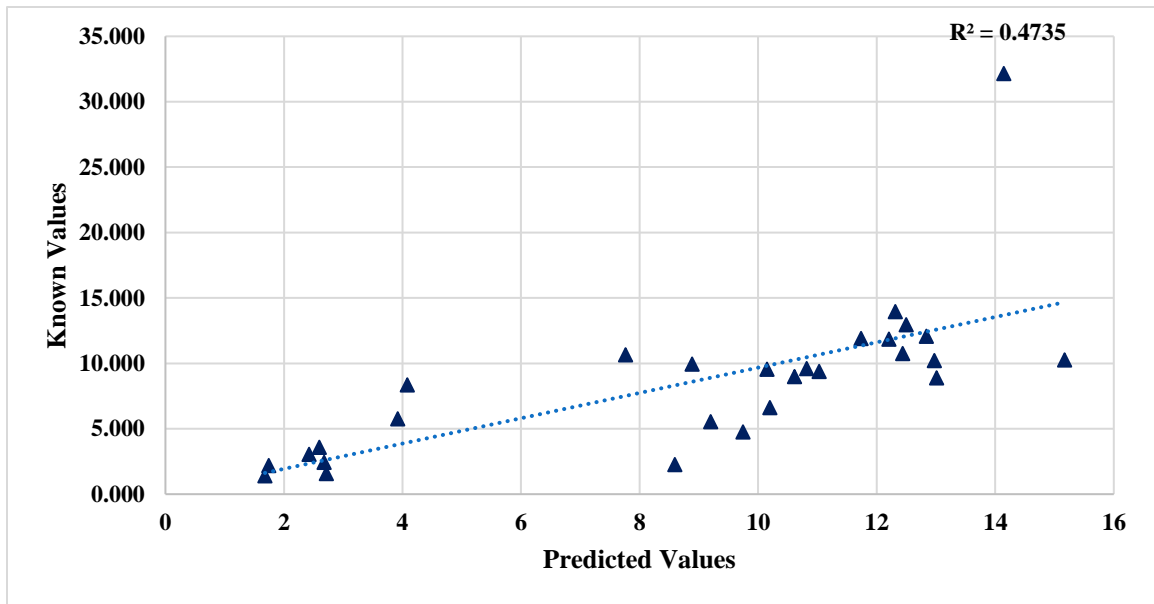


Figure 44. Results of Fe₂O₃ Using Line Classification.

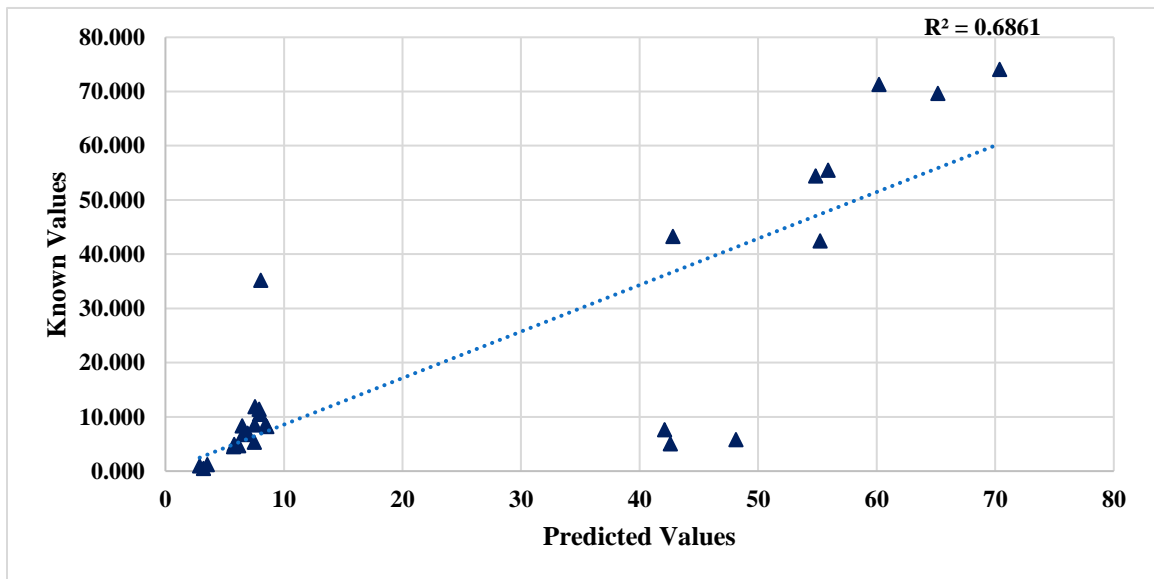


Figure 45. Results of CaO Using Line Classification.

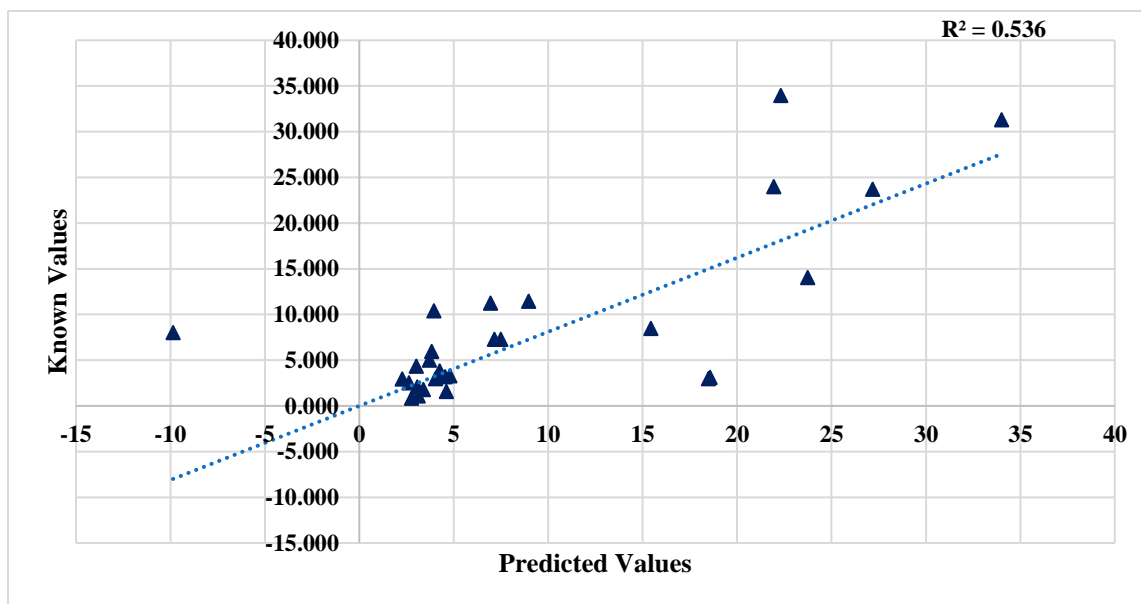


Figure 46. Results of MgO Using Line Classification.

Two-Dimensional Ratio classification. Figures 47 through 51 show the results for the Ratio classification method. Carbonates except Lehigh Asphalt Carbonate are classified correctly for split training purposes compared to the Two-Dimensional Line classification method (See Table 4). However, the accuracy of prediction of trap rocks and non-carbonates are yet to be improved. For this purpose, a precise model for trap rocks and non-carbonates must be defined which is discussed in the next section.

Table 4

Outliers of Two-Dimensional Ratio Classification

Outlier	Threshold Value	Classified as:
Lehigh Asphalt Carbonate	17.668	Non-Carbonate

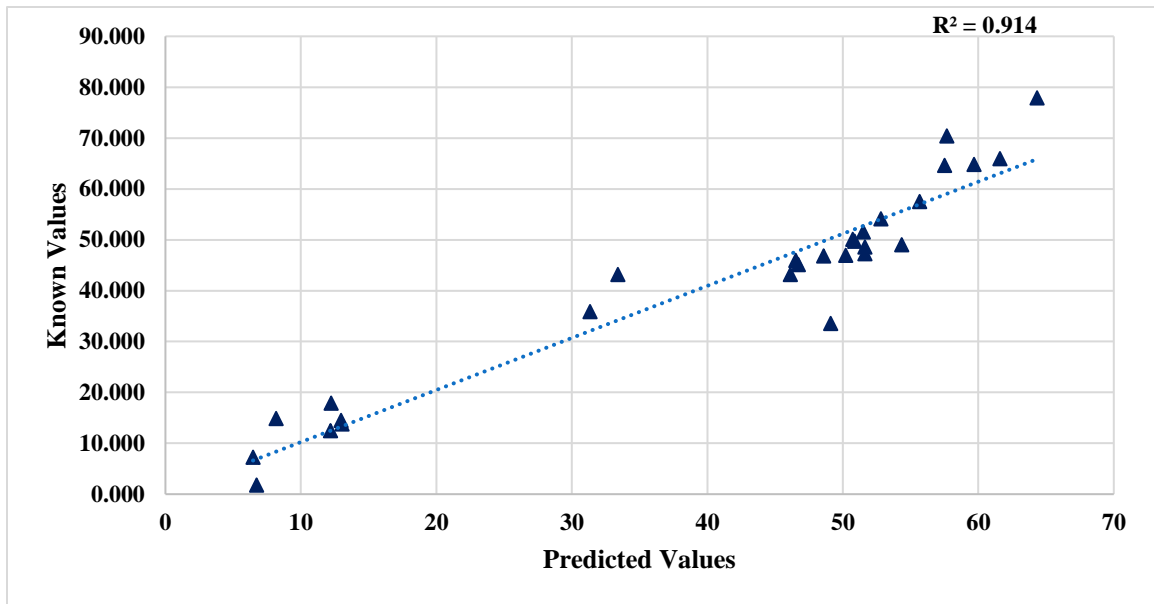


Figure 47. Results of SiO₂ Using Ratio Classification.

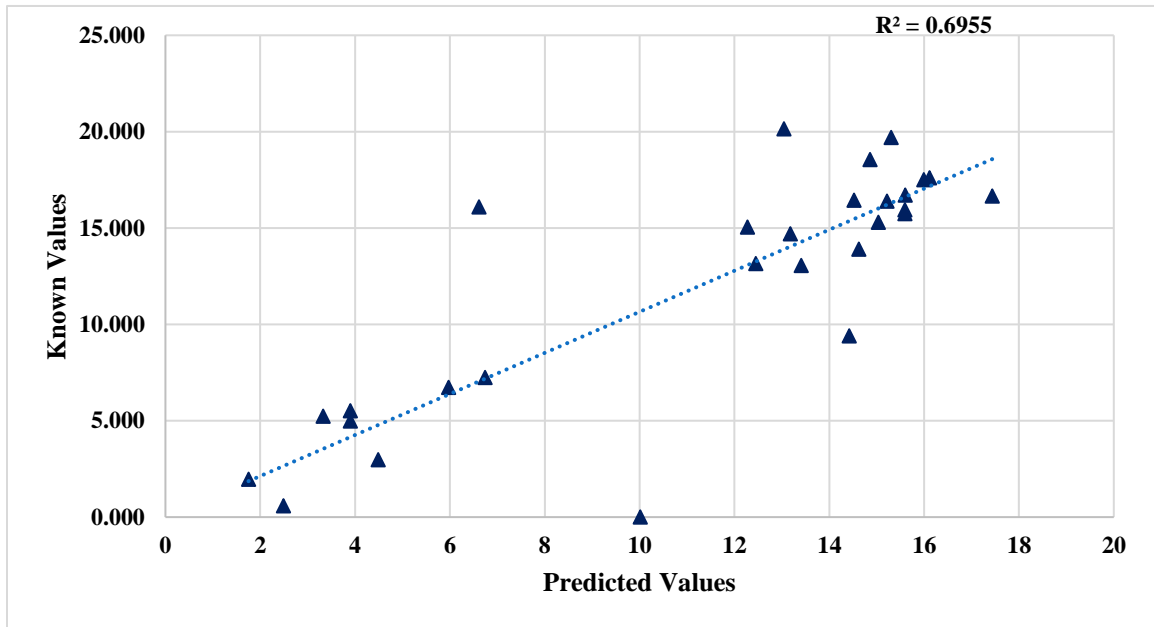


Figure 48. Results of Al₂O₃ Using Ratio Classification.

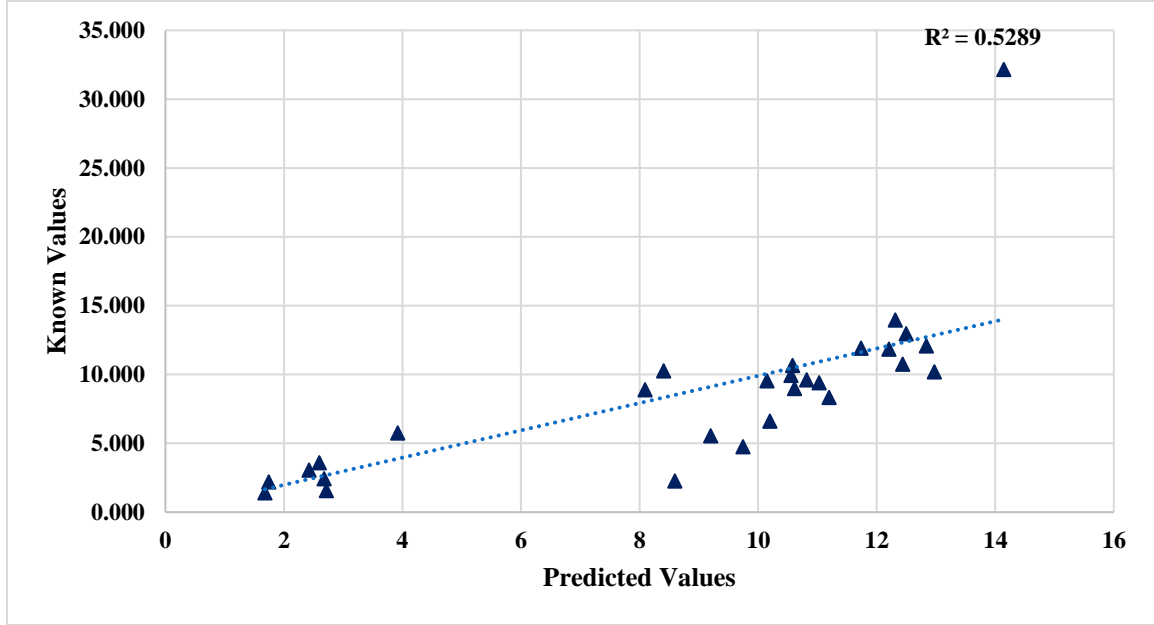


Figure 49. Results of Fe₂O₃ Using Ratio Classification.

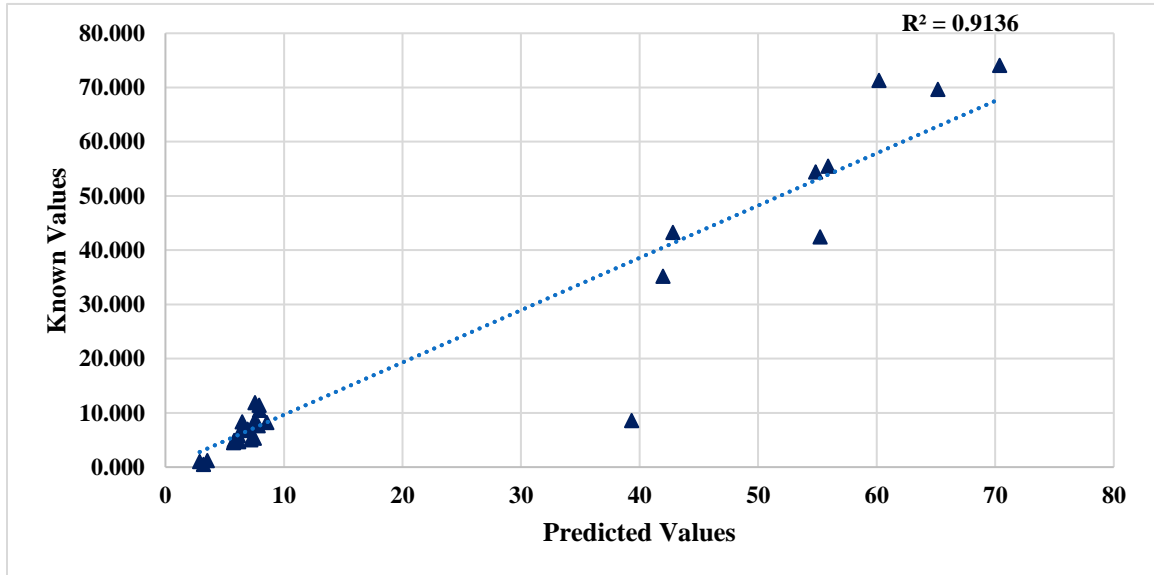


Figure 50. Results of CaO Using Ratio Classification.

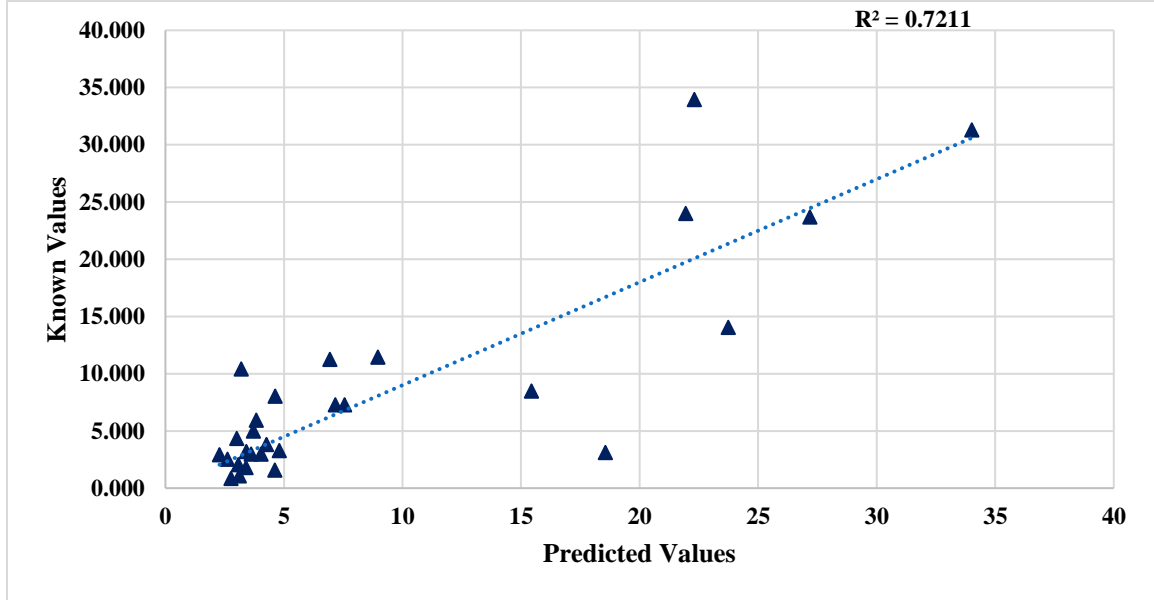


Figure 51. Results of MgO Using Ratio Classification.

Three-Way Split classification. The Three-Way Split classification technique discussed in Chapter 3 is the most effective way to classify the aggregate rocks. Based on the initial guess of composition based of the Base Model, the rocks are classified into three broad categories namely carbonates, trap rocks and non-carbonates.

$$Threshold\ Value = \left(\frac{SiO_2}{CaO}\right)^2 * Fe_2O_3$$

The squaring effect of the ratio set apart carbonates from non-carbonates. Lehigh Asphalt Carbonate is again classified as Non-Carbonate which later identified as a contaminated rock by NJDOT. Some trap rocks are classified as non-carbonates as shown in Table 5. This can be explained by the metamorphism of trap rocks due to the weathering process where the CaO and Fe₂O₃ contents are washed away. Figure 52

through 56 shows the results for the split training using the Three Way Split classification technique.

Table 5

Outliers of Three-Way Split Classification

Outlier	Threshold Value	Classified as:
Fanwood Trap Rock	6539.836	Non-Carbonate
Kingston Trap Rock	8052.592	Non-Carbonate
Kingston Trap Rock 15219	991.4638	Non-Carbonate
OWT Orange Basalt	1744.469	Non-Carbonate
Lehigh Asphalt Carbonate	8411.455	Non-Carbonate
Tilcon Diabase	18852.28	Non-Carbonate
Westfield Trap Rock	1189.668	Non-Carbonate

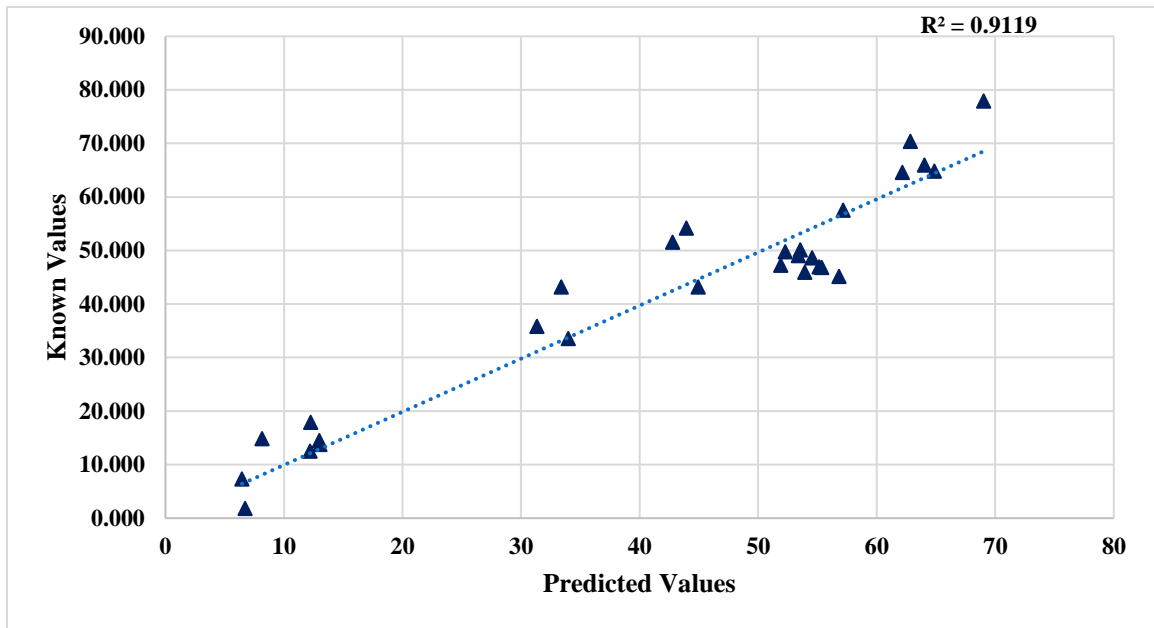


Figure 52. Results of SiO₂ Using Ratio Square Classification.

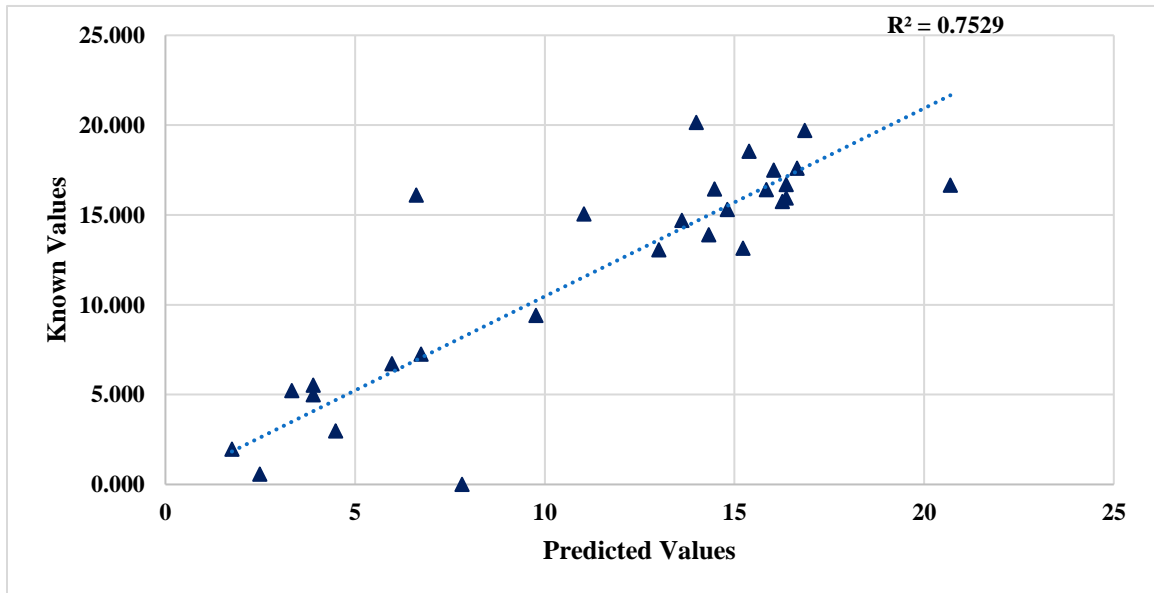


Figure 53. Results of Al₂O₃ Using Ratio Square Classification.

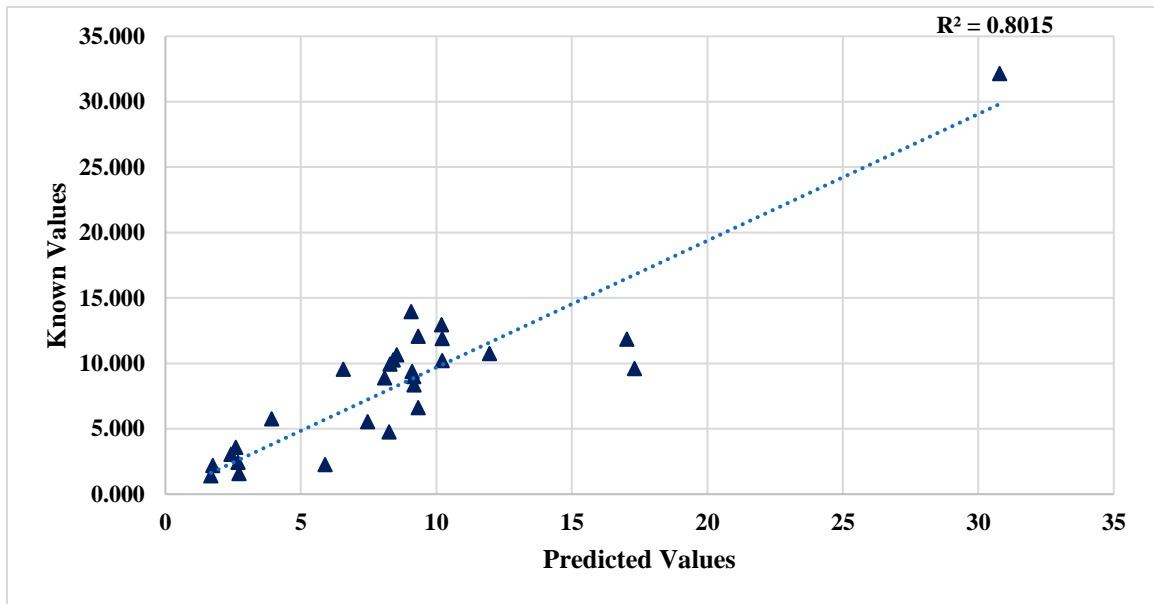


Figure 54. Results of Fe₂O₃ Using Ratio Square Classification.

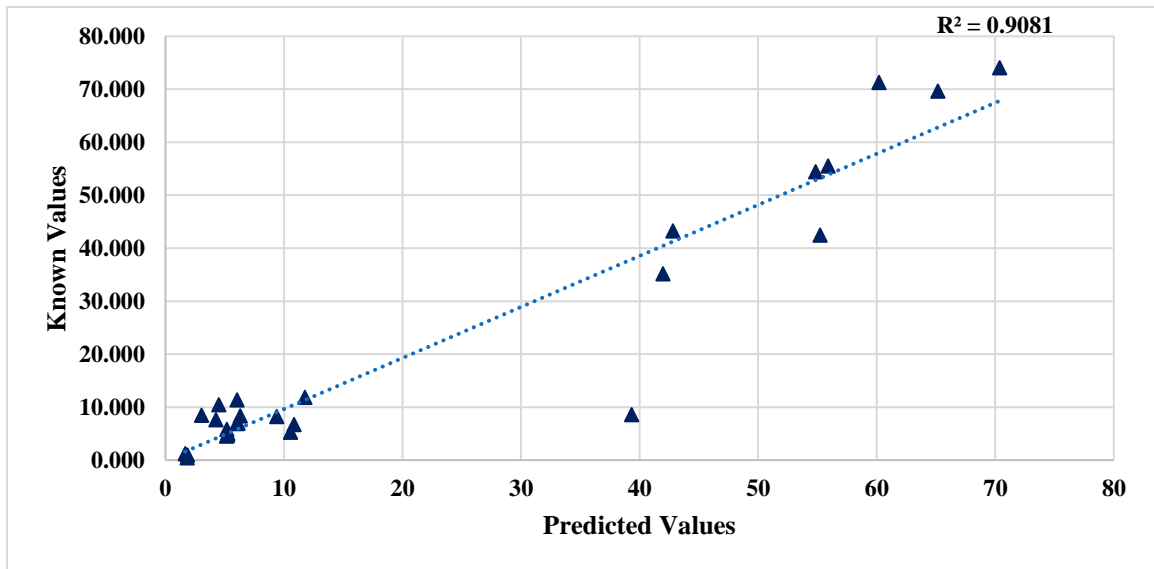


Figure 55. Results of CaO Using Ratio Square Classification.

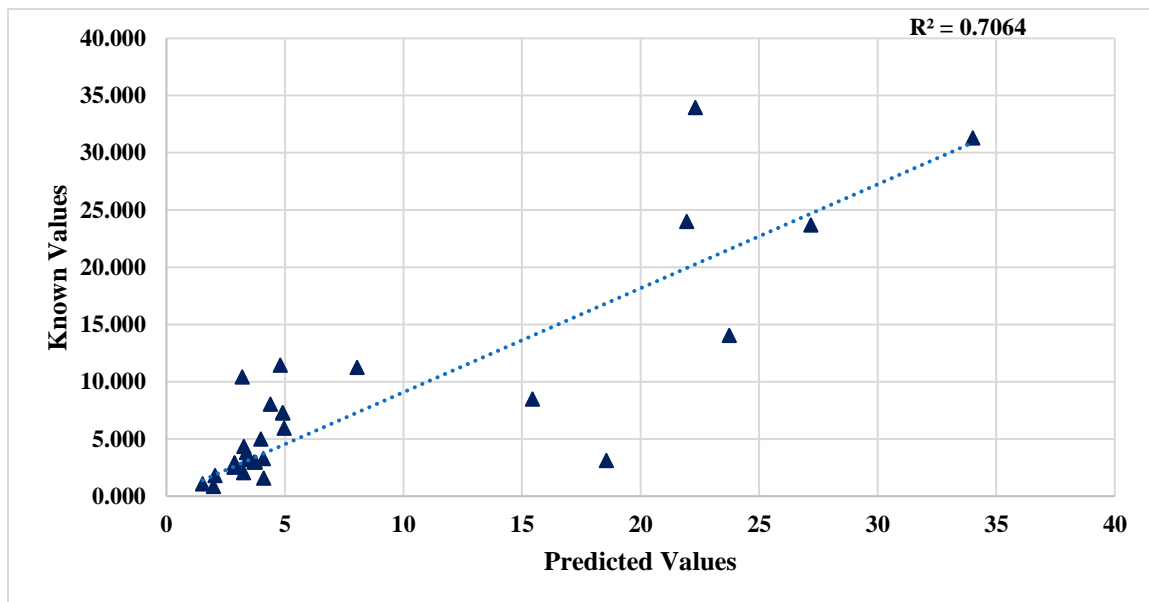


Figure 56. Results of MgO Using Ratio Square Classification.

Accuracy of Models

The accuracy of each model is determined using R square values and ANOVA analysis.

R Square values. R^2 values show the percentage of variation of the predicted results. When the R^2 value is higher, the model fits the data better. Table 6 shows the R^2 values for each model compared for each compound and Table 7 shows the R^2 values for carbonates, trap rocks and non-carbonates for each split training classification methods. Split Training with Y Scaling combined with the Three Way Split Classification shows the highest R^2 values. Y Scaling improved the accuracy of minor compound predictions since this method considered all compounds with equal priority.

Table 6

R Square Values of Each Method Against Each Compound

R Square Value	SiO₂	Fe₂O₃	Al₂O₃	CaO	MgO
Base Model	.8589	.6103	.3691	.8421	.4914
Y Scaling	.8722	.6956	.4924	.8469	.6178
Split Training	.9109	.753	.5276	.9271	.7123
Split Training with Y Scale					
One Dimensional Classification	.9021	.72	.5011	.9829	.7251
Split Training with Y Scale					
Two-Dimensional Line Classification	.7341	.5261	.4735	.6861	.536
Split Training with Y Scale					
Two-Dimensional Ratio Classification	.914	.6955	.5289	.9136	.7211
Split Training with Y Scale					
Three-Way Split Classification	.9119	.7529	.8015	.9081	.7064

Table 7

R Square Values of Carbonates, Trap Rocks and Non-Carbonates for Various Split Training Methods

R Square Value	Carbonates	Trap Rocks	Non-Carbonates
One Dimensional Classification	.806	.873	.983
Two-Dimensional Line Classification	.819	.687	.710
Two-Dimensional Ratio Classification	.932	.713	.978
Three-Way Split Classification	.932	.747	.969

ANOVA (Analysis of Variance). ANOVA is a statistical method developed by Ronald Fisher in 1918 to analyze the variance of more than two groups. This is also called the Fisher analysis of variance. This is an extended version of the t- and z-test. The assumptions considered while running ANOVA for the prediction results are as follows:

1. The weighted average errors of each compound of aggregates are normally distributed.
2. Independence of cases: Each LIBS test at various locations and on different samples are independent of each other.
3. Homogeneity: The variance between the aggregate groups are approximately equal.

A two-way ANOVA analysis is conducted on the average weighted error of each compound for all aggregates.

ANOVA for various PLSR models. The two-way ANOVA analysis is conducted on the results for the various spectrum analysis methods. Figure 57 through 59 shows the results of the ANOVA analysis to assess the accuracy of the different spectrum pre-processing techniques and split training strategies. X-axis represents the P-value associated with each analysis method which is the significance level of the interaction term. Y-axis represents each method of analysis as follows:

- 1- Base Model
- 2- Y-Scaling
- 3- Split Training
- 4- Split Training with Y-Scaling

When the P-value on the X-axis is lower, this indicates that the method is successful. Figure 57 shows that Split Training with Y-Scaling (#4 in Figure 57) is the best method because it has the lowest error for carbonates. Figure 58 for trap rock and Figure 59 for non-carbonates also indicates that method #4 is the most accurate.

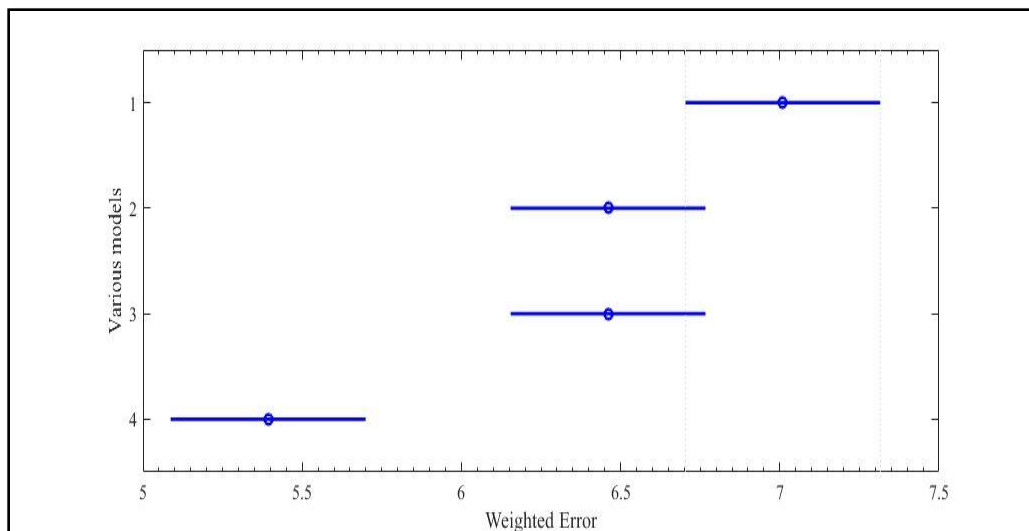


Figure 57. ANOVA Results of Various Models for Carbonates.

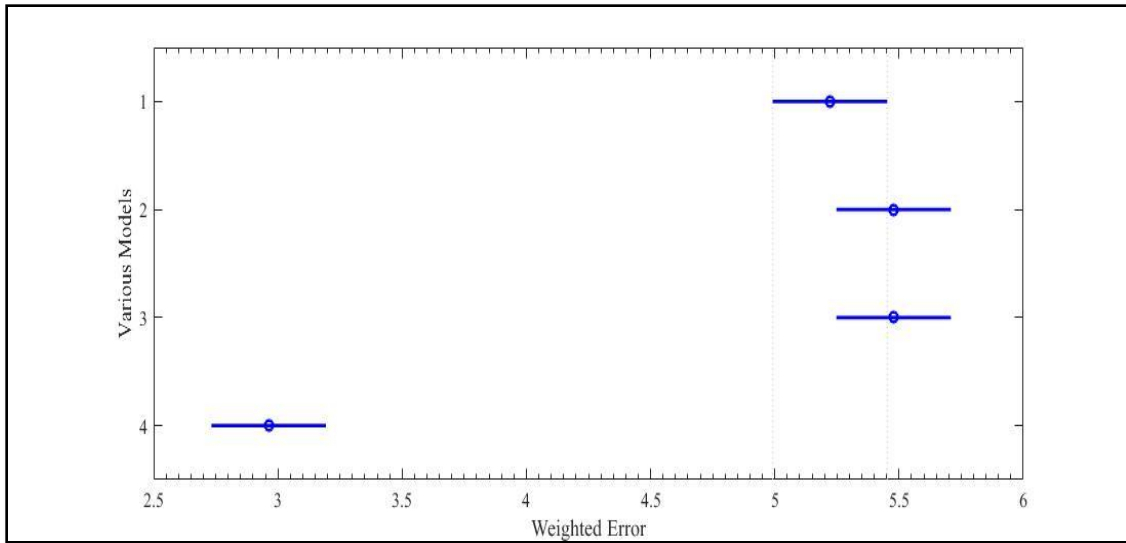


Figure 58. ANOVA Results of Various Models for Trap Rocks.

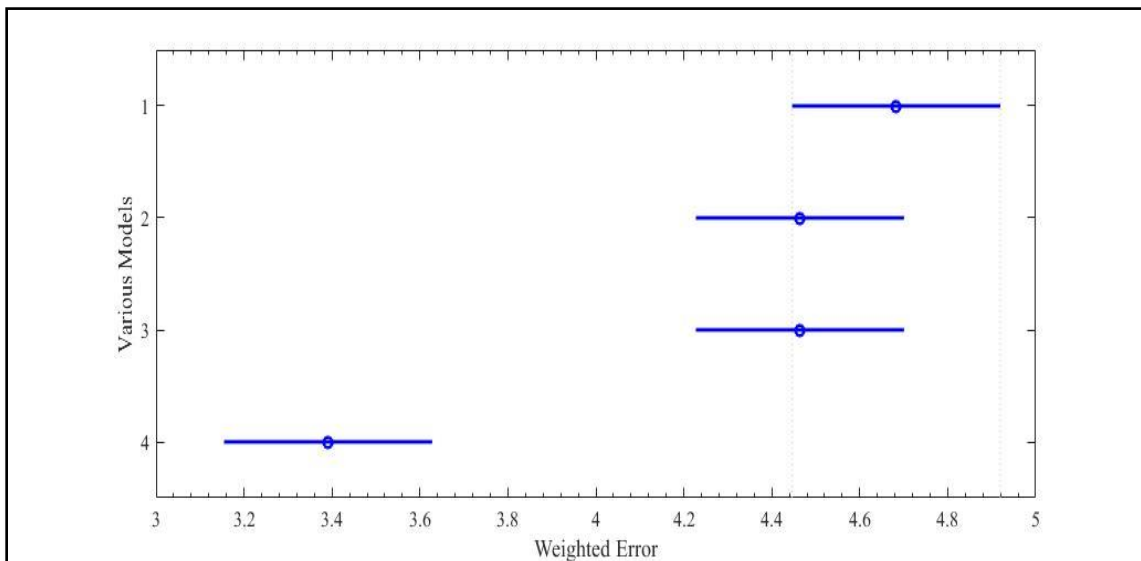


Figure 59. ANOVA Results of Various Models for Non-Carbonates.

ANOVA for various classifications. Two-way ANOVA is also conducted to determine the relative accuracy of the various classification methods. Figures 60 through 62 show the results from the ANOVA analysis for various split training classification

methods. X-axis represents the error of each classification method. Y-axis represents each method of classification as follows:

- 1- One Dimensional classification
- 2- Two- Dimensional Line classification
- 3- Two- Dimensional Ratio classification
- 4- Three-Way Split classification

Figure 60 displays the results of the ANOVA analysis for carbonates. Methods #3 and #4 are equally accurate with the lowest error. ANOVA analysis on trap rocks (Figure 61) shows that method #1 is more accurate compared to the other three methods.

ANOVA analysis on non-carbonates (Figure 62) shows that methods #1, #3 and #4 are significantly different from method #2. However, method 4 is selected because it has slightly less error than methods #1 and #3.

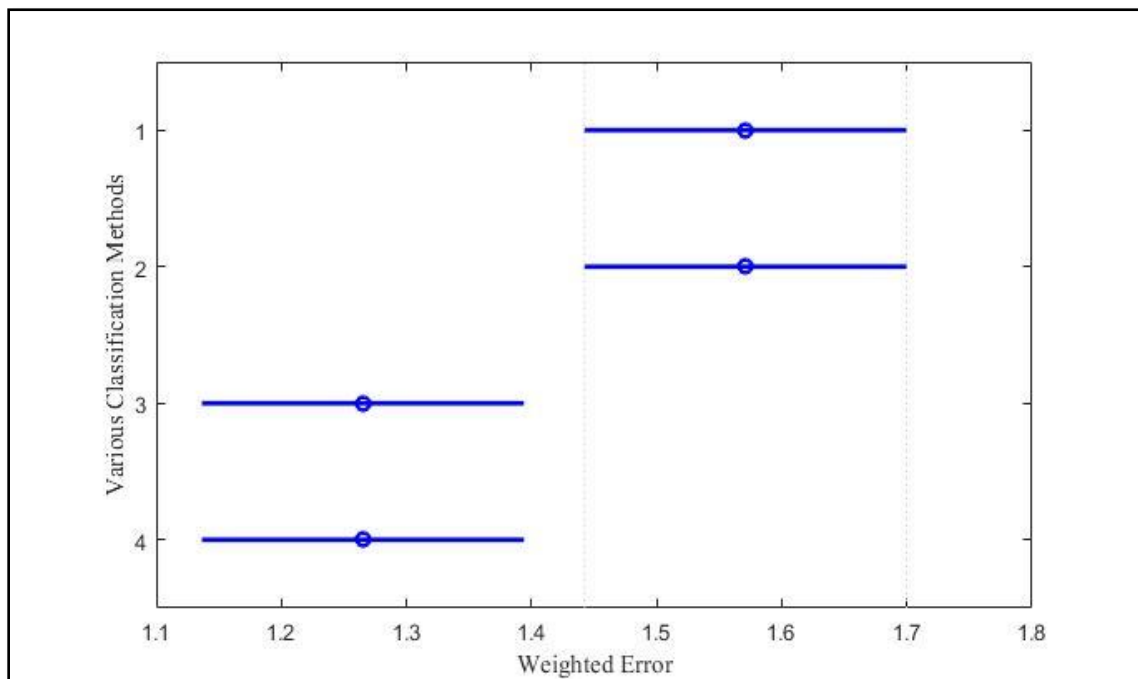


Figure 60. ANOVA Results of Various Split Training Methods for Carbonates.

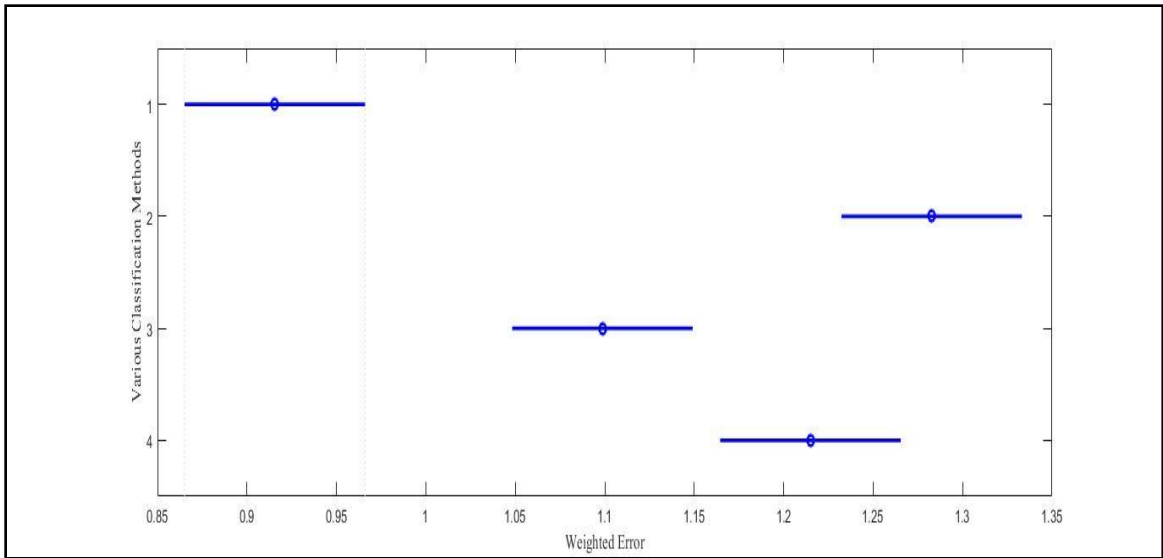


Figure 61. ANOVA Results of Various Split Training Methods for Trap Rocks.

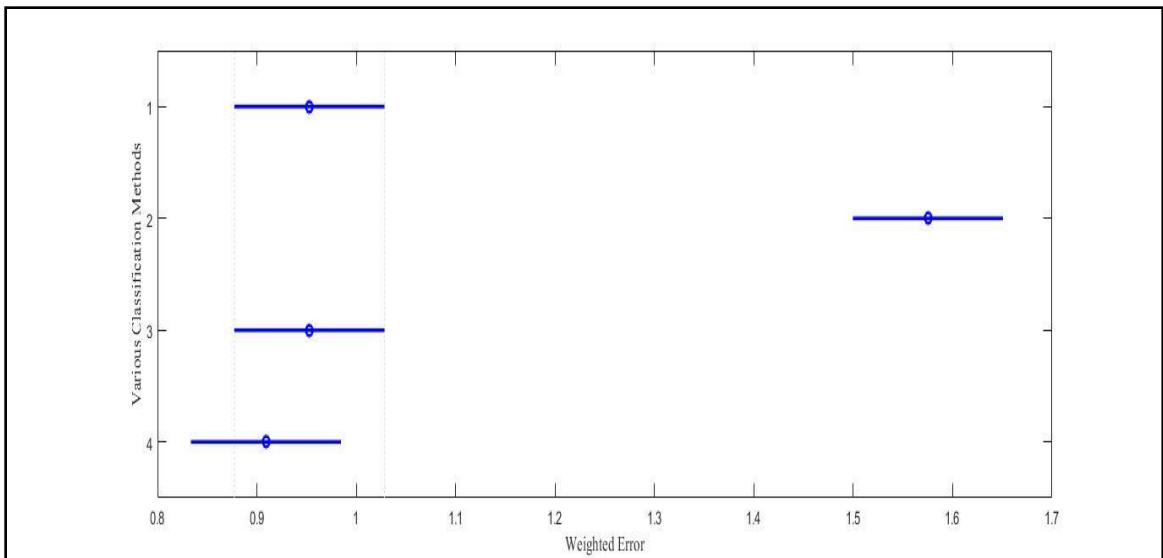


Figure 62. ANOVA Results of Split Training Methods for Non-Carbonates.

High-Pass Filter of LIBS Spectrum

In order to improve the accuracy of the LIBS-PLSR analysis model, a filtering technique is implemented to eliminate the Bremsstrahlung baseline while preserving the

remaining information. A MATLAB code is developed that will filter the spectral data obtained.

Moving Average Subtraction (MAS). To remove the baseline of the LIBS data, a moving average of the data is created with an adjustable value, N , which will take the average of the N values before and after each data point between $N:(12,288-N)$. Values 1: N and $(12,288-N): 12,288$ are assigned a zero value. By adjusting the N value, the peaks of the original data are eliminated, leaving only the baseline. This resulting baseline is then subtracted from the original data, and all negative values of intensity are set to zero. This method removes the baseline height from the maximum intensity of the peaks with the assumption that the relevant data is shifted in intensity by the baseline. Figures 63 and 64 show the effect of moving average subtraction.

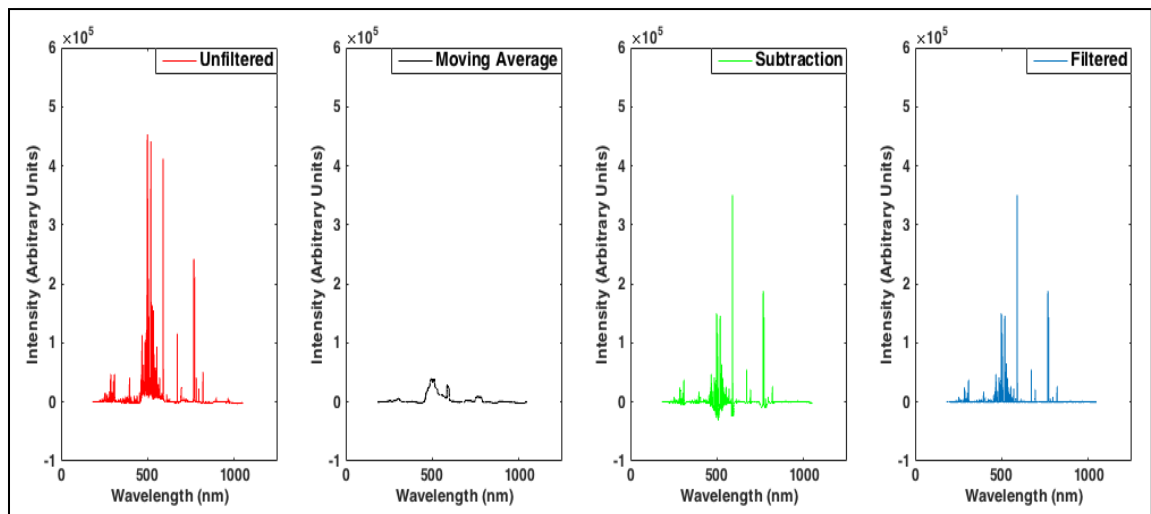


Figure 63. Left to Right: Unfiltered Atkinson Quartzite Data, Moving Average of Data, Subtraction of Data, Subtraction of Moving Average from Original Data, Filtered Data Adjusted to Eliminate Negative Values.

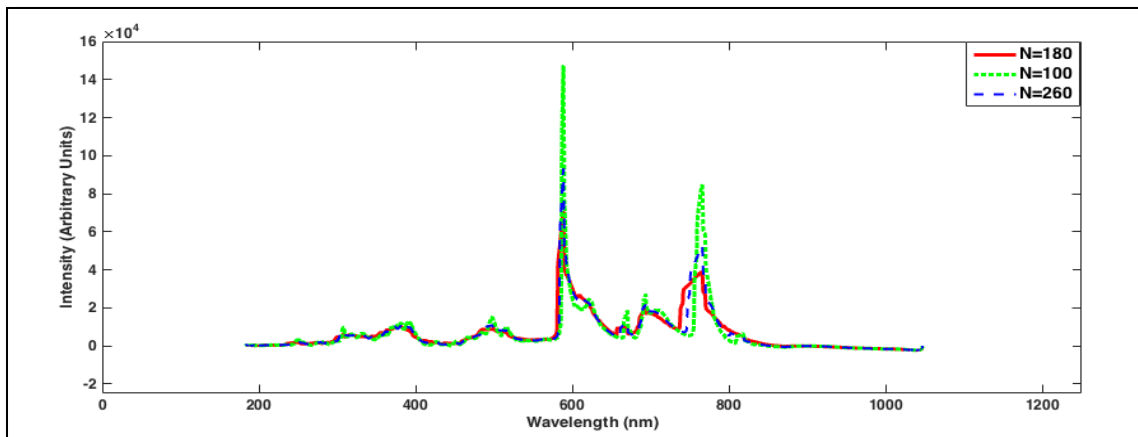


Figure 64. Subtraction from MAS Filtration Method Showing the Moving Average N=180 to Best Conserve Relevant Information.

Moving Slope Analysis (MSA). An array consisting of 12,288 zero points is created. The original data is then scanned point to point to determine the instantaneous slope. If the slope, $((J+1)-J)/1$, is greater than or equal to 100, the corresponding J point in the zero array is assigned the value. By adjusting the slope value, the original peak data is preserved. This method preserves relative intensity when removing the baseline, with the assumption that the baseline overshadows relevant information.

The effectiveness of the MAS filtering technique is maximized by varying the N value used for the average to determine which value will result in the greatest preservation of intensity peak data. An average of 361 data points surrounding each individual point, N=180 value is shown to best preserve the data while still eliminating the baseline as shown in Figure 65. The MSA filtering technique is maximized similarly by determining the slope value that results in the most effective conservation of the sharp intensity peak data as shown in Figure 66. The effectiveness of the filters is determined by comparing the results of the filtered and unfiltered models to the XRF values. A student's t-test was performed with 95% confidence that the true value lies within the

uncertainty of the mean. Figures 67 through 69 show the results of MSA and MAS filtering methods. The figures show that the results of the unfiltered data, MAS N 180 filter data and MSA slope 100 filter data are within the 95 percent confidence interval, hence significantly not different. Either technique removed the broadening of the spectrum but it did not make any improvements in the predicted results.

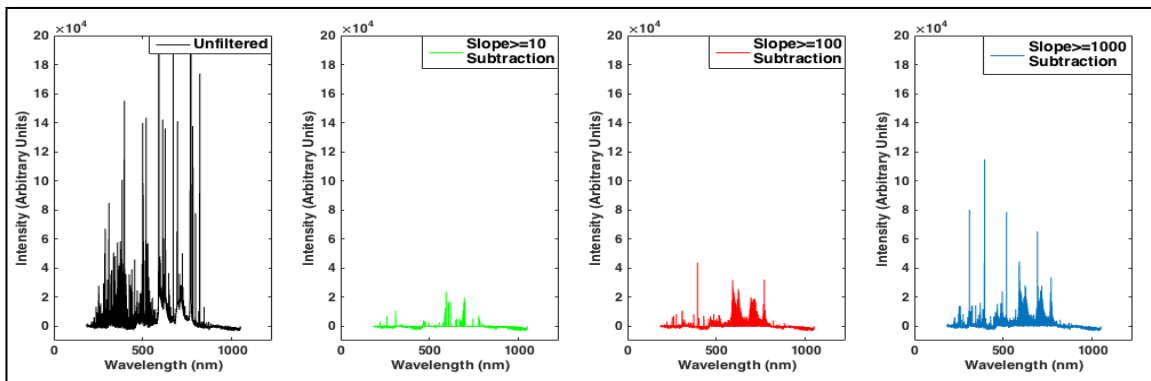


Figure 65. Left to Right: Unfiltered Atkinson Quartzite Data, Moving Slope Analysis Data, Showing Preservation of Intensity Information, Filtered Data Subtracted from Unfiltered Data Leaving Only the Baseline.

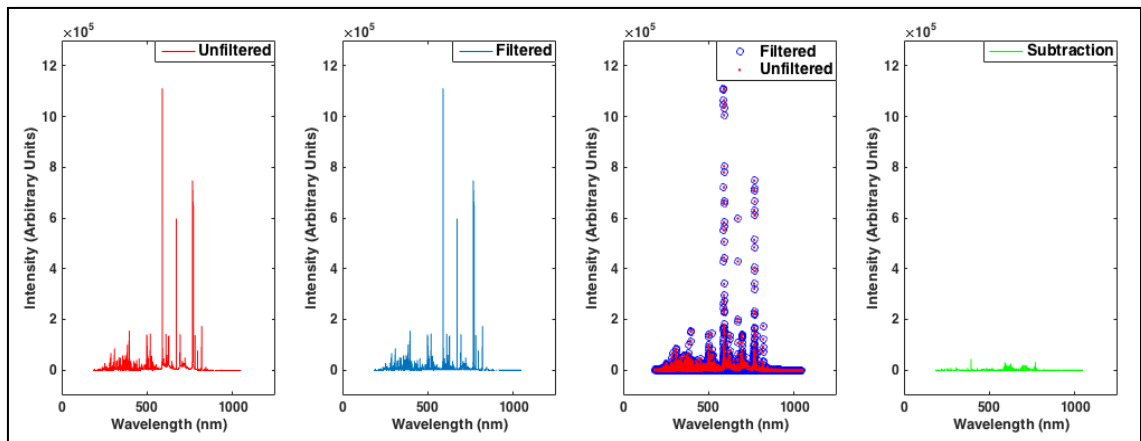


Figure 66. Left to Right: Unfiltered Atkinson Quartzite Data, Moving Slope Analysis Preserving Data with Slope ≥ 10 , Moving Slope Analysis Preserving Data with Slope ≥ 100 , Moving Slope Analysis Preserving Data with Slope ≥ 1000 .

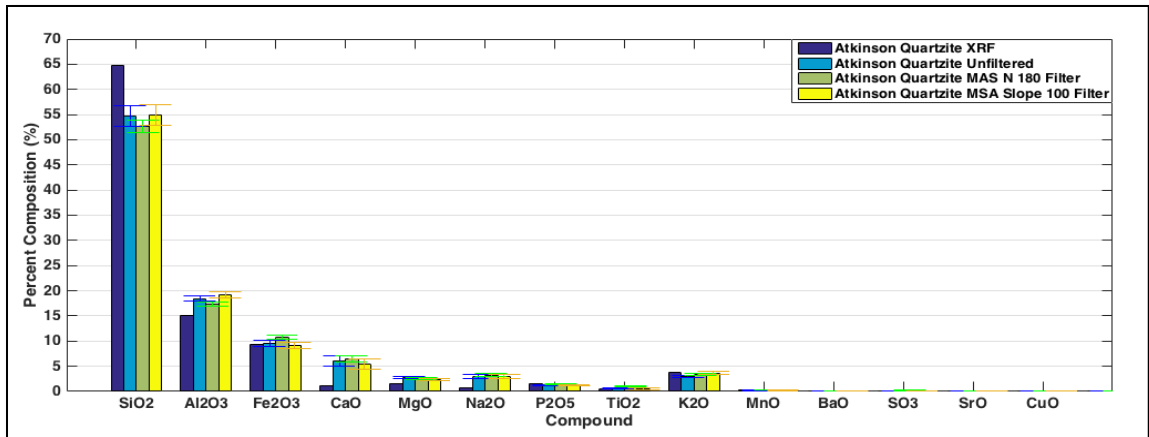


Figure 67. Comparing the Output of the PLSR Calculation of Atkinson Quartzite, Error Bars Showing Uncertainty of Data with 95% Certainty.

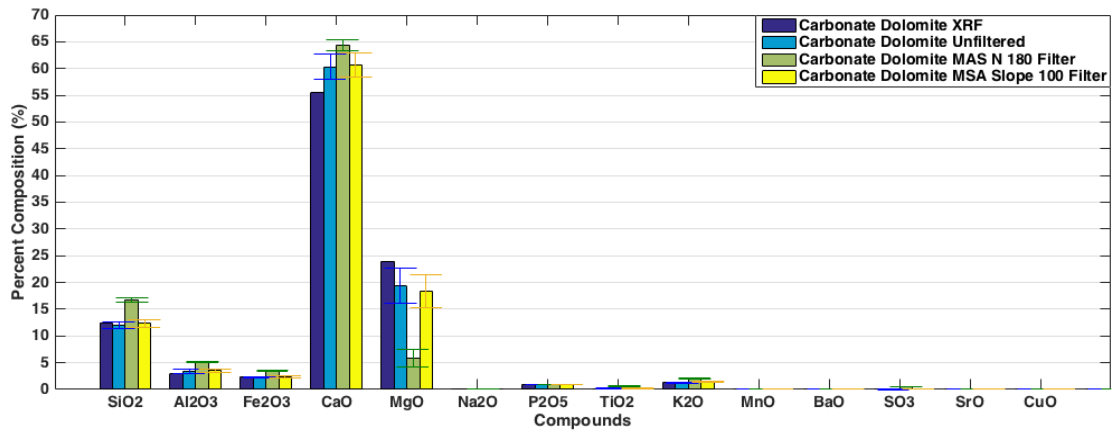


Figure 68. Comparing the Output of the PLSR Calculation of Carbonate Dolomite, Error Bars Showing Uncertainty of Data with 95% Certainty.

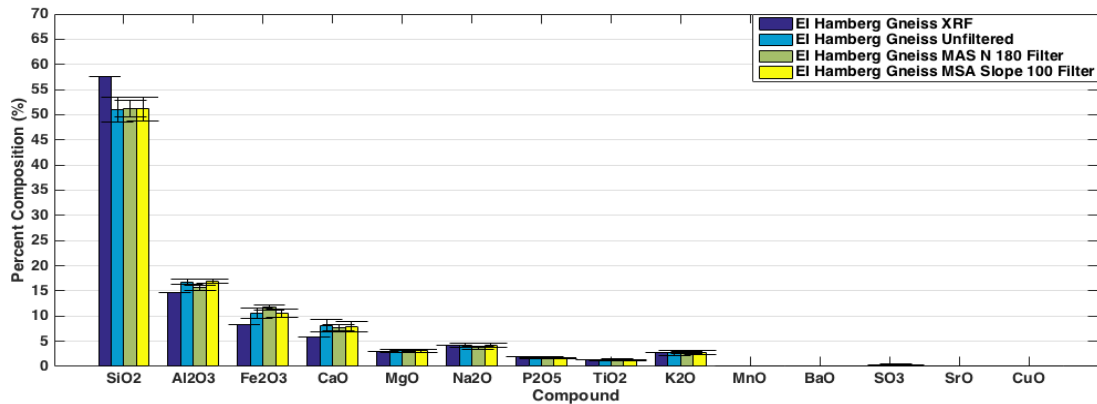


Figure 69. Comparing the Output of the PLSR Calculation of EI Hamburg Gneiss, Error Bars Showing Uncertainty of Data with 95% Certainty.

Frequency cut off and slope detection. This method uses a high-pass filter, in which each laser pulse reading has an associated cutoff frequency. The values lower than this cutoff will be removed from the data. The assumption is that this technique will remove any noise in the data generated by these frequencies. The goal of this method is that the identified broadening of the spectrum will be removed. This method will find the standard deviation of the derivative of LIBS spectra. Using the standard deviation and a chosen slope threshold, an edge detection system will be utilized to differentiate the abrupt spikes in the data as well as gradual increases. The gradual increases in the spikes are assumed to create the broadening of the spectrum and hence it is filtered out. All slope changes in the 'Y' direction that are not equal to or greater than the chosen slope are filtered out because any small or gradual changes in the 'Y' direction of the data are considered to be noise. Figure 70 shows the filtered and unfiltered spectrums after high-pass filtering. Although the broadening of the spectrum is successfully removed, the analysis of the filtered data does not improve the accuracy of the results. Therefore,

filtering of the spectral data is not done before analysis of the data. Figure 71 shows the comparison of results using filtered and unfiltered spectrums and shows that there is very little improvement in accuracy.

Although the high-pass filter removes the broadening of the spectrum, there is no improvement in the model predictions. Hence, the idea of removing the spectral broadening is no longer considered.

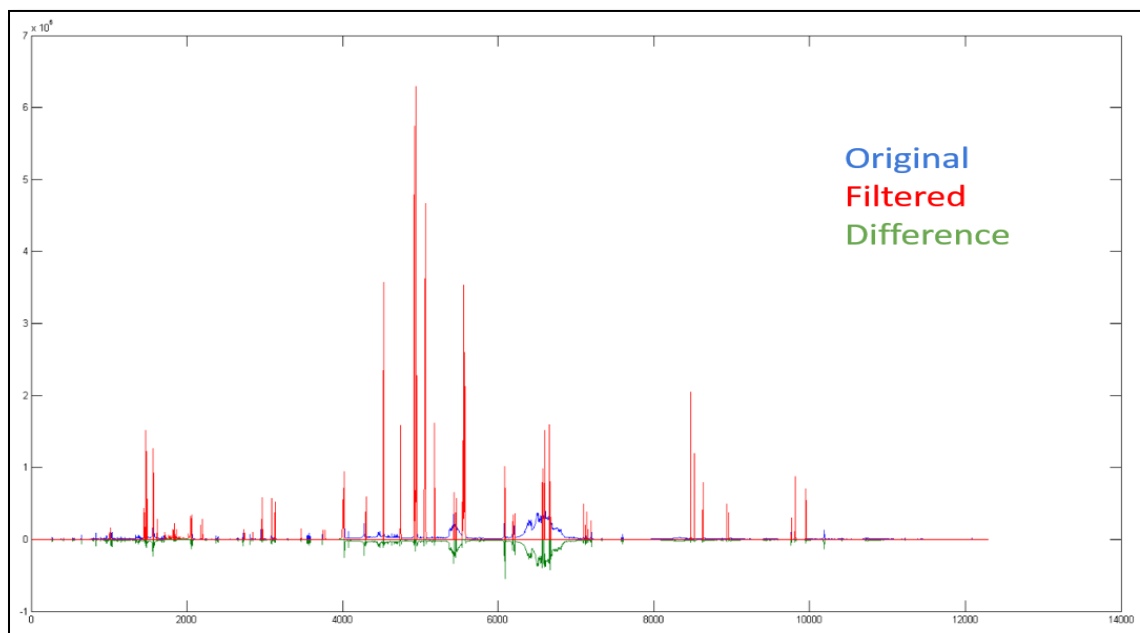


Figure 70. High Pass Filtering of LIBS Spectrum.

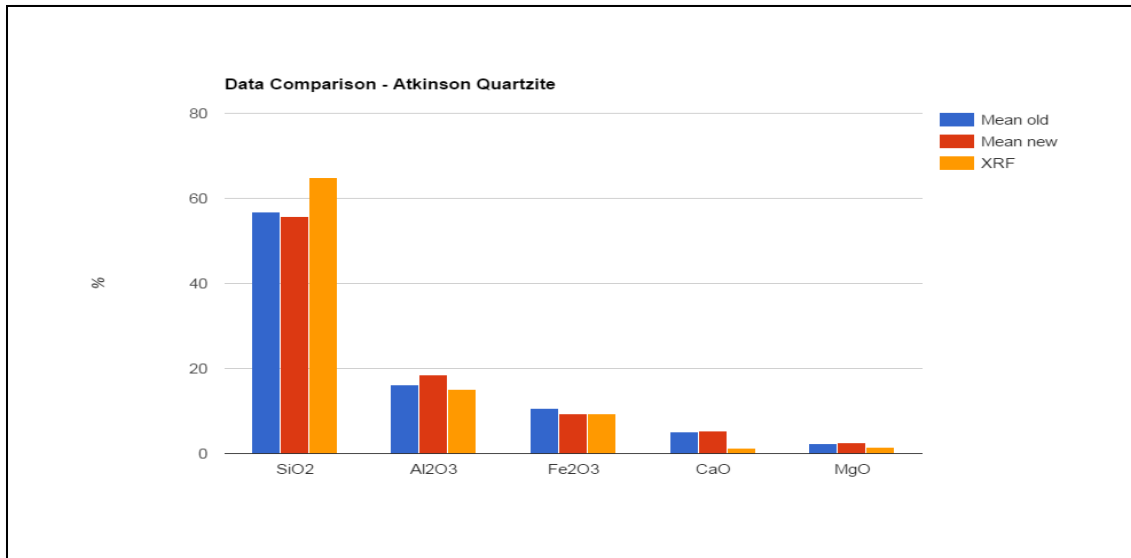


Figure 71. Results of High Pass Filtering of LIBS Spectrum

Determination of a Suitable Sample Size

Testing set size is determined based on the number of samples required for a stabilized prediction. Figure 72 shows predictions of Woodboro Carbonate for various testing set size. X-axis shows the total number of testing data used for each prediction and Y-axis shows the predicted values for the percentage of SiO₂. As per the figure, a minimum of 30 data points is recommended. The number of samples tested is of greater importance than the number of locations tested per sample. Thus, a testing set size of 10 samples with 3 locations per sample is selected.

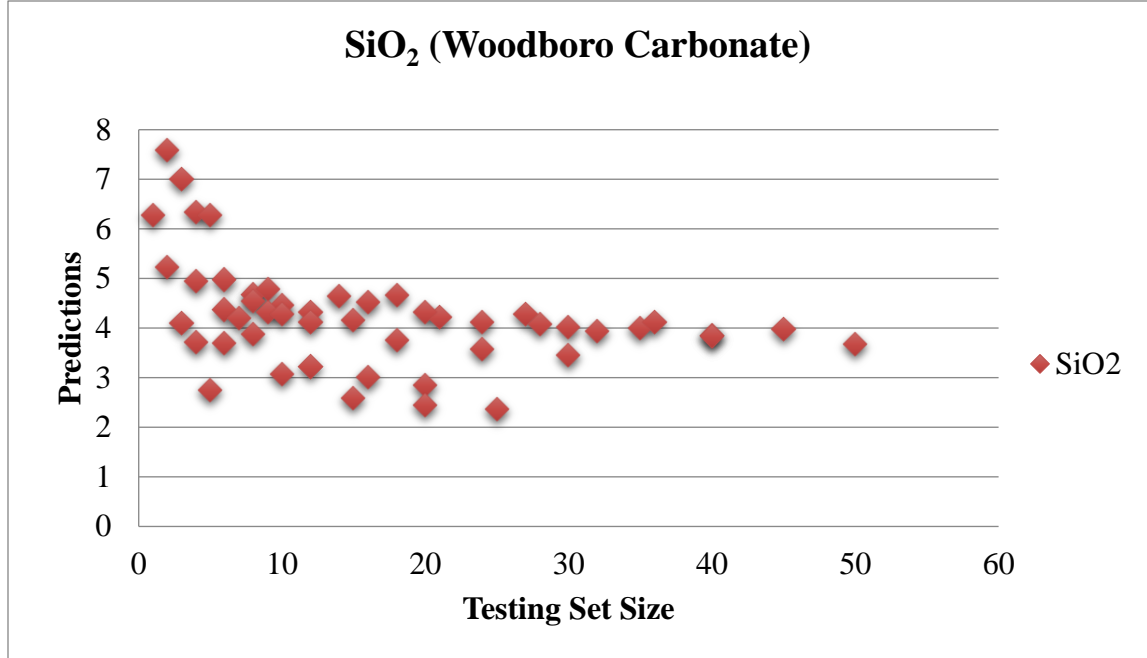


Figure 72. Testing Set Size.

Development of a User-Friendly Program

A Graphic User Interface (GUI) program is developed using MATLAB to analyze the LIBS spectrum. Figure 73 shows the GUI for the Laser Data Analysis Tool. It gives options for the various operating modes such as training the model, testing single aggregates at a time and testing a set of aggregates. In the training mode, number of PLS components are calculated by default or by manual input. For each testing mode, testing threshold defaults are 150 for carbonate and 500 for non-carbonate. Carbonate threshold classify rocks into Carbonates and Non-Carbonates while non-carbonate threshold classifies rocks between Non-Carbonates and Trap Rocks. A custom threshold option is also provided. The user can select the input data and run the program. A *help* option is also provided to address any questions users would have about running the program. The directory to which results will be saved can be changed using *Settings*.

A GUI for updating the calibration data is also provided. Figure 74 shows the interface of the update calibration tool. It provides the options to input the laser calibration data as a folder and the corresponding XRF data as an excel spreadsheet.

A stand-alone deployable software for these programs has been developed which could be installed and used in any system without MATLAB. This software program will not allow users to make changes to the code or available features.

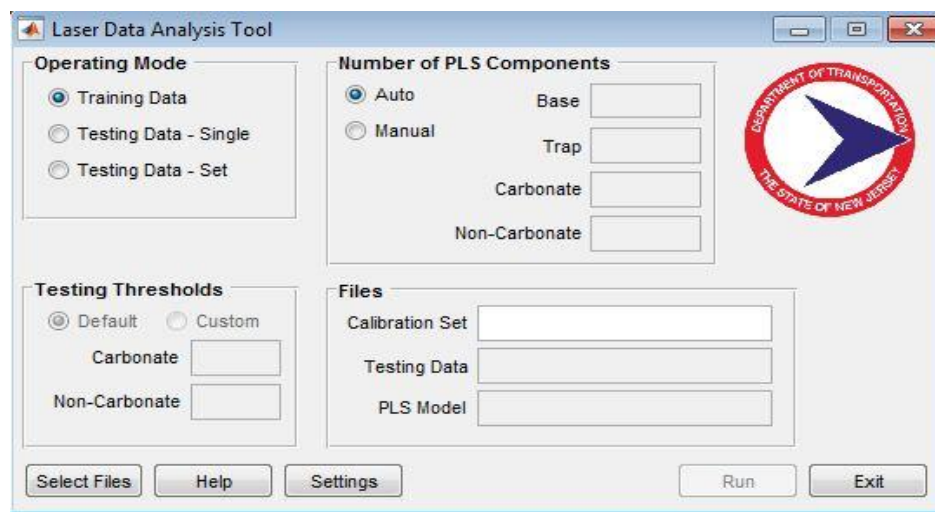


Figure 73. Laser Data Analysis Tool.

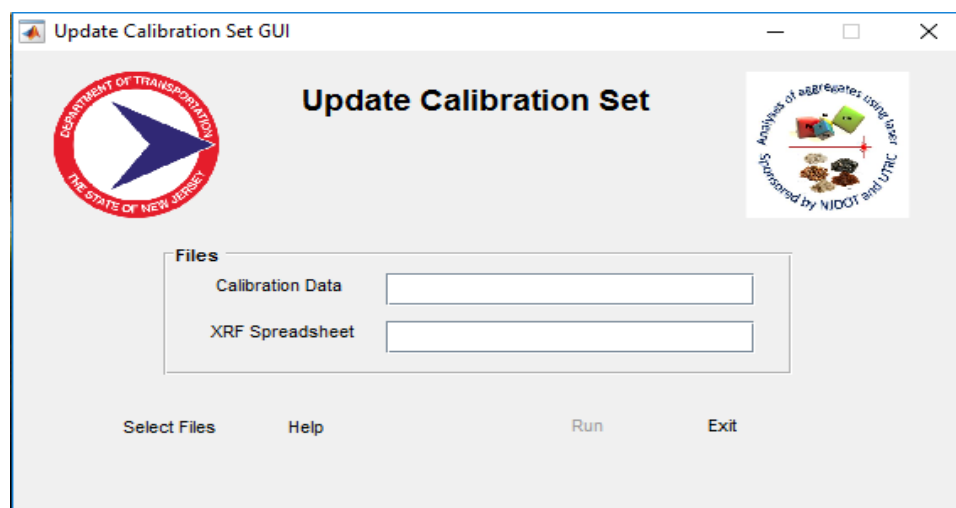


Figure 74. Update Calibration Tool.

Testing of the Portable Equipment to Assess Ruggedness and Impact of Environmental Factors

Vibration/impact test. To test the durability and the resiliency of the portable laser system, the equipment is loaded onto the back of a truck which is then subjected to high speeds and roadways with poor driving conditions. Sudden jerks and vigorous impacts due to potholes, rutting, and overall inconsistencies in the roadway, as well as abrupt braking are used to simulate realistic transportation conditions. The following tests were conducted on the same samples of the same batch of aggregates before and after the vibration/ impact testing. Figures 75 through 77 depict the results from the vibration/ impact testing on Carbonate Dolomite, Plumstead Argillite Belt and Bechtelsville Gneiss.

The results are similar before and after the vibration/impact field test. The small variations can be attributed to the typical shot-to-shot variations within the aggregate samples and are within the experimental error thresholds.

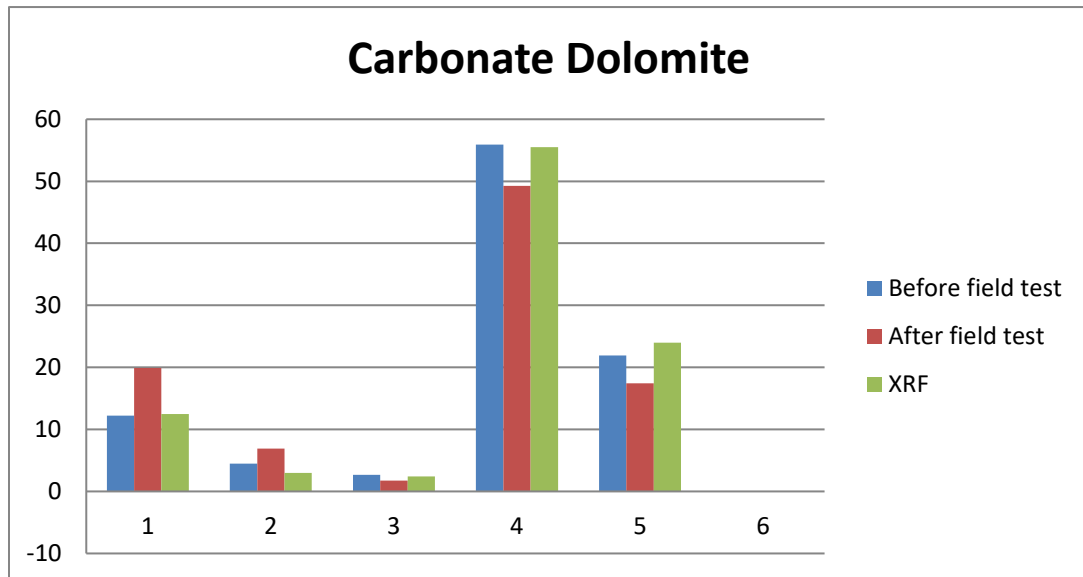


Figure 75. Vibration/ Impact Test Results, Carbonate Dolomite.

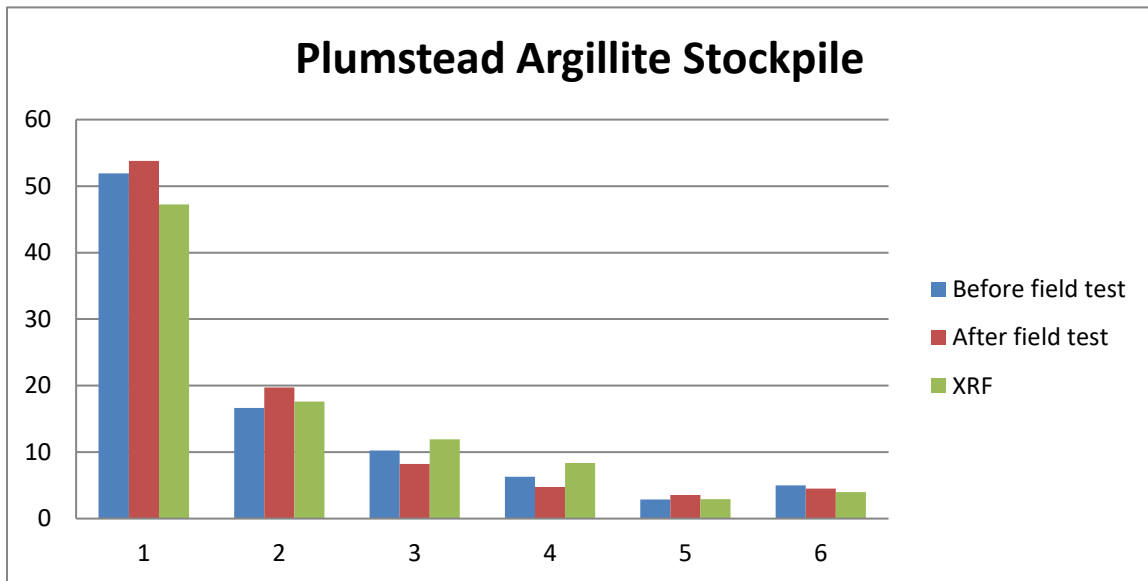


Figure 76. Vibration/ Impact Test Results, Plumstead Argillite Stockpile.

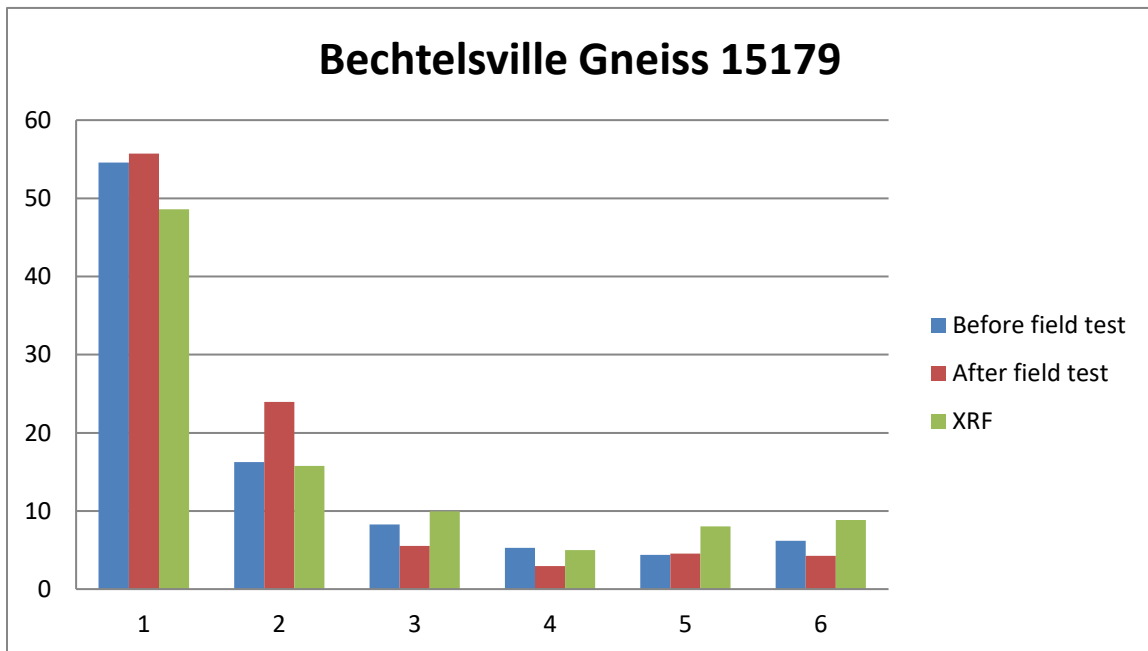


Figure 77. Vibration/ Impact Test results, Bechtelsville Gneiss 15179.

Temperature test. The equipment is kept in the field and allowed to equilibrate to the atmospheric temperature during a 4-hour time frame. Tests are then conducted on the same sample of aggregates from the same stockpile of rocks at various temperatures to depict the field conditions. Finally, these results are compared with the results obtained in the laboratory at a room temperature of 68 °F.

Figures 78 through 79 show the results of temperature testing for Carbonate Dolomite and Plumstead Argillite stockpile. The results show a wide variation of results. Testing at temperatures of approximately 79 °F and 68 °F give results comparable to the XRF values. However, testing at 54 °F and 32 °F show a wide variation from accepted values and therefore it is concluded that this equipment should be utilized at temperatures above 60 °F and under low humidity conditions.

The poor performance of the equipment, at lower temperatures is explained by the spectrums obtained at temperatures 34 °F and 68 °F as shown in Figures 80 and 81. The first and third fiber optic channels of the spectrometer give negative light intensities. The Aurora module of the spectrometer is not specified for use outside of the laboratory in freezing temperatures or in humid conditions, which affects the data collection and the results. The ultra Quantel laser is manufactured for harsh environments and an anti-freeze cooling reagent is used as coolant. This minimized the negative effects of temperature on the laser. Some spectrum processing is done to shift the negative values of the spectrum, but it did not improve the analysis.

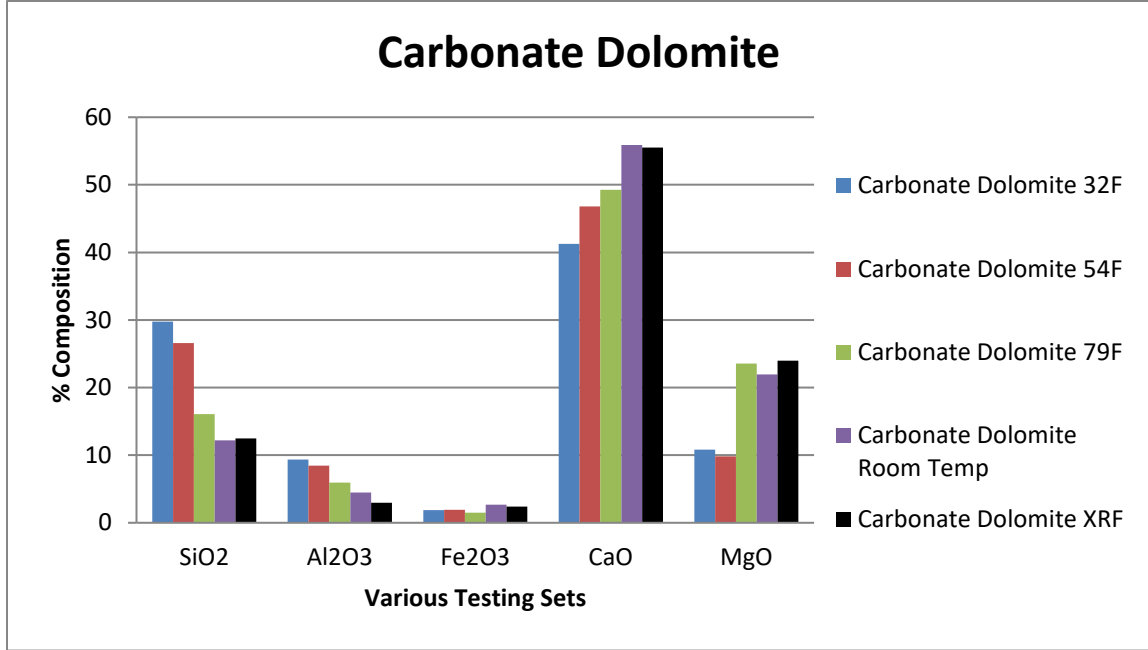


Figure 78. Temperature Test Results, Carbonate Dolomite.

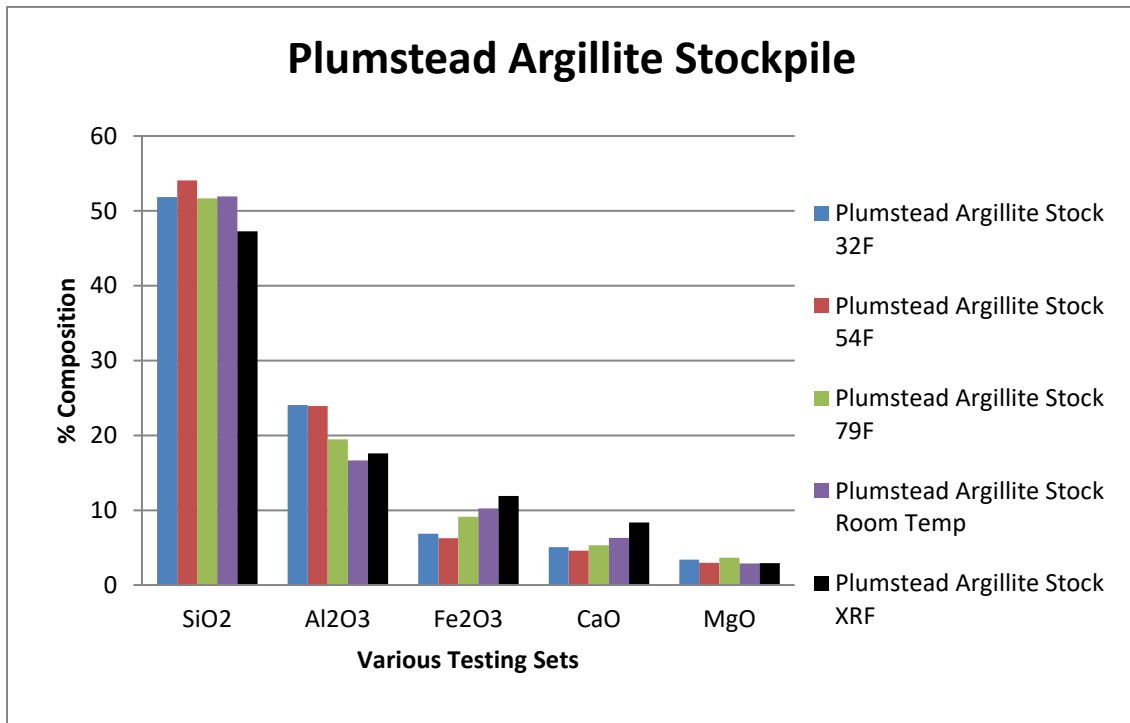


Figure 79. Temperature Test Results, Plumstead Argillite Stockpile.

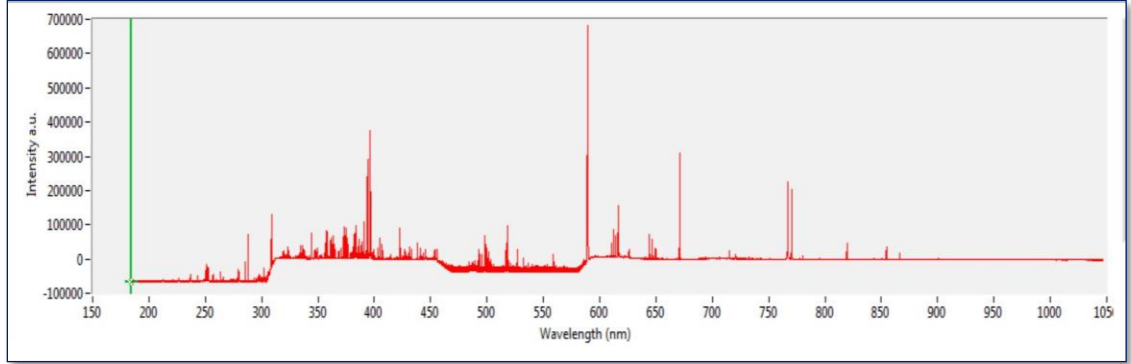


Figure 80. LIBS Spectrum Obtained at 34 deg. F.

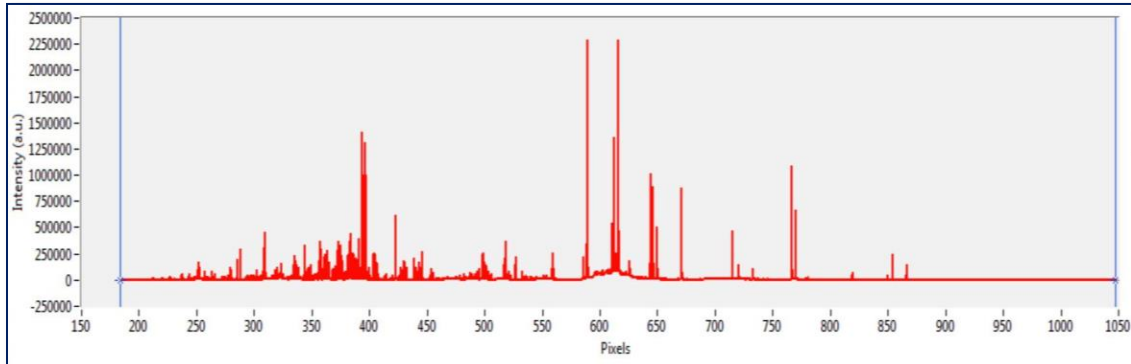


Figure 81. LIBS Spectrum Obtained at 68 deg. F. (Laboratory Condition).

Effect of aggregate moisture content on results. The sample's moisture content was studied to see if the results are affected. The aggregate samples are soaked in water for 24 hours. They are then wiped with a damp cloth and no other sample preparation is done before testing. These samples are tested before and after soaking. Figures 82 and 83 show the results of the tests. X-axis represents the test results before soaking and Y-axis represents the test results after 24 hours of soaking. Each point represents the compounds predicted. The figures show that test's before and after soaking gives the same results and the moisture content of the sample doesn't affect the LIBS test results. This concludes that the samples collected after a rainy day will not impact the accuracy of the results.

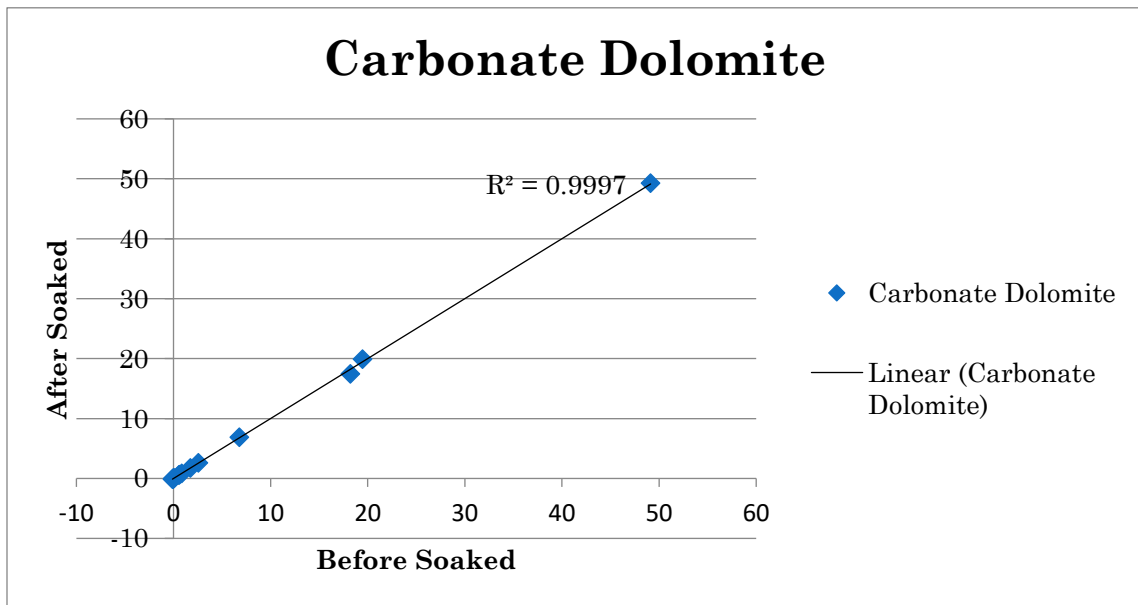


Figure 82. Aggregate Moisture Content Test Results, Carbonate Dolomite.

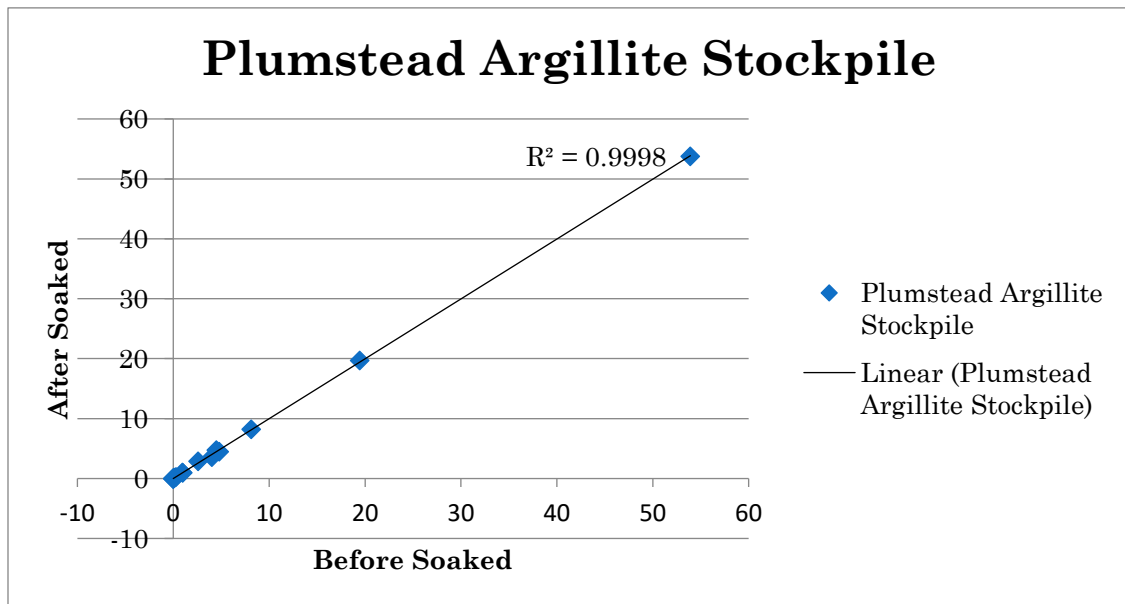


Figure 83. Aggregate Moisture Content Test Results, Plumstead Argillite Stockpile.

Building a more affordable and portable equipment setup. Since the most expensive piece of equipment in the setup is the spectrometer, testing is done using a high, as well as a low-resolution spectrometer. The low-resolution spectrometer is much more affordable than the current high resolution spectrometer that is being used. Data is collected from the same sample and location of an aggregate of Atkinson Quartzite. The Aurora module of high resolution spectrometer has a resolution of 12288 points. Figure 84 shows the results for the lower resolution spectrometer. Although various resolutions give more or less the same result as that of the higher resolution spectrometer, the results are slightly better for lowest resolution (1/20th). This may be due to the reduced sensitivity of the low-resolution spectrometer to the signal noises.

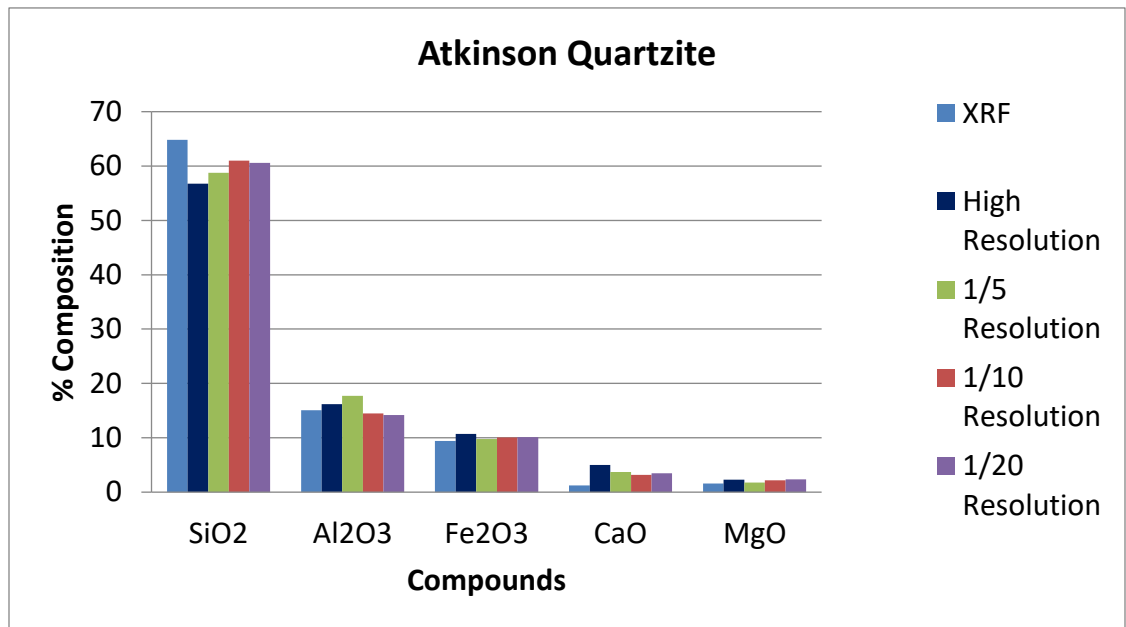


Figure 84. Testing of the Equipment Using Low Resolution Spectrometer.

To conclude, Split Training combined with Y-Scaling using a Three-Way Split classification is the most efficient model to predict the chemical composition of aggregates using LIBS technology. This chapter also proves that the portable equipment

is feasible for field testing. This equipment can be made more affordable in future using a lower resolution spectrometer.

Chapter 5

Conclusions

Summary of Findings

Throughout this study, Laser Induced Breakdown Spectroscopy (LIBS) is used to obtain characteristic light spectra for various types of aggregates collected from various quarries and sources in New Jersey and surrounding states. This involves firing a high energy, short laser pulse at a sample to vaporize a small amount of the sample material, which then fluoresces due to the high temperature of the resulting plasma. The emitted light contains a unique spectrum of wavelengths corresponding to the elements present in the aggregate. X-Ray Fluorescence (XRF) tests were also conducted on each sample by the NJDOT and served as the source of calibration data. Partial Least Square Regression analysis is used to develop the predictive model for the laser spectra utilizing the known XRF values that are provided.

Various tests were conducted to finalize the system standards and specifications for the LIBS setup. The most reliable timing was determined to use a flashlamp-Q-Switch delay of 180 μ s and a spectrometer delay of 6.3 μ s for the Ultra Quantel laser. A spectrum of accumulated data of 100 laser pulses were collected to accommodate the variability in test data due to randomness in the system and to minimize the shot to shot variations due to aggregate heterogeneity.

Various spectrum preprocessing methods were utilized for this research study and the most optimal methodology is determined to be Split Training with Y Scaling. Negative light intensities assumed as noise in the spectrum are zeroed. Each spectrum is normalized based on the total light intensity such that the sum of all light intensity values

is 1. Reverse adjustments are made on the final predicted values. Y-Scaling has applied to the X-Ray Fluorescence chemical composition by scaling the data of each composition between 0 and 1. This will force the PLSR algorithm to consider all the compounds with equal priority.

The preprocessed spectra are then used to develop functional models using PLSR. An optimum number of PLS components are used to calibrate each models. An initial guess of the chemical composition of unknown sample is made using a broad-based Model. This broad-based Model is developed using all the aggregates in the calibration data set. The rocks are then classified into Carbonates, Trap Rocks or Non-Carbonates using a Three-Way Split classification. The final predictions are made using these precise models for better accuracy. Various error analysis is done to ensure the accuracy of the model. The conclusions from the model testing are the following.

- Split Training with Y-Scaling using a Three-Way Split classification is found to be the best model with an overall accuracy of 90%. Table 8 shows how accurate the model fits the data.
- 35 rocks were used to calibrate the model with 10 Carbonates, 8 Trap Rocks and 17 Non-Carbonates.

Table 8
Accuracy of the Model Selected for Final Use

R Square Value	SiO₂	Fe₂O₃	Al₂O₃	CaO	MgO
Split Training with Y Scale Three-Way Split Classification	.9119	.7529	.8015	.9081	.7064

- Three unknown rocks, North Church Franklin Gravel and Westfield Gravel and Westerly Granite were tested using the model and the predicted result has an R Square value of 0.9249. These aggregates consist of water transported particles of rocks are very heterogeneous and are not used for calibrating the model.
- A standard testing set size is determined as 10 samples with 3 locations per sample to represent the aggregate stockpile. The initial 200 laser shots are neglected to eliminate the surface dust contamination and also to stabilize the peak light intensity collected. The accumulated data of succeeding 100 shots are saved per locations.
- No sample preparation is needed for this testing. Brush the sample with a damp cloth to remove the surface dust.
- Testing for a single stone type takes less than an hour to collect the LIBS spectrum, analyze the data and predict the result.

Various high pass filtering methods are considered to remove the broadening of the spectrum. This idea of smoothing the spectrum is not pursued further in this study as

it did not produce significant improvement in test results. A user-friendly GUI program is developed for easy analysis of LIBS data. The user can browse the data needed to be analyzed. Manual input options are also provided for the number of PLS components and for the carbonate, non-carbonate threshold values. Software for the data analysis program is developed, named “Laser Analysis Tool,” which can be installed and used in any system without MATLAB. A program for expanding the calibration set in future is developed, which will automatically create the analysis input file needed for the model training.

The equipment is made portable and can transported in the back of a vehicle and taken to the field for on-site testing. It is then tested for various field conditions to ensure the feasibility of LIBS testing as a portable tool. The summary of the portable equipment test is found to be the following.

- The equipment is built to handle the vibrations and the impact caused by poor roadway and driving conditions.
- The equipment is tested for various atmospheric temperatures by allowing it to cool/heat to the atmospheric temperature in 4hrs. It is found that the portable equipment gives reliable test results at 60⁰F or above. The equipment should be stored in a temperature controlled room during winter to avoid the damage to the spectrometer caused by the freezing weather.
- The aggregate samples with high moisture content were also tested with no impact on the accuracy of the results obtained.
- This equipment is also tested with a low cost, temperature controlled, lower resolution spectrometer (Flame Miniature Spectrometer from Ocean Optics) and

found producing similar results with the same accuracy. Thus the equipment can be made 50% more affordable in the future.

A manual is developed for the end users that includes the safety precautions, operation and maintenance of the equipment and trained the NJDOT personnel to equip them to use the equipment.

In conclusion,

- Laser Induced Breakdown Spectroscopy can be used to quantify the chemical composition of aggregate stone samples.
- Partial Least Square Regression Analysis can be used to develop predictive models to predict the aggregate composition.
- Split Training with Y Scaling with a Three-Way Split classification produce accurate results.
- A Graphical User Interface program facilitates rapid model testing and future refining of the models.
- The equipment is feasible and affordable as a portable tool for field use and is efficient in terms of time and cost compared to XRF.

Future Recommendations

A lower resolution spectrometer can be used for the LIBS testing which will serve the purpose and ensure the accuracy of the results. This spectrometer will be a solution to make it more portable. Its temperature controlled feature helps to use the equipment in a wide range of atmospheric weather conditions.

References

- [1] The Geology of New Jersey, Division of Science, Research and Technology, Department of Environmental Protection, Trenton, New Jersey, 1999.
- [2] Bedrock Geologic Maps of New Jersey, Division of Water Science and Geoscience, Trenton, New Jersey, 1996.
- [3] Geological Time, Virtual Fossil Museum, 1999.
- [4] R. L. Folk, "Petrology of Sedimentary Rocks," Hemphil Publishing Company, Austin, Texas, 1974.
- [5] T. Pallis, "New Jersey Brownstone," Unearthing New Jersey, New Jersey Geological Survey, Department of Environmental Protection, Trenton, New Jersey, 2007.
- [6] Franklin Mineral Museum, Franklin Mineral Museum, Franklin, New Jersey, 2013.
- [7] Steven. H and W. C. K. Panarese, Design and Control of Concrete Mixtures, 13 ed., Washington, DC: Portland Cement Association, 1998.
- [8] J. Gilluly, A. C. Waters and A. O. Woodford, Principles of Geology, San Fracisco, California: W.H. Freeman and Company, 1968.
- [9] P. Kandhal and E. Bishara, Evaluation of Limestone Aggregates in Asphalt Wearing Courses, Alabama: National Center for Asphalt Technology, Auburn University, 1992.
- [10] Rock and Mineral Identification for Engineers, US Department of Transportation, Federal Highway Administration, Washington DC, 1991.
- [11] K. Hobart, "Geology.Com," 2015.
- [12] Rock Identification and Classification, The Universtiy of Auckland, New Zealand, 2005.
- [13] D. John and R. M. Anderson, "Material Production, Mix Design and Pavement Design Effects on Moisture Damage," Moisture Sensitivity of Asphalt Pavements: A National Seminar, San Diego, California, 2003.
- [14] G. H. Rowe, "Applied Geology of Wellington Rocks for Aggregate and Concrete," School og Geography, Environment, and Earth Sciences, University of Wellington, New Zealand, 2010.
- [15] S. R. Koirtyohann, "A History of Atomic Absorption Spectrometry," Analytical Chemistry, vol. 63, no. 21, 1991.

- [16] R. J. Porra, W. A. Thompson and P. E. Kriedemann, "Determination of accurate extinction coefficients and simultaneous equations for assaying chlorophylls a and b extracted with four different solvents: verification of the concentration of chlorophyll standards by atomic absorption spectroscopy," *Biochimica et Biophysica Acta (BBA)-Bioenergetics*, vol. 975, no. 3, pp. 384-394, 1989.
- [17] R. E. Wolf, "What is ICP-MS?," U.S. Geological Survey, 2005.
- [18] B. Fryer, S. E. Jackson and H. P. Longerich, "The Design, Operation and Role of the Laser Ablation Microprobe Coupled with an Inductively Couple Plasma Mass Spectrometer in the Earth Science," *The Canadian Mineralogist*, vol. 33, pp. 303-315, 1995.
- [19] J. e. a. Ludden, "Applications of LAM-ICP-MS Analysis to Minerals," *The Canadian Mineralogist*, vol. 33, pp. 419-434, 1995.
- [20] S. A. Nelson, *Mineral Chemistry*, Tulane University, 2013.
- [21] K. Wirth and A. Barth, "X-Ray Fluorescence (XRF)," Carleton College, 2013.
- [22] T. E. L. Tour, "Analysis of rocks using X-Ray Fluorescence Spectrometry," *Rigaku Journal*, 1987.
- [23] J. Goodge, "Electron probe micro-analyzer (EPMA)," Carleton College, 2012.
- [24] M. I. Pownceby, C. M. MacRae and N. C. Wilson, "Mineral Characterization by EPMA mapping," *Minerals Engineering*, vol. 20, no. 5, pp. 444-451, 2007.
- [25] D. A. Cremers and L. J. Radziemski, *Handbook of Laser-Induced Breakdown Spectroscopy*, John Wiley & Sons, Ltd, 2006.
- [26] Photonics, "An Introduction to Laser-Induced Breakdown Spectroscopy," Applied Photonics Ltd, North Yorkshire, UK, 2001.
- [27] W. Pierce, S. M. Christian, M. J. Myers and J. D. Myers, "Field-Testing for Environmental Pollutants Using Briefcase Sized Portable LIBS System," in 3rd International Conference on Laser Induced Plasma Spectroscopy and Applications, Malaga, Spain, 2004.
- [28] E. A. Taffe, "Development of a portable LIBS-device for quality assurance in concrete repair," *Concrete Repair, Rehabilitation and Retrofitting II*, London, 2009.
- [29] AppliedSpectra, "What is LIBS?."
- [30] R. Gonzalez, P. Lucena, L. M. Tobarria and J. J. Laserna, "Standoff LIBS Detection of Explosive Residues Behind A Barrier," *The Royal Society of Chemistry*, 2009.

- [31] V. Lazic, A. Palucci, S. Jovicevic, M. Carapanese, C. Poggi and E. Buono, "Detection of explosives at trace levels by laser-induced breakdown spectroscopy (LIBS)," in Chemical, Biological, Radiological, Nuclear, and Explosives (CBRNE) Sensing XI, Orlando, Florida, 2010.
- [32] G. Qian-jin, H. Yu, Y. Xin, X. Li and X. Li, "Experimental Study on High Alloy Steel Sample by Laser-Induced Breakdown Spectroscopy," Spectroscopy and Analysis, vol. 30, no. 3, pp. 783-790, 2010.
- [33] C. Aragon, A. Aguilera and J. Campos, "Determination of Carbon Content in Molten Steel using Laser-Induced Breakdown Spectroscopy," Applied Spectroscopy, vol. 47, no. 5, pp. 606-608, 1993.
- [34] K. R. Awadshesh, Y. Fang-Yu and P. S. Jagadish, "Laser-induced breakdown spectroscopy of molten aluminium alloy," Applied Optics, vol. 42, no. 12, pp. 2078-2084, 2003.
- [35] M. Rosalie, A. C. David and M. L. Bostian, "Use of laser-induced breakdown spectroscopy for the differentiation of pathogens and viruses on substrates," Applied Optics, vol. 51, no. 7, pp. B57-B64, 2012.
- [36] Rai, K. Nilesh and A. K. Rai, "LIBS-an efficient approach for the determination of Cr in industrial wastewater," Journal of hazardous materials, vol. 150, no. 3, pp. 835-838, 2008.
- [37] J. Cunat, S. Palanco, F. Carrasco, M. D. Simon and J. J. Laserna, "Portable instrument and analytical method using laser-induced breakdown spectrometry for in-situ characterization of speleothems in Karstic caves," Royal Society of Chemistry, vol. 20, pp. 295-300, 2005.
- [38] M. Anzano Jesús, M. A. Villoria, A. Ruiz-Medina and R. J. Lasheras, "Laser-induced breakdown spectroscopy for quantitative spectrochemical analysis of geological materials: Effects of the matrix and simultaneous determination," Analytica chimica acta, vol. 575, no. 2, pp. 230-235, 2006.
- [39] W. Chesner and N. McMillan, "Automated Laser Spectrographic Pattern Matching for Aggregate Identification," Highway Idea Program, 2012.
- [40] NJDOT, "Petrographic Analysis to Determine Lithological Composition of Coarse Aggregate," New Jersey Department of Transportation Standard Specifications for road and Bridge construction, New Jersey, 2007.
- [41] Ontario Laboratory Testing Manual, "Petrographic Analysis to determine Lithological Composition of Coarse Aggregate," Ministry of Transportation, Ontario, 2001.

- [42] F. Rosenblatt, "The Perception: A Probabilistic Model for Information Storage and Organization in the Brain," *Psychological Review*, pp. 386-408, 1958.
- [43] wikimedia.org.
- [44] e. a. Koujelev, "Laser-Induced breakdown spectroscopy with artificial neural network processing for material identification," *Planetary and Space Science*, vol. 58, pp. 682-690, 2010.
- [45] Ramil, A. J. Lopez and A. Yanez, "Appliciation of Artificial neural networks for the rapid classification of archeological ceramics by means of laser induced breakdown spectroscopy (LIBS)," *Applied Physics*, vol. 92, no. 1, p. 197, 2008.
- [46] M. Boueri, V. Motto-Ros, W.-Q. Lei, L.-J. Zheng, Jin Yu and U. d. Lyon, "Identification of Polymer Materials Using Laser-Induced Breakdown Spectroscopy combined with Artificial Neural Networks," *Applied Spectroscopy*, vol. 65, pp. 307-314, 2011.
- [47] Jolliffe, *Principal Component Analysis*, Wiley StatsRef: Statistics Reference Online, 2014.
- [48] H. Abdi and L. J. Williams, "Principal Component Analysis," *WIREs Comp Stat*, vol. 2, pp. 433-459, 2010.
- [49] Rasmus and A. K. Smilde, "Principal Component Analysis," *Royal Society of Chemistry*, vol. 6, pp. 2812-2831, 2014.
- [50] Unnikrishnan, K. S. Choudhari, S. D. Kulkarni, R. Nayak, V. B. Kartha and C. Santhosh, "Analytical predictive capabilities of Laser Induced Breakdown Spectroscopy (LIBS) with Principal Component Analysis (PCA) for plastic classification," *RSC Advances*, pp. 25872-25880, 2013.
- [51] G. M.-A. Morales, "Partial Least Squares (PLS) methods: Origins, Evolution and Application to social sciences," Complutense University of Madrid, Spain.
- [52] H. Abdi, *Partial Least Squares (PLS) Regression*, Texas: The University of Texas at Dallas, 2003.
- [53] S. Wold, M. A. Sjostrom and L. B. Eriksson, "PLS REgression: A basic tool of chemometrics," Institute of Chemistry, Umea, Sweden, Sweden, 2001.
- [54] Z. Wang, J. Feng, L. Li, W. Ni and L. Zheng, "A Non-linearized PLS Model Based on Multivariate Dominant Factor for Laser-induced Breakdown Spectroscopy Measurements," State Key Lab of Power Systems, Department of Thermal Engineering, Tsinghua-BP Clean Energy Center, Tsinghua University, Beijing, China.

Appendix A

X-Ray Fluorescence Data of Rocks

Below is a summary of XRF results provided by the NJDOT. Note that this list only includes samples used for model calibration. Additional samples and chemical composition results have recently been received and will be incorporated into future models.

Rock Names	SiO ₂	Al ₂ O ₃	Fe ₂ O ₃	CaO	MgO	Na ₂ O	P ₂ O ₅	TiO ₂	K ₂ O	MnO
Allen Myers Carbonate	13.8	6.725	2.195	43.25	31.3	0	0.7485	0.2265	1.235	0.0918
Andreas Lehigh Carbonate	42.75	19.8	5.485	20.8	4.985	0.5855	0.687	0.8165	3.185	0.072
Bechtessville Gneiss	51.55	15.3	9.61	5.3	5.945	8.275	1.135	1.435	1.02	0.1155
Braen Franklin Carbonate	1.81	0.581	1.405	71.3	23.7	0	0.5725	0	0.05845	0.2
Carbonate Dolomite	12.5	2.97	2.42	55.5	24	0	0.8705	0.1795	1.3	0.06685
Dyer Quarry Diabase	46.8	17.5	10.65	7.625	7.285	6.795	0.9015	1.455	0.5945	0.1645
EI Hamburg Gneiss	57.5	14.7	8.34	5.795	2.975	4.115	1.9	1.25	2.86	0.0925
Eureka Milford Quartzite	65.95	20.15	4.75	0.99	2.98	1.355	0.474	0.6405	2.285	0.0999
Fanwood Traprock	43.2	15.95	10.75	8.22	11.25	8.45	0.7115	0.889	0.247	0.167
Hanson Glen Gneiss	54.15	13.15	11.85	6.715	3.295	3.205	2.185	1.9	2.215	0.178

Kingston Argillite	41.45	17.8	12.1	7.32	8.17	8.595	1.003	0.7935	2.11	0.238
Kingston Trap Rock	45.95	16.7	12.065	10.465	7.275	4.235	0.985	1.161	0.65	0.202
Lehigh Asphalt Carbonate	35.85	7.25	8.885	35.2	3.195	0.775	1.27	1.41	3.965	0.124
New Hope Crushed Stone Carbonate	17	6.065	2.05	44.15	26.7	1.445	0.3336	0.3395	1.475	0.0858
OW Traprock Orange Basalt	43.2	16.1	10.25	8.575	10.4	9.41	0.6765	0.8265	0.2545	0.188
Westfield Traprock	45.3	17.1	12.25	7.88	7.215	7.625	0.728	0.7815	0.786	0.1965
Pioneer Laflin Quartzite	66.2	24.35	3.145	0.3775	1.265	0.5595	0.3795	0.654	2.795	0.0666
Temple Quartzite	87.8	8.87	0.2575	0.1365	0.469	0	0.378	0.904	0.931	0
Atkinson Quartzite	64.8	15.05	9.39	1.21	1.575	0.756	1.64	0.545	3.79	0.245
Woodboro Carbonate	14.85	5.23	3.055	69.65	3.11	0	0.932	0.5775	1.865	0
Plumstead Argillite Belt	49.75	16.4	12.95	6.955	2.055	3.585	1.795	1.345	4.015	0.2345
Plumstead Argillite Stockpile	47.25	17.6	11.9	8.34	2.93	3.98	1.57	1.17	4.17	0.2195
Tilcon Diabase	46.95	16.45	13.95	11.4	3.805	3.435	1.53	1.325	0.7145	0.195
Newhope Carbonate	17.9	5.52	3.585	54.45	14.05	0.7885	0.943	0.574	1.71	0.118

Eastern Wantage Carbonate	14.5	4.99	1.565	42.45	33.95	0	0.574	0.1875	1.55	0.0295
Tilcon Oxford Carbonate	7.29	1.96	5.755	74.05	8.47	0	0.742	0.356	0.301	0.336
Plumstead Argillite Lockatong	50.1	18.55	10.2	6.93	2.52	4.55	1.48	1.165	3.645	0.186
Tilcon Oxford Gneiss	64.6	13.05	5.545	4.935	1.79	4.98	1.38	0.697	1.83	0.1085
Eastern Hamburg Gneiss Losee	70.4	13.9	2.27	4.655	0.8475	4.33	1.31	0.255	1.77	0.04575
Moore's Argillite Traprock Ind	33.55	9.4	32.15	11.85	1.08	0.2355	1.27	2.35	6.135	0.516
Bechtelsville Gneiss 15179	48.6	15.75	9.93	5.005	8.025	8.84	0.605	1.115	1.53	0.1075
Plumstead Argillite 15165	49.05	19.7	6.61	4.525	4.995	10.15	0.908	0.6985	2.64	0.1285
Tarheel Quartzite	77.9	0	8.98	0.461	4.34	1.09	1.505	1.37	3.86	0.186
Kingston Traprock 15219	45.15	16.65	9.54	8.49	11.45	6.125	0.803	1.095	0.4265	0.165
Pyramid Gneiss	45.75	0	33	4.985	0.6225	0.099	1.33	3.875	7.95	0.439

Appendix B

Algorithm for Three-Way Split Classification

plsregress function as per MATLAB 2015 (Copyright 2007-2010 The MathWorks, Inc.)

```
%%%%%%%%%%  
%%%%%%%%%%  
% function laseranalysis(rock_data, PLS, ncomp_in, mode_custom_thresh)  
%  
% This function handles the training and testing of a PLS model to predict  
% the chemical components of an observed data set. In training mode, this  
% function will take the observed X data and known Y data as well as the  
% number of PLS components to use and train a PLS model, saving the beta  
% matrix for use in testing. In testing mode, the function loads the saved  
% beta matrix and creates a predicted chemical composition for the observed  
% data set.  
%  
% Inputs:  
% rock_data - struct containing X and Y data with same number of  
% observations and corresponding rows aligned (training) or a matrix  
% containing all of the X data (testing)  
% (X - observed data set. In training this contains the spectrometer data  
% for all aggregate stones. In testing, this contains the spectrometer  
% data for just one aggregate stone.  
%  
% Y - known data set. In training, this contains the known composition  
% of all aggregate stones. For testing, enter 0 for this input.)  
%  
% PLS - struct containing PLS generated in training mode. Only used in  
% testing mode. For training mode, this input will be null.  
%  
% ncomp - number of PLS components to be used in training the PLS model.  
% In training mode enter the number of PLS components to use or enter a  
% number <= 0 to automatically use the maximum PLS components. In testing  
% mode, enter 0 for this input.  
%  
% mode - 'train' or 'test' (obtained from GUI)  
%  
% Outputs:  
% Training mode - Saves the PLS model in a struct; contains beta matrix  
% necessary for testing.  
% Testing mode - Saves the predicted chemical composition for the input  
% observed spectrometer data.  
%%%%%%%%%%  
%%%%%%%%%%
```

```

function laseranalysis(rock_data, PLS, ncomp_in, mode, thresholds, resultsFigName,
settingsSave_dir, TStamp)
%% TRAINING MODE %%
if(strcmp(mode,'train'))
    w = waitbar(0,'Generating PLS Model...','Name','Please Wait...');
    try
        frames = java.awt.Frame.getFrames();
        frames(end).setAlwaysOnTop(1);
    catch
    end

    % LOAD DATA IF FUNCTION IS CALLED FROM GUI
    if(ischar(rock_data))
        disp('Loading Rock Data.')
        rock_data = load(rock_data);
        rock_data = rock_data.rock_data;
        X = rock_data.X;

        disp('Loading Y Data.')
        Y = rock_data.Y;
        classer = rock_data.C;
    end

    %%%%%%%%%%%
    % PREPROCESSING STAGE %

    %%%%%%%%%%%
    % NOTE %
    %%%%%%%%%%%
    % This stage can eventually contain all of the different types of
    % preprocessing techniques we want to test. This includes the split
    % training technique, Y-scaling, and normalizing the data to total
    % light emission.

    %%%%%%%%%%%
    %%%%%%%%%%%

    waitbar(1/10,w);
    % Remove light intensity values less than 0.
    [m,n]=size(X);

    disp('Removing negative light intensity values.')
    for i=1:m
        for j=1:n
            if X(i,j)<0

```

```

        X(i,j)=0;
    end
end
end
waitbar(3/10,w);
% Normalizing Data to Total Light Emission
disp('Normalizing spectra to total light emissions.')
```

% Initializing total light intensity.

```

total_light_int=zeros(m,1);

for i=1:m
    for j=1:n
        total_light_int(i) = total_light_int(i) + X(i,j);
    end
end

% Determine Xnorm
Xnorm = zeros(m,n);
for i=1:m
    for j=1:n
        Xnorm(i,j) = X(i,j)/total_light_int(i);
    end
end
waitbar(4/10,w);
% Perform Y Scaling
numCol= size(Y,2);

% Initialize minmax matrix. Currently 2x24, but it can be of varying
% size.
minmax_base = zeros(2, numCol);
for i = 1:numCol

    maxVal = max(Y(:,i));
    minVal = min(Y(:,i));
    minmax_base(2,i) = minVal;
    minmax_base(1,i) = maxVal;
    val_range = maxVal-minVal;
    if(val_range == 0)
        Yscaled(:,i) = 0;
    else
        Yscaled(:,i) = (Y(:,i) - minVal)/val_range;
    end

end
waitbar(5/10,w);
```

```

% NOTE: Do Y scaling for Carb and Nonc models after splitting into
% separate matrices

% Determine pls components if set to 'Auto'
% THIS NEEDS TO BE DONE SEPARATELY FOR EACH OF THE SPLIT
TRAINING
% MODELS

ncomp_base_in = ncomp_in.Base;
if ncomp_base_in<=0;
    disp('Determining optimal number of PLS components for Base model.')
    ncomp = 25;

    % Find PLS regression for starting number of ncomp
    [~,~,~,~,~,PCTVAR] = plsregress(Xnorm,Yscaled,ncomp);
    pctvar_count = 0;
    PCTVAR = 100*PCTVAR;

    % Set ncomp to max number that explains >1% of variation
    for i = 1:ncomp
        if (PCTVAR(2,i) >= 1)
            pctvar_count = pctvar_count + 1;
        else
            break;
        end
    end
    ncomp = i - 1;
    disp(['Number of Base PLS components automatically set to ', num2str(ncomp), '!']);
else
    ncomp = ncomp_base_in;
end
waitbar(7/10,w);
% PLS REGRESSION
disp('Generating Broad Base PLS Model.')
 [~,~,~,~,betamat,PCTVAR] = plsregress(Xnorm,Yscaled,ncomp);

% Creates a structure with all of the PLS Model variables to be saved as a
% .mat file.
PLS_Model_base = struct('Date', date, 'PercentVariation', PCTVAR, 'Beta', betamat,
'MinMax', minmax_base);
PLS_Model_base.NComp = ncomp;

% SPLIT TRAINING
Ycarb = [];
Xcarb = [];
Ynonc = [];

```

```

Xnonc = [];
Ytrap = [];
Xtrap = [];
for i = 1:size(Y,1)
    switch classer(i)

        case 'c'
            Ycarb = cat(1,Ycarb,Y(i,:));
            Xcarb = cat(1,Xcarb,Xnorm(i,:));
        case 'n'
            Ynonc = cat(1,Ynonc,Y(i,:));
            Xnonc = cat(1,Xnonc,Xnorm(i,:));
        case 't'
            Ytrap = cat(1,Ytrap,Y(i,:));
            Xtrap = cat(1,Xtrap,Xnorm(i,:));
        otherwise
            error('Error in XRF Sheet used in Calibration. Unknown classification')
    end
end

% Calculate ncomp for carbonate rocks
ncomp_carb_in = ncomp_in.Carbonate;
if ncomp_carb_in<=0;
    disp('Determining optimal number of PLS components for Carbonate model.')
    ncomp_carb = 25;

    % Find PLS regression for maximum number of ncomp
    [~,~,~,~,~,PCTVAR] = plsregress(Xcarb,Ycarb,ncomp_carb);
    pctvar_count = 0;
    PCTVAR = 100*PCTVAR;
    % Set ncomp to max number that explains >1% of variation
    % Stop searching if two components in a row are found to explain
    % less than 1%.
    for i = 1:ncomp_carb
        if (PCTVAR(2,i) >= 1)
            pctvar_count = pctvar_count + 1;
        else
            break;
        end
    end
    ncomp_carb = i - 1;
    disp(['Number of Carbonate PLS Model components automatically set to ',
num2str(ncomp_carb),'.']);
else
    ncomp_carb = ncomp_carb_in;
end

```

```

% Perform Y scaling for Carbonate rocks
minmax_carb = zeros(2, numCol);
for i = 1:numCol

    maxVal = max(Ycarb(:,i));
    minVal = min(Ycarb(:,i));
    minmax_carb(2,i) = minVal;
    minmax_carb(1,i) = maxVal;
    val_range = maxVal-minVal;
    if(val_range == 0)
        Yscaled_carb(:,i) = 0;
    else
        Yscaled_carb(:,i) = (Ycarb(:,i) - minVal)/val_range;
    end

end

%-----
% Calculate ncomp for noncarbonate rocks
ncomp_nonc_in = ncomp_in.Carbonate;
if ncomp_nonc_in <= 0;
    disp('Determining optimal number of PLS components for Non-Carbonate model.')
    ncomp_nonc = 25;

    % Find PLS regression for maximum number of ncomp
    [~,~,~,~,~,PCTVAR] = plsregress(Xnonc, Ynonc, ncomp_nonc);
    pctvar_count = 0;
    PCTVAR = 100*PCTVAR;
    % Set ncomp to max number that explains >1% of variation
    % Stop searching if two components in a row are found to explain
    % less than 1%.
    for i = 1:ncomp_nonc
        if (PCTVAR(2,i) >= 1)
            pctvar_count = pctvar_count + 1;
        else
            break;
        end
    end
    ncomp_nonc = i - 1;
    disp(['Number of Non-Carbonate PLS Model components automatically set to ',
num2str(ncomp_nonc),'.']);
else
    ncomp_nonc = ncomp_nonc_in;
end

% Perform Y scaling for NonCarbonate rocks
minmax_nonc = zeros(2, numCol);

```

```

for i = 1:numCol

    maxVal = max(Ynonc(:,i));
    minVal = min(Ynonc(:,i));
    minmax_nonc(2,i) = minVal;
    minmax_nonc(1,i) = maxVal;
    val_range = maxVal-minVal;
    if(val_range == 0)
        Yscaled_nonc(:,i) = 0;
    else
        Yscaled_nonc(:,i) = (Ynonc(:,i) - minVal)/val_range;
    end

end

%-----
ncomp_trap_in = ncomp_in.Trap;
if ncomp_trap_in<=0;
    disp('Determining optimal number of PLS components for Traprock model.')
    ncomp_trap = 25;

    % Find PLS regression for maximum number of ncomp
    [~,~,~,~,~,PCTVAR] = plsregress(Xcarb,Ycarb,ncomp_trap);
    pctvar_count = 0;
    PCTVAR = 100*PCTVAR;
    % Set ncomp to max number that explains >1% of variation
    % Stop searching if two components in a row are found to explain
    % less than 1%.
    for i = 1:ncomp_trap
        if (PCTVAR(2,i) >= 1)
            pctvar_count = pctvar_count + 1;
        else
            break;
        end
    end
    ncomp_trap = i - 1;
    disp(['Number of Traprock PLS Model components automatically set to ',
num2str(ncomp_trap),'.']);
else
    ncomp_trap = ncomp_trap_in;
end

% Perform Y scaling for Traprocks
minmax_trap = zeros(2, numCol);
for i = 1:numCol

    maxVal = max(Ytrap(:,i));

```



```

minVal = min(Ytrap(:,i));
minmax_trap(2,i) = minVal;
minmax_trap(1,i) = maxVal;
val_range = maxVal-minVal;
if(val_range == 0)
    Yscaled_trap(:,i) = 0;
else
    Yscaled_trap(:,i) = (Ytrap(:,i) - minVal)/val_range;
end

end

waitbar(8/10,w);

% PLS REGRESSION Trap
disp('Generating Trap Rock PLS Model.')
[~,~,~,~,betamat,PCTVAR] = plsregress(Xtrap,Yscaled_trap,ncomp_trap);

% Creates a structure with all of the PLS Model variables to be saved as a
% .mat file.
PLS_Model_trap = struct('Date', date, 'PercentVariation', PCTVAR, 'Beta', betamat,
'MinMax', minmax_trap);
PLS_Model_trap.NComp = ncomp_trap;

% PLS REGRESSION CARB
disp('Generating Carbonate Rock PLS Model.')
[~,~,~,~,betamat,PCTVAR] = plsregress(Xcarb,Yscaled_carb,ncomp_carb);

% Creates a structure with all of the PLS Model variables to be saved as a
% .mat file.
PLS_Model_carb = struct('Date', date, 'PercentVariation', PCTVAR, 'Beta', betamat,
'MinMax', minmax_carb);
PLS_Model_carb.NComp = ncomp_carb;

% PLS REGRESSION NONC
disp('Generating Non-Carbonate Rock PLS Model.')
[~,~,~,~,betamat,PCTVAR] = plsregress(Xnonc,Yscaled_nonc,ncomp_nonc);

% Creates a structure with all of the PLS Model variables to be saved as a
% .mat file.
PLS_Model_nonc = struct('Date', date, 'PercentVariation', PCTVAR, 'Beta', betamat,
'MinMax', minmax_nonc);
PLS_Model_nonc.NComp = ncomp_nonc;

waitbar(8.5/10,w);

```

```

% Create PLS structure that contains PLS models for base, carbonate,
% and noncarbonate all together and save. This is the file the user
% should load when testing the system as it contains all of the
% necessary PLS models.
PLS_Model_All = struct('Base', PLS_Model_base, 'Carbonate', PLS_Model_carb,
'NonCarbonate', PLS_Model_nonc, 'Trap', PLS_Model_trap);
save_dir = check_create_dir('LAT Results\Training Data - PLS
Models',settingsSave_dir,3);
save([save_dir,'PLS-Model-All-', TStamp, '.mat'], 'PLS_Model_All');

waitbar(10/10,w);
disp(['PLS Model saved to ', settingsSave_dir,'\LAT Results\Training Data - PLS
Models'])
disp('Model calibration complete.')
delete(w)
waitfor(msgbox(['PLS Model saved to ', settingsSave_dir,'\LAT Results\Training Data
- PLS Models'],'Model Calibration Complete'))
end
%% TESTING MODE %%
close all;
if(strcmp(mode,'test')) || (strcmp(mode, 'testset'))
w = waitbar(0,'Processing testing data...','Name','Please Wait...');
try
frames = java.awt.Frame.getFrames();
frames(end).setAlwaysOnTop(1);
catch
end
setdata = rock_data;
sampnum = numel(setdata);
save_dir = check_create_dir('LAT Results\Testing Data -
Analysis',settingsSave_dir,3);
means=cell(sampnum+1,25);
chem = {'SiO2' 'Al2O3' 'Fe2O3' 'CaO' 'MgO' 'Na2O' 'P2O5' 'TiO2' 'K2O' 'MnO' 'BaO'
'SO3' 'SrO' 'CuO' 'ZrO2' 'ZnO' 'Y2O3' 'Rb2O' 'Ga2O3' 'Cl' 'Cr2O3' 'NiO' 'CeO2'
'Nb2O5'};
means(1,2:25)=chem;
stddev=means;
resultsFigure = figure('WindowStyle', 'normal','NumberTitle','Off');
if(sampnum == 1)
set(resultsFigure,'Name',['Single Test: ' resultsFigName ' Results']);
else
set(resultsFigure,'Name',['Set Test: ' resultsFigName ' Results']);
end
resultsTabGroup = uitabgroup(resultsFigure);
resultsTabArray = [];
for c = 1:sampnum

```

```

waitbar((1/15+14/15*(c/sampnum)),w)
rock_data = setdata{c};
% LOAD BETA MATRIX
dir = pwd;
disp([setdata{c},':'])
disp('Loading PLS model.')
if(ischar(PLS))
    load(PLS);
end
betamat = PLS_Model_All.Base.Beta;

% Obtain name of rock from rock_data filename.
rock_type = rock_data(1:length(rock_data)-4);

if(ischar(rock_data))
    disp('Loading X Data.')
    rock_data = load([settingsSave_dir 'LAT Results\Testing Data - Conversion to
mat\' TStamp \' rock_data]);
    X = rock_data.test_rock_data;
end

% Preprocessing stage
% Should use the same techniques as in training.

[m,n]=size(X);
% Center Clipping
for i=1:m
    for j=1:n
        if X(i,j)<0
            X(i,j)=0;
        end
    end
end

% Normalizing Data to Total Light Emission
disp('Normalizing spectra to total light emission.')

% Initializing total light intensity.

total_light_int = zeros(1,m);

for i=1:m
    for j=1:n
        total_light_int(i) = total_light_int(i) + X(i,j);
    end
end

```

```

% Initialize Xnorm
Xnorm = zeros(m,n);
for i=1:m
    for j=1:n
        Xnorm(i,j) = X(i,j)/total_light_int(i);
    end
end

% MAKE INITIAL PREDICTION
Ypredicted = [ones(size(Xnorm,1),1) Xnorm]*betamat;

% Obtain beta and minmax from carbonate or non-carbonate models based
% on carbonate threshold. Beta is used for prediction, minmax is used
% for reverse Y scaling.

% Edit: Reverse Y scaling has been changed back to just using the Base
% min_max values rather than split based on Carbonate content.
min_max = PLS_Model_All.Base.MinMax;

numCol = size(Ypredicted,2);
for i = 1:numCol
    val_range = min_max(1,i)-min_max(2,i);
    Ypredicted(:,i) = (Ypredicted(:,i)*val_range) + min_max(2,i);
end

% Use prediction matrix to determine whether the rock is carbonate,
% non-carbonate, or trap, and then make another prediction using the
% corresponding PLS Model.

% Ratio for classification
thresratio =
mean((Ypredicted(:,1)./abs(Ypredicted(:,4))).^2.*abs(Ypredicted(:,3)));
disp(num2str(thresratio))
if (thresholds == [-1,-1])
    carbthresh=150;
    noncarbthresh=500;
else
    carbthresh=thresholds(1);
    noncarbthresh=thresholds(2);
end

if(thresratio <= carbthresh)
    betamat = PLS_Model_All.Carbonate.Beta;
    min_max = PLS_Model_All.Carbonate.MinMax;
    disp('Classified as Carbonate')

```

```

elseif (theshratio<=noncarbthresh)
    betamat = PLS_Model_All.Trap.Beta;
    min_max = PLS_Model_All.Trap.MinMax;
    disp('Classified as Trap')
else
    betamat = PLS_Model_All.NonCarbonate.Beta;
    min_max = PLS_Model_All.NonCarbonate.MinMax;
    disp('Classified as Non-Carbonate')
end

% Make new prediction based on split training decision.
Ypredicted = [ones(size(Xnorm, 1), 1) Xnorm] * betamat;

% Perform reverse Y scaling on predicted matrix.
numCol = size(Ypredicted,2);
for i = 1:numCol

    val_range = min_max(1,i)-min_max(2,i);
    %if(range == 0)
    % Ypredicted(:,i) = 0;
    %else
    Ypredicted(:,i) = (Ypredicted(:,i)*val_range) + min_max(2,i);
    %end
    YpredLength = length(Ypredicted(:,i));
    for j=1:YpredLength
        if Ypredicted(j,i)<0
            Ypredicted(j,i)=0;
        end
    end
end

% MEAN AND STD. DEV. CALCULATIONS
% Initialize mean and std. dev. variables
Ymean = zeros(1,size(Ypredicted,2));
Ystd = zeros(1,size(Ypredicted,2));
Ymode = zeros(1,size(Ypredicted,2));
Ymedian = zeros(1,size(Ypredicted,2));

% Calculate mean and std. dev. for each column.
for i = 1:size(Ypredicted,2)
    Ymean(i) = mean(Ypredicted(:,i));
    Ystd(i) = std(Ypredicted(:,i));
    Ymedian(i) = median(Ypredicted(:,i));
end

% DISPLAY RESULTS IN FORMATTED TABLE

```

```

resultsTabArray(c) = uitab(resultsTabGroup, 'Title',rock_type);
Ymstd = cat(1,Ymean,Ystd,Ymedian);
t = uitable('Parent', resultsTabArray(c), 'Data', Ypredicted, 'ColumnName', chem);
set(t,'Position',[0 80 560 315])
h = uitable('Parent', resultsTabArray(c), 'Data', Ymstd, 'ColumnName', chem,
'RowName', {'Mean','Std.','Median'});
set(h,'Position',[0 0 560 80])
%data extraction for excel
rockname=setdata{c};
means(c+1,1)= {rockname(1:end-4)};
stddev(c+1,1)= {rockname(1:end-4)};

means(c+1,2:25)= num2cell(Ymean);
stddev(c+1,2:25)= num2cell(Ystd);

% COMPILER RESULTS STRUCTURE
Gap{1,24} = [];
lGap{1,1} = [];
ExcelRockSum{c} =
[chem;num2cell(Ypredicted);Gap;num2cell(Ymean);num2cell(Ystd)];
ERScol = size(ExcelRockSum{c},1) - 3;
ExcelRockSumLabels = {}
for lblC = 2:ERScol
    ExcelRockSumLabels{lblC,1} = ['Sample ' num2str(lblC-1)];
end
ExcelRockSumLabels = [ExcelRockSumLabels;lGap;'Mean';'Std.'];
ExcelRockSum{c} = [ExcelRockSumLabels ExcelRockSum{c}];
end
delete(w)
if exist('actxserver','file')
w2 = waitbar(0,'Exporting to Excel...','Name','Please Wait...');
try
    frames = java.awt.Frame.getFrames();
    frames(end).setAlwaysOnTop(1);
catch
end
if(strcmp(mode,'test'))
    ExcelName = 'Single Test';
elseif(strcmp(mode,'testset'))
    ExcelName = 'Testing Set';
end
cd(save_dir)
warning('off','MATLAB:xlswrite:AddSheet')
xlswrite([ExcelName ' Results Summary ' TStamp '.xls'],means,'Mean Values')
xlswrite([ExcelName ' Results Summary ' TStamp '.xls'],stddev,'Standard
Deviations')

```

```

waitbar(3/10,w2)
for xw = 1:length(ExcelRockSum)
    xlswrite([ExcelName ' Results Summary ' TStamp
'.xls'],ExcelRockSum{xw},setdata{xw}(1:end-4))
    waitbar((3/10)+(6/10)*(xw/length(ExcelRockSum)),w2)
end
disp(['Prediction report spreadsheet saved to ', save_dir])
fprintf('\n')
objExcel = actxserver('Excel.Application');

objExcel.Workbooks.Open(fullfile(cd,[ExcelName ' Results Summary ' TStamp
'.xls'])); % Full path is necessary!
try
    objExcel.ActiveWorkbook.Worksheets.Item(1).Delete;
catch
end

try
    for cc = 1:length(ExcelRockSum)+2
        invoke(objExcel.ActiveWorkbook.Worksheets.Item(length(ExcelRockSum)-
cc+1), 'Activate')
        objExcel.Cells.Select;
        objExcel.Selection.Columns.AutoFit;
    end
catch
end

% Save, close and clean up.
objExcel.ActiveWorkbook.Save;
objExcel.ActiveWorkbook.Close;
waitbar(1,w2)
objExcel.Quit;
objExcel.delete;
msgbox(['An Excel spreadsheet containing a summary of this test has been saved in:'
save_dir])
else
    warning('ActiveX process could not be created, excel summary not saved ')
end
cd(dir);
delete(w2)
end

```